Electrical Engineering
Mekelweg 4,
2628 CD Delft
The Netherlands
http://ewi.tudelft.nl/

2009

MSc THESIS

Interference Analysis, Measurements and Performance Evaluation of IEEE 802.11n in the presence of other IEEE 802.11b/g/n WLANs

Iman Ghaseminezhad Marandi

IRCTR-A-011-09

Abstract

The IEEE 802.11n standard is a promising technology for near future Wireless LAN's. By utilizing enhanced techniques like MIMO communication and OFDM digital modulation extremely high data rates over large distances are possible for wireless communications. Predecessors like 802.11b/g standards are succesfully outnumbered and a strong competitor to other rising WLAN techniques e.g., UWB and Wimax is born.

With the rapid migration of 802.11n into WLAN a new scenario arises where 802.11n networks and other nearby located 802.11b/g/n networks operate simultaneously. Forced to share the medium, interference between the networks is often inevitable, causing performance degredation in such way that the promised maximum data rates and communcation distances cannot be guaranteed. The objective of this thesis is to study these interference scenarios and gain a clear understanding of the consequences and effects of interference on the performance of the networks under consideration. In this regard real life measurements are performed and an analysis has been carried out. Our main focus will be on an 802.11n WLAN operating within the range of another 802.11b/g/n WLAN. We will observe the dramatic impact on the performance of the networks with respect to network throughput and packet loss rate. Consequently, the results of our study will address the eminent interference problem that the rapid growing WLANs are facing.

Interference Analysis, Measurements and Performance Evaluation of IEEE 802.11n in the presence of other IEEE 802.11b/g/n WLANs

THESIS

submitted in partial fulfillment of the
requirements for the degree of

MASTER OF SCIENCE

in

ELECTRICAL ENGINEERING

by

Iman Ghaseminezhad Marandi
born in Tehran, Iran

Electrical Engineering
Faculty of Electrical Engineering, Mathematics and Computer Science
Delft University of Technology, Delft, The Netherlands

Interference Analysis, Measurements and Performance Evaluation of IEEE 802.11n in the presence of other IEEE 802.11b/g/n WLANs

by Iman Ghaseminezhad Marandi

Abstract

The IEEE 802.11n standard is a promising technology for near future Wireless LAN's. By utilizing enhanced techniques like MIMO communication and OFDM digital modulation extremely high data rates over large distances are possible for wireless communications. Predecessors like 802.11b/g standards are succesfully outnumbered and a strong competitor to other rising WLAN techniques e.g., UWB and Wimax is born.

With the rapid migration of 802.11n into WLAN a new scenario arises where 802.11n networks and other nearby located 802.11b/g/n networks operate simultaneously. Forced to share the medium, interference between the networks is often inevitable, causing performance degredation in such way that the promised maximum data rates and communcation distances cannot be guaranteed. The objective of this thesis is to study these interference scenarios and gain a clear understanding of the consequences and effects of interference on the performance of the networks under consideration. In this regard real life measurements are performed and an analysis has been carried out. Our main focus will be on an 802.11n WLAN operating within the range of another 802.11b/g/n WLAN. We will observe the dramatic impact on the performance of the networks with respect to network throughput and packet loss rate. Consequently, the results of our study will address the eminent interference problem that the rapid growing WLANs are facing.

Student Number : 1170740
Laboratory : IRCTR, Electrical Engineering Dept., TU Delft
Codenumber : IRCTR-A-011-09

Committee Members :

Advisor:	Dr. H. Nikookar, IRCTR, TU Delft
Mentor:	I. Budiarjo M.Sc, IRCTR, TU Delft
Chairman:	Prof. L.P.Ligthart, Director IRCTR, TU Delft
Member:	T. Mol, Manager Device Competence Center, KPN
Member:	Ing. V. Hayes, Economics of Infrastructure, TBM, TU Delft

To my Parents

Contents

List of Figures

List of Tables

Acknowledgements

This research work has been performed as a collaboration work between KPN and IRCTR-TU Delft.

Special thanks go to Dr. H. Nikookar for his supervision and guidance in accomplishing this work. The interesting discussions that we had contributed very positively to this thesis. My thanks go to I. Budiarjo for his useful comments and suggestions. Further, my gratitude goes to all the professors of the EWI faculty for their efforts and knowledge, for without them, I would not come this far. In particular, Prof. Ligthart for chairing my graduation committee and giving me the chance to carry out my MSc thesis with IRCTR.

Furthermore, I would like to thank Theo Mol and Jaap Biesheuvel from KPN , who gave me the chance to gain more experience in the industry. Thanks for allways helping me during my measurements, the practical tips you gave me, making available all the resources I needed and the good times at the office. Also thanks to all the other collegues at the former DCC: Paul, Eric, Marcel, Fred, Richard, Peter, Edwin, Fred, Richard and the rest.

I also would like to express my sincere gratitude to Ing. V. Hayes and his collegues at TBM for the discussions and meeting which are acknowledged. Specially, the punctuality and accuracy of Vic Hayes' approach led to comments and advice which became a valuable input to this work. His efforts to improve the quality of the thesis are highly appreciated.

Last but not least, I am very grateful to my family and friends. My parents and brothers for their unlimited love and support, my dearest friends for the good times and for allways being there, other friends for their friendship and company, and last but definitely not least, *Niousha* for her endless love, her presence and her trust and faith in me.

Iman Ghaseminezhad Marandi
Delft, The Netherlands
August 21, 2009

1 Introduction

One of the promising techniques for Wireless Local Area Networks (WLAN) is the IEEE 802.11 family developed by the IEEE Committee. As data applications like multimedia services and other broadband purposes are demanding higher data rates and higher ranges, the evolution of the WLANs is going very fast in order to meet to these demands. IEEE introduced its first WLAN standardization in 1997 and from that moment amendments to this and new standards have been repeatedly developed and introduced. The first standard, the Legacy [13], operates on the 2.4 GHz frequency band and has a maximum data rate of 2 Mbit/s covering a range of about 20 meters when used indoor.

1.1 Background information

1.1.1 History WLAN

Through time, amendments to the Legacy WLAN led to new standards like the 802.11a and 802.11b. And every new standard had a new feature on top of the older one improving either the data rate or the range or both. 802.11a for example, has a maximum data rate of 54 Mbit/s, but it only covers short ranges because of the high operating frequency of 5 GHz. For this reason 802.11a was not such a success. Nevertheless, the next standard, the 802.11b was the first one to be widely accepted. It has a maximum data rate which is lower than that of its predecessor, but it operates in the lower 2.4 GHz ISM band, allowing a better indoor performance as it can propagate more through walls and doors. Another standard that is widely used currently is 802.11g operating at 2.4 GHz but reaching maximum data rates of 54 Mbit/s while using Orthogonal Frequency Division Multiplexing (OFDM) as modulation technique. OFDM has proven to be more bandwidth efficient than the Direct Sequence Spread Spectrum (DSSS) used in the 802.11b standard, making the higher data rates possible.

Until today 802.11g is the only official standard providing data rates as much as 54 Mbit/s. However, this rate is degraded by all the overhead for protocol management services at higher layers, i.e. security and reliability purposes. The new amandment to the legacy standards is already in development reaching up to even higher data rates and greater coverage distances. Several drafts of this new standard have been approved already, yet for the time being there is no official standard.

Some years ago in 2004 IEEE formed a new Task Group N (TGn) that should develop this successor to the existing standards. The new standard was given the name 802.11n and it was expected to reach much higher data rates and still cover large communication distances, i.e. maximum data rates that can reach up to 600 Mbit/s covering a range

of about 70 meters [9]. The two proposals with the best prospects for the 802.11n standard were from the groups named Tgnsync and WWiSE (World-Wide Spectrume Efficiency) each composed of all kinds of developers and manufacturers of electronic devices. After a real struggle between these competitors i.e., repeated ballots over and over again, together lasting a couple of years [1], in July 2005 finally the parties decided to join and work together to create a single merged proposal. From that moment on several drafts of the standard have been created, though still unapproved, but slowly leading to a final standard. Among these drafts, Draft 2.0 (D2.0 is implemented in the newest wireless routers by nearly all manufacturers of networking electronics. All over the world the networking products with implemented D2.0 are sold in electronics shops and warehouses and it is already a widely used electronic device in households in the Western countries. In July 2009 finally, the 802.11n standard is send to the IEEE Standards Board as an official candidate standard.

1.1.2 802.11n Features

In order to provide the high physical data rates in 802.11n WLANs, the standard makes use of Multi Input Multi Output (MIMO) communication where multiple transmitter and receiver antennas ensure higher data rates. Together with Orthogonal Frequency Division Multiplexing (OFDM), MIMO features such as spatial division multiplexing and space-time block coding (STBC) cope with the multipath character of the channel and the fading of signals in order to enable reliable data transfer at high rates at larger distances. Even more, transmission bandwidths of 40 MHz wide are supported, where 802.11a/b/g operate through 20 MHz channels. Besides the operation in the 2.4 GHz band, also operation in the 5 GHz band is supported with much more available frequency space. These innovations on 802.11n make it possible to achieve data rates up to 600 Mbit/s and increase range of reception. Because of these new features and the high performance of the standard, the future prospects of 802.11n WLANs are very promising.

1.2 Motivation

The ever growing demand for higher data rates in wireless networks and the massive use of wireless devices in the license free 2.4 GHz Industrial, Scientific and Medical (ISM) frequency band, has really caused a lot of occupancy on these bands. Providing this free frequency space by the frequency regulators in The United States (FCC) and Europe (ETSI), has created a whole list of electronic devices contributing to the occupancy of the bands, e.g., microwave ovens, Bluetooth devices, Dect telephones and not to be missed the WLANs. Indeed, WLANs occupy a major part of the ISM band, because of their large communication channels of 20 MHz and 40 MHz for an 802.11n WLAN. Since the available bandwidth in the ISM band is 80 MHz, there is only enough space for 2 non-overlapping 802.11n WLANs.

At this point already the problem that arises can be addressed. Multiple simultaneously operating wireless devices must share the same medium, but since there is not enough space, networks will operate at the same frequency channels and inevitebly are forced to share the available bandwidth in such way that interference is avoided. With

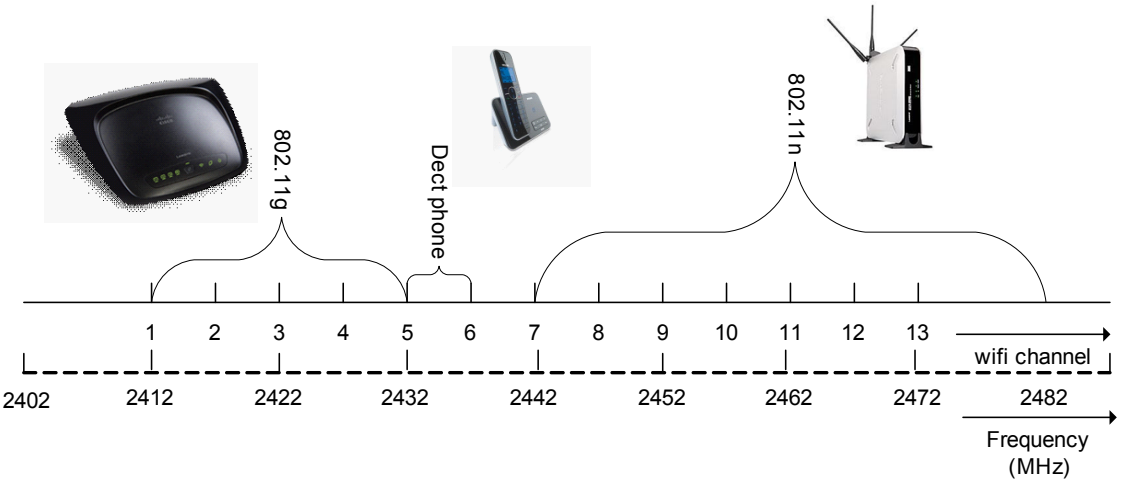

Figure 1.1: Common operation in the 2.4 GHz frequency band

the arrival of 802.11n, available frequency space will be even more sparse (Figure 1.1 and sharing of the medium has to be carried out even in a greater extent. That medium sharing will take place is a fact, but in which extent it will occur and whether or not it will lead to interference, plus all the effects it will have on the performance of the networks under consideration is rather unknown. This unknown territory serves as motivation of this work.

According to the author's knowledge which is based on background and literature study, still not much study is devoted to this subject if not, no study at all. Other works are performed on 802.11n WLANs but within scenarios that differ from ours. From this point of view, our work will contribute in order to obtain more insight into the problem of interference scenarios between 802.11n WLANs and other 802.11b/g/n WLANs.

1.3 Thesis Objectives

The arrival of 802.11n based networking devices on the market, leads to an substantial increase of medium sharing scenarios in the 2.4 GHz band, e.g., between 802.11n and UWB networks [11, 12]. Apart from UWB networks, medium sharing also occures due to the presence of other 802.11b/g/n WLANs operating in the same frequency band and located in the range of an 802.11n WLAN. The effect that medium sharing has to such networks can result in degradation of the network performance in terms of network throughput and even more in terms of probability of error given that the medium sharing turns into interference. The network throughput and probability of error are properties that define the quality of the communication within a network.

The goal of this work is to study medium sharing scenarios, concerning 802.11b/g/n WLANs and gain a clear understanding of the consequences and effects of medium sharing, if not interference on the performance of the concerning networks. Our main focus will be on 802.11n WLANs operating nearby other 802.11b/g WLANs or another

802.11n WLAN, which consequently have to share the medium. The network throughput and the probability of error serve as a measure of the performance of the systems. The study is performed by means of real life measurements and by carrying out an interference analysis.

1.4 Related work

Thorough studies on the performance of 802.11n networks are performed earlier in [9, 10] with results confirming the improvement of the performance with respect to packet error rate and throughput. Interference scenarios are discussed in [11] existing of colocated 802.11g/n networks and 802.15.4 sensor networks. In this work interference is analyzed through measurements which resulted in negative effects on the performance of the 802.15.4 networks with respect to packet delivery ratio, due to the interfering 802.11n WLAN. In [12] the interference between 802.11n networks and UWB networks is analyzed and an interference nulling model is proposed. With interference nulling the multiple antennas in the MIMO system featured by the 802.11n system, are utilized such that interferers can be nulled out. Finally, a short overwiew is given in [10] of Bluetooth devices experiencing interference from colocated 802.11n networks. Here the negative effects on the signal detecting capabilities of the Bluetooth device are pointed out.

Our work considers a different scenario containing an 802.11n WLAN experiencing interference from another 802.11b/g/n network and being the interfering source with respect to another 802.11b/g/n network. As we will go through this work, we will see that not allways these scenarios will lead to interference, due to operation of the medium access mechanism that allows the networks to share the medium in stead of causing interference upon each other. Obviously the medium sharing scenarios widely exist in many districts of many big cities (and even small towns) in Western countries. Further more, we use the probability of bit error and the network throughput as measures for the performance of the networks.

1.5 Thesis Outline

Chapter 2 covers the basic concepts and techniques behind the 802.11n standard and discusses in more detail the elemental features of the standard, e.g. MIMO, Space Time Block Coding (STBC) and spatial mapping and describes how medium sharing is controlled by the MAC layer. In Chapter 3 the results of the measurement phase are discussed that consisted of measurements with new 802.11n devices like routers and wireless adaptars. Different measurement locations and various devices are considered to cover important medium sharing and interference scenarios. Chapter 4 discusses the interference analysis that is carried out. Finally, in Chapter 5 conclusions are drawn from the results obtained per chapter and recommendations are provided for future work.

IEEE 802.11n

2

In order to reach the goal of this thesis, i.e. measuring and analyzing the interference between co-existing 802.11n and 802.11b/g networks, we must know and understand at least the basics and -for specific cases- deeper detailes of the still not-standardized 802.11n standard. The amandment to the legacy IEEE 802.11 standards offers higher data rates and covers greater distances, while still allowing interoperability with its precursors. This chapter covers the basic concepts and techniques behind the 802.11n standard (see 2.2) and discusses in more detail the elemental features of the standard, e.g. MIMO (see 2.1), Space Time Block Coding (STBC) and spatial mapping (see 2.2.7.2) that make the high data rates possible. In addition, the 802.11n physical layer and the physical layer data packets are discussed in subsections 2.2.1 and 2.2.2 respectively and the frequency band allocation (see 2.2.8) and transmit power mask (see 2.2.9) are covered. Further, a section is devoted to the 802.11n Medium Access Control (MAC) layer to provide a better understanding of how the medium should be used by multiple users simultaneuously. Since every new IEEE 802.11 standard is an amandment to the 802.11 legacy, preknowledge of the older standards would be favourable [13, 14, 15, 16].

2.1 MIMO

Multiple-input multiple-output (MIMO) is a technique using multiple antennas at the transmitter and the receiver enabling spatial diversity - resulting in *diversity gain* - and *multiplexing* to increase data rates. Multiplexing utilizes the multipath character of the channel to send independent data over independent paths. This way MIMO copes with the multipath fading of the channel and takes benefit from it in such way that higher spectral efficiency will be achieved, provided that there is accurate knowledge of the channel at the receiver. Often, a trade-off has to be made between the two techniques: a high transmission rates is obtained by spatial multiplexing and increasing the reliability is done by transmit diversity. Additionally, Inter Symbol Interference (ISI) and interference from other users can be reduced when using the antennas in a smart way. Furthermore *array gain* is also obtained by MIMO which is the increased received SNR resulting from a coherent combining effect of the wireless signals at a receiver. These benefits together contribute to significant performance gains and are discussed in more detail in [20, Chap. 1]. The acquired performance advantages have on the other hand also some added cost. These include costs for the deployment of multiple antennas, their power requirements and their higher complexity.

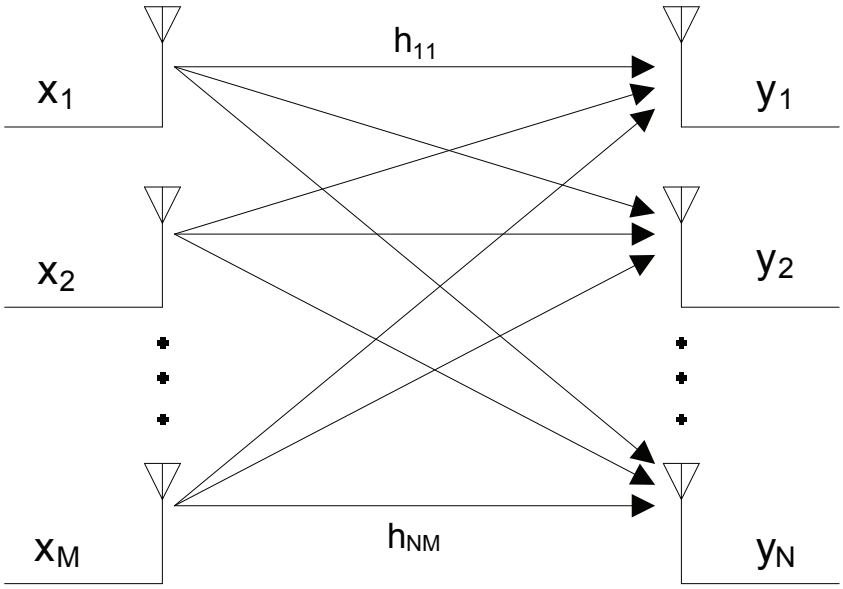

Figure 2.1: MIMO system

2.1.1 Narrowband MIMO Model

Let us consider a narrowband MIMO model, i.e., a narrowband communication system consisting of M transmit and N receive antennas like the one shown in Figure 2.1. A suitable representation of this system is

$$\mathbf{y}=\mathbf{H}\mathbf{x}+\mathbf{n}, \tag{2.1}$$

which in a more specific form is

$$\begin{bmatrix} y_1 \\ \vdots \\ y_N \end{bmatrix} = \begin{bmatrix} h_{11} & \cdots & h_{1M} \\ \vdots & \ddots & \vdots \\ h_{N1} & \cdots & h_{NM} \end{bmatrix} \begin{bmatrix} x_1 \\ \vdots \\ x_M \end{bmatrix} + \begin{bmatrix} n_1 \\ \vdots \\ n_N \end{bmatrix}$$

In this model $\mathbf{y}$ is the received N-dimensional symbol, $\mathbf{x}$ is the M-dimensional transmitted symbol, $\mathbf{H}$ is the $N \times M$ matrix of channel gains h_{ij} representing the gain from transmit antenna j to receive antenna i and $\mathbf{n}$ is the N-dimensional noise vector. The information about the channel which determines the gains in the $\mathbf{H}$-matrix, depends on whether one looks to the channel from the transmitter side or the receiver side, also known as *channel state information* (CSI) at the transmitter (CSIT) or at the receiver (CSIR). For a static channel a pilot sequence can be transmitted to obtain the matrix entries. If there is a return channel, the information at the receiver can be send back to provide the transmitter with knowledge about the channel. When there is no channel information neither at the receiver nor the transmitter, then, in order to fill in the $\mathbf{H}$-matrix, an assumption must be made for the channel distribution, in the common case a zero-mean spatially white model (ZMSW) like is done in [19, Chap. 10]. This model assumes the channel entries to be independent and indentically distributed (i.i.d.) zero-mean, unit-variance, complex circularly symmetric Gaussian random variables.

2.1.2 MIMO Channel Capacity

The multiplexing technique used in MIMO increases channel capacity. This capacity gain obtained from multiple antennas heavily depends on the available channel information at either the receiver or transmitter, the channel SNR, and the correlation between the channel gains on each antenna element. Having a system with only one transmitter and one receiver, a single input single output (SISO) system, results in a channel capacity that can be easily derived from Shannon's channel capacity formula [8], that is

$$C = B \log_2(1 + \gamma|h|^2), \tag{2.2}$$

where γ is the signal to noise ratio at the receiver and h is the gain of the SISO channel. Consequently we know from [19] that the capacity of a MIMO system with M transmit and N receive antennas is

$$C = B \log_2 \det[\mathbf{I}_N + \mathbf{H}\mathbf{R}_\mathbf{x}\mathbf{H}^H] \tag{2.3}$$

where $\det[\cdot]$ is the determinant of a matrix, $\mathbf{R}_\mathbf{x}$ is the covariance matrix of the transmitted vector $\mathbf{x}$ and X^H denotes the conjugate transpose of the matrix X. Depending on the availabilty of CSIT and CSIR the covariance matrix $\mathbf{R}_\mathbf{x}$ can be optimized such way to gain maximum capacity from the channel, because more information on CSIT and CSIR gives more knowledge about the $\mathbf{H}$ matrix. In the next subsection we will see how to decompose the MIMO channel to increase capacity.

2.1.2.1 Parallel Decomposition

In order to increase the capacity of a MIMO system, paralled decomposition of the MIMO channel can be applied where the MIMO channel is decomposed into R parallel independent channels. Multiplexing independent data onto these independent channels, results in an increase of the data rate by a factor R which is called the multiplexing gain. Let us consider again the equation

$$\mathbf{y} = \mathbf{H}\mathbf{x} + \mathbf{n}, \tag{2.4}$$

where $\mathbf{H}$ is the $N \times M$ channel matrix. $\mathbf{H}$ can be converted into R parallel, non-interfering single input single output channels using the singular value decompostion (SVD), i.e.

$$\mathbf{H} = \mathbf{U}\mathbf{\Sigma}\mathbf{V}^\mathbf{H}, \tag{2.5}$$

where $\mathbf{U}$ and $\mathbf{V}$ are unitary $N \times N$ and $M \times M$ matrices, respectively; $\mathbf{\Sigma}$ is a $N \times M$ diagonal matrix with only positive entries. These entries are the singular values σ_i of $\mathbf{H}$ with the property that $\sigma_i = \sqrt{\lambda_i}$ with λ_i the ith largest eigenvalue of $\mathbf{H}\mathbf{H}^\mathbf{H}$. We can

define $\mathbf{\Sigma}$ as

$$\mathbf{\Sigma} = \begin{pmatrix} \sigma_1 & & & & & \\ & \sigma_2 & & \mathbf{0} & & \\ & & \ddots & & & \\ & & & \sigma_{R_H} & & \\ & & & & 0 & \\ & \mathbf{0} & & & & \ddots \\ & & & & & & 0 \end{pmatrix} \tag{2.6}$$

The number of positive singular values of $\mathbf{H}$ is equal to the rank of $\mathbf{H}$ denoted by $R_{\mathbf{H}}$ with the condition $R_{\mathbf{H}} \leq \min(M,N)$ and M and N being the number of transmit and receive antennas respectively. If $\mathbf{H}$ is full rank, then $R_{\mathbf{H}} = \min(M,N)$ which means that the communication takes place in a rich scattering environment, with the presence of multipath. In the absence of multipath, the rank of $\mathbf{H}$ will be rather low and only one major nonzero eigenvalue will be present. Another factor that influences the rank of the $\mathbf{H}$-matrix is the correlation between the MIMO channels. These channels should be uncorrelated in order to have high capacity gain. Correlation between channel gains could lead to $\mathbf{H}$ having only rank 1. In communication systems the parallel decomposition is obtained via transmit precoding and receiver shaping by applying a transformation on the channel input $\mathbf{x}$ and output $\mathbf{y}$, i.e. $\mathbf{x} = \mathbf{V}\widetilde{\mathbf{x}}$ with $\widetilde{\mathbf{x}}$ the input vector and $\mathbf{y}$ multiplied by $\mathbf{U^H}$, resulting in

$$\begin{aligned} \widetilde{\mathbf{y}} &= \mathbf{U}^H(\mathbf{H}\mathbf{x} + \mathbf{n}) \\ &= \mathbf{U}^H(\mathbf{U}\mathbf{\Sigma}\mathbf{V}^H\mathbf{x} + \mathbf{n}) \\ &= \mathbf{U}^H(\mathbf{U}\mathbf{\Sigma}\mathbf{V}^H\mathbf{V}\widetilde{\mathbf{x}} + \mathbf{n}) \\ &= \mathbf{U}^H\mathbf{U}\mathbf{\Sigma}\mathbf{V}^H\mathbf{V}\widetilde{\mathbf{x}} + \mathbf{U}^H\mathbf{n} \\ &= \mathbf{\Sigma}\widetilde{\mathbf{x}} + \widetilde{\mathbf{n}} \end{aligned} \tag{2.7}$$

Here $\widetilde{\mathbf{n}} = \mathbf{U}^H\mathbf{n}$ where $\mathbf{n}$ and $\widetilde{\mathbf{n}}$ are identically distributed. Accordingly, after these transformations the MIMO channel is decomposed into $R_{\mathbf{H}}$ parallel independent channels with the i^{th} channel having input $\widetilde{x}^i$, output $\widetilde{y}^i$ and channel gain σ^i. The parallel decompositions leads to an increase in channel capacity enabling high data rates up to 600 Mbit/s when using a 4x4 MIMO system where there will be $4/times4 = 16$ parallel independent channels.

2.2 802.11n PHY Layer Specifications

As mentioned before the IEEE 802.11n standard hase been in the development stage since 2004 and from that time one draft after another has been approved to continue with the next draft. Currently this process has reached draft 8.0 already and a date for the final version of the standard has not been announced yet. The engineer that wants to do research on the subject is left with a difficult task, because the standard is not yet finished and officialized. In addition, the approved drafts are not even accessible to

everyone. Nevertheless, through some effort and subscribtion at the IEEE society some of the drafts were available and made it possible to have this chapter with the 802.11n specifications be based on draft 4.00 (D4.00) [18]. Since this work focuses on the physical part of the interference (BER's, modulation, coding, etc.), this chapter consideres only the technical specifications of the physical layer of the standard, from here on denoted as PHY.

2.2.1 PHY Interface

In order to provide service to the higher MAC layer, the PHY layer consists of two functions:

- The PHY convergence function that has the task to adapt the capabilities of the Physical Medium Dependent (PMD) system to the PHY service, supported by the Physical Layer Convergence Procedure (PLCP). PLCP is a method that enables the PHY Sublayer service Data Units (PSDU) to be in a framing format, called the PLCP Protocol Data Unit (PPDU) suitable for sending and receiving user data and management information between two or more stations (STA).

- A PMD system whose function defines the charactetistics and method of transmitting and receiving data through a wireless medium between two or more STA's.

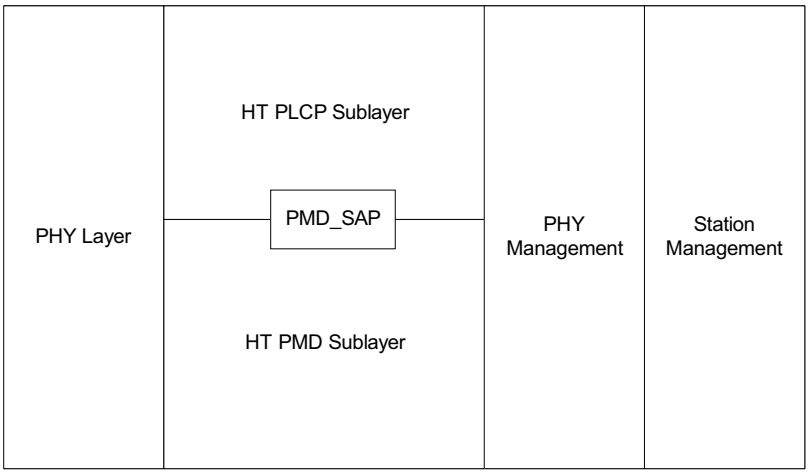

Figure 2.2: PHY layer model [18]

In figure 2.2 these functions are shown within the reference model of the PHY layer. The PMD Service Access Point (SAP) in the middle of the two sublayers is where the interactions between the two are defined. The PHY layer interfaces with the MAC through a TX_ VECTOR containing packet transmit parameters and the RX_ VECTOR with packet receive parameters which are specified in [18, Ch. 20.2].

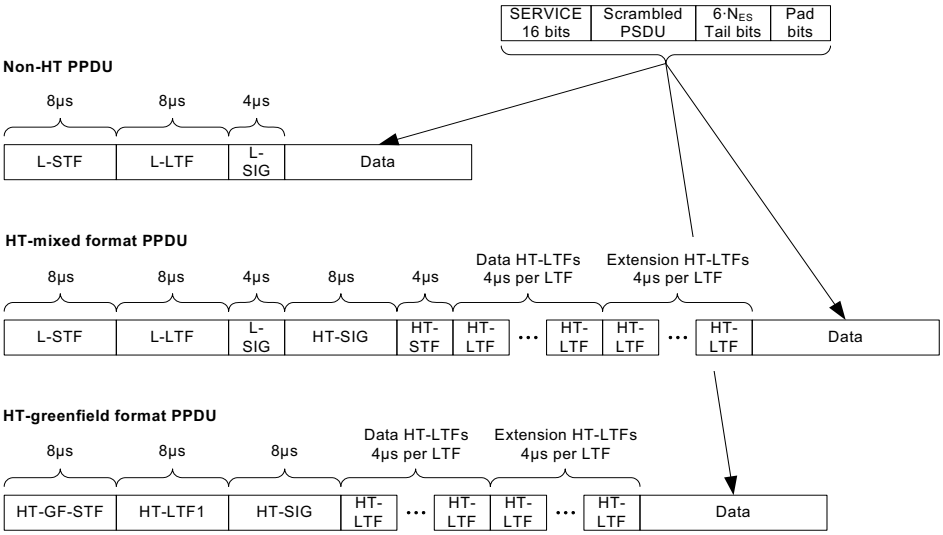

Figure 2.3: PPDU formats [18]

2.2.2 PPDU Formats

As can be seen Figure 2.2, the sublayers are in High Throughput (HT) format. This is the new format introduced in the standard that makes the higher data rates and ranges possible and the form of a PPDU in this format is shown in figure 2.3 together with the PPDU in the legacy format in the figure denoted as 'Non-HT PPDU' where packets are transmitted in the legacy 802.11a/g format defined in [14, Ch. 17] and [16, Ch. 19]. The HT PPDU's have two formats which are the HT Mixed format and HT Greenfield format. In the mixed mode, as indicated by the name, packets of both formats, the legacy and the HT, can be transmitted and received. In the HT Greenfield format only transmission/reception of HT packets are possible and the non-HT packets are not supported. To keep the work manageable, we will only consider the HT Mixed format in this study. The elements within this packet as shown in 2.3 are as follows:

- L-STF: Legacy Short Training Field
- L-LTF: Legacy Long Training Field
- L-SIG: Legacy Signal Field
- HT-SIG: HT Signal Field
- HT-STF: HT Short Training Field
- HT-LTF1: First HT Long Training Field
- HT-LTF's: Additional HT Long Training Fields
- Data: Data field including PSDU

MCS Index	Modulation	R	N_{BPSC}	N_{SD}	N_{SP}	N_{CBPS}	N_{DBPS}	Data Rate (Mbps)	
								800 ns GI	400 ns GI
8	BPSK	1/2	1	108	6	216	108	27.0	30.0
9	QPSK	1/2	2	108	6	432	216	54.0	60.0
10	QPSK	3/4	2	108	6	432	324	81.0	90.0
11	16-QAM	1/2	4	108	6	864	432	108.0	120.0
12	16-QAM	3/4	4	108	6	864	648	162.0	180.0
13	64-QAM	2/3	6	108	6	1296	864	216.0	240.0
14	64-QAM	3/4	6	108	6	1296	972	243.0	270.0
15	64-QAM	5/6	6	108	6	1296	1080	270.0	300.0

Table 2.1: MCS rate dependent parameters for 40 MHz channels and $N_{SS} = 2$

Symbol	Stands for
N_{BPSC}	Number of coded bits per single carrier
N_{CBPS}	Number of coded bits per symbol
N_{CBPSS}	Number of coded bits per symbol per spatial stream
N_{DBPS}	Number of data bits per symbol
N_{SS}	Number of spatial streams
N_{ES}	Number of FEC encoders
N_{STS}	Number of space time streams
N_{TX}	Number of transmit chains
R	Coding Rate
GI	Guard Interval length

Table 2.2: MCS parameters

These elements are discussed in more detail in the subsections that are to follow. Apart from the TX_ VECTOR, also the channel bandwidth (20 MHz or 40 MHz) and the Modulation and Coding Scheme (MCS) parameters define the structure of the transmitted PPDU. MCS is a value determining the modulation, coding and number of spatial streams (SS) used for transmission and is carried in the HT Signal Field. In Table 2.1 a small part of this MCS scheme is depicted for transmission with 40 MHz bandwidth channels and $N_{SS} = 2$, i.e. two spatial streams. The entire MCS scheme can be found in [18, Ch. 20.6]. The table returns a number of parameters that depend on the desired or the maximum achievable data rate determined by the MCS index. What these parameters stand for is denoted in Table 2.2 together with some other frequently used parameters during this chapter. An interesting parameter in these tables is the Guard Interval (GI), an extension to the OFDM symbol length to cope with Inter Symbol Interference (ISI). This parameter can be set to 800ns as in the 802.11a/g standards, but also 400ns to achieve even higher data rates as indicated.

2.2.3 Transmitter Structure

The transmitter used to transmit the HT signals is shown in figure 2.4 in the form of a block diagram with all the building blocks it consists of. The different blocks and their

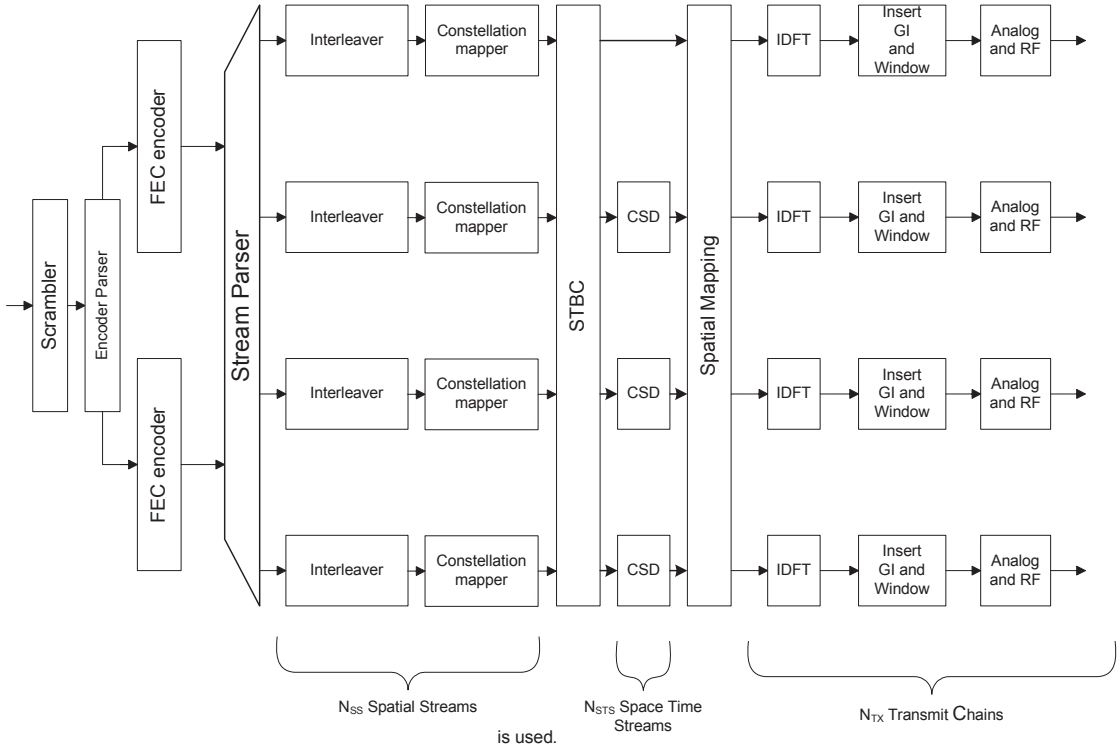

Figure 2.4: Transmitter Block Diagram [18]

functions are briefly discussed here.

- **Scrambler**: Scrambles the data string to prevent long sequences of zeros or ones.
- **Encoder Parser**: De-multiplexes the scrambled bits among N_{ES} FEC encoders. This process is done in a Round Robin manner.
- **FEC Encoders**: Provides error correction by encoding the data through binari convolutional encoders together with a puncturing device or an Low Density Parity Chech (LDPC) encoder
- **Stream Parser**: Divides the output strings of the encoders into N_{SS} spatial streams that will be sent to different interleaver and mapping devices.
- **Interleaver**: Interleaves the bits of each spatial stream by putting them in a different order to enable te correction of long bursty errors.

Parameter	Value	Parameter	Value
N_{SD}: Number of data subcarriers	108	T_{GIS}: Short GI	0.4μs
N_{SP}: Number of pilot subcarriers	6	T_{SYM}: OFDM symbol length	4μs
N_{ST}: Total number of subcarriers	114	T_{SYMS}: Short GI OFDM symbol length	3.6μs
N_{SR}: Number of subcarriers over half the BW	58	T_{L-SIG}	4μs
Δ_F: Subcarrier frequency spacing	312.5 KHz	T_{HT-SIG}	8μs
T_{FFT}: FFT/IFFT period	3.2μs	T_{HT-STF}	4μs
T_{GI}: Guard interval length	0.8μs	$T_{HT-LTF1}$	4μs
T_{GI2}: Double GI	1.6μs	$T_{HT-LTFs}$	4μs

Table 2.3: Timing related constants

- **Constellation Mapper**: Maps the bit sequence from the interleaver of each spatial stream to constellation points dependent on the modulation type (BPSK, QPSK, 16-QAM, 64-QAM).
- **STBC**: Creates STBC codes by spreading the constellation points from N_{SS} spatial streams into N_{STS} space time streams.
- **CSD**: Cyclic shift is inserted to prevent beamforming when similar signals are transmitted in different space time streams.
- **Spatial Mapping**: Maps the space time streams to different transmit chains.
- **IDFT**: The Inverse Discrete Fourier Transform transforms the complex constellation points from the frequency domain to the time domain.
- **GI and Window insertion** Inserting Guard Interval and smoothing the edges of each symbol to increase spectral decay.

Accordingly, on the receiver side the same processes are performed in reverse order.

2.2.4 Transmitted signals: Mathematical Representation

This subsection describes the mathematical form in which the HT signals are transmitted. To do so first a set of constants are defined in Table 2.3 which are used in the signal equations. When transmitted by the 802.11n device the different PPDU fields discussed before are concatenated in the way depicted in Figure 2.5. Each new field starts after

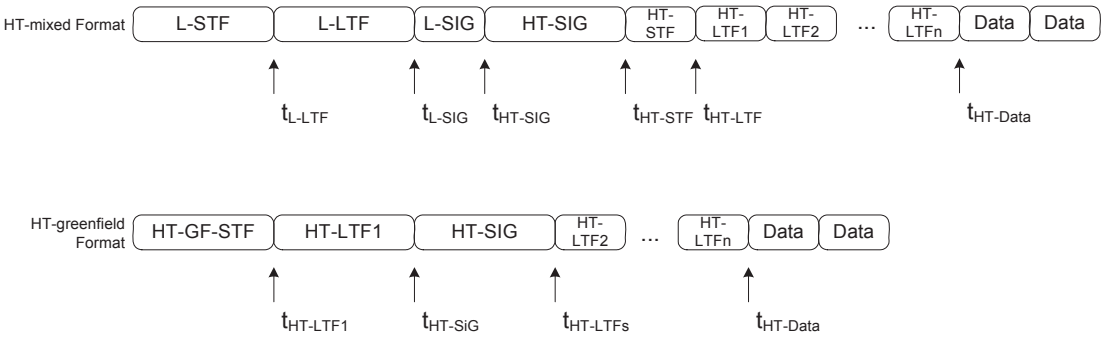

Figure 2.5: PPDU fields in time [18]

time offset t_{Field} The values of t_{Field} can be found in Table 2.3. Consequently the radio frequency (RF) signal that is being transmitted is of the form

$$r_{RF}(t) = \mathrm{Re}\{r(t)e^{j2\pi f_c t}\}, \tag{2.8}$$

where $\mathrm{Re}\{\cdot\}$ stands for the real part of a complex number and f_c is the carrier center frequency. The time dependent function $r(t)$ in this formula exists of the different fields and is for transmit chain i_{TX} given by

$$\begin{aligned} r^{i_{TX}}_{PPDU}(t) = {} & r^{i_{TX}}_{L\_STF}(t) \\ & + r^{i_{TX}}_{L\_LTF}(t - t_{L\_LTF}) \\ & + r^{i_{TX}}_{L\_SIG}(t - t_{L\_SIG}) \\ & + r^{i_{TX}}_{HT\_SIG}(t - t_{HT\_SIG}) \\ & + r^{i_{TX}}_{HT\_STF}(t - t_{HT\_STF}) \\ & + \sum_{i_{LTF}=1}^{N_{LTF}} r^{i_{TX},i_{LTF}}_{HT\_LTF}(t - t_{HT\_LTF} - (i_{LTF}-1)T_{HT_LTFs}) \\ & + r^{i_{TX}}_{HT\_DATA}(t - t_{HT\_DATA}) \end{aligned} \tag{2.9}$$

The time boundaries for the fields indicated by t_{Field} have the same values as their associated time constants with the same indices in Table 2.3. The time domain baseband waveforms in this equation are derived through the discrete Fourier transform according to

$$r^{(i)}_{Field}(t) = \frac{1}{\sqrt{N_{Field}}} w_{T_{Field}}(t) \sum_{k=1}^{K} X^{(i)}_k e^{j2\pi k \Delta_F t}, \tag{2.10}$$

which is a general representation of all fields for the i^{bf} complex number on the k^{th} subcarrier. In this equation $\frac{1}{\sqrt{N_{Field}}}$ implies a scaling factor to ensure that the total power of a field summed over all transmit chains has a maximum of 1 and the values for N_{Field} to reach this for the different fields are stated in table 2.4. Further on in

Field	N_{Field}
L_STF	24
L_LTF	104
L_SIG	104
HT_SIG	104
HT_STF	24
HT_LTF	114
HT_DATA	114

Table 2.4: Scaling factor variable N_{Field} for each field

this chapter we will see that these values equal the number of non-zero elements in the complex OFDM symbol of the concerned field. In (2.10) $w_{T_{Field}}(t)$ is a time windowing function defining the boundaries of each field and Δ_F is the frequency spacing between the subcarriers.

2.2.5 High Throughput Preamle: Short and Long Training Field

The HT-STF and HT-LTF are belonging to the High Throughput packets preamble to realise Automatic Gain Control (AGC) and channel estimation respectively. The HT-STF OFDM symbol is QPSK modulated and is of the form:

$$\begin{aligned} HTSTF_{-58,58} = \sqrt{1/2}\{&0,0,1+j,0,0,0,-1-j,0,0,0,1+j,0,0,0,\\ &-1-j,0,0,0,-1-j,0,0,0,1+j,0,0,0,0,0,0,0,-1-j,0,0,0,-1-j,0,0,0,1+j,\\ &0,0,0,1+j,0,0,0,1+j,0,0,0,1+j,0,0,0,0,0,0,0,0,0,0,0,0,0,0,0,1+j,0,\\ &0,0,-1-j,0,0,0,1+j,0,0,0,-1-j,0,0,0,-1-j,0,0,0,1+j,0,0,0,0,0,0,0,0,\\ &-1-j,0,0,0,-1-j,0,0,0,1+j,0,0,0,1+j,0,0,0,1+j,0,0,0,1+j,0,0\} \end{aligned} \tag{2.11}$$

The factor $\sqrt{1/2}$ serves as normalization factor for the QPSK modulation. This factor is different depending on the type of modulation and ensures that for different mappings, the transmitted signal's average power is still the same. The HT-LTF field is a bit more complicated than the HT-STF field, since the number of HT-LTF fields N_{LTF} is related to the number of space time streams created in the transmitter. N_{LTF} is at least equal to the number of STS NL_{STS}. When STBC is applied even two types of LTF fields exist: a part necessary for the demodulation of the HT-DATA field, called DATA HT-LTFs that are allways present, and a second part of HT-LTFs that are used to examine extra spatial dimensions of the MIMO channel that are not utilized by the HT-DATA field, called Extension HT-LTFs. The total number of HT-LTFs is the sum of the two types

Field Name	**Number of reserved bits**	**Explanation and Interpretation**
Modulation and Coding Scheme	7	Index indicating which MCS from the MCS table is used
CBW 20/40	1	0: 20 MHz Channel 1: 40 MHz Channel
HT Length	16	Number of bytes in the PSDU in the range 0-65535
STBC	2	Set to point the difference between the number of STS, N_{STS} and the number of SS, N_{SS}. Value is '00' if $N_{STS} = N_{SS}$

Table 2.5: HT SIGNAL field bits; bits are transmitted with LSB first

of fields. A BPSK modulated HT-LTF symbol is given by

$$\begin{aligned} HTLTF_{-58,58} = \sqrt{1/2}\{&1,1,-1,-1,1,1,-1,1,-1,1,1,1,1,1,1,\\ &-1,-1,1,1,-1,1,-1,1,1,1,1,1,1,-1,-1,1,1,-1,1,-1,1,-1,-1,-1,-1,-1,1,1,\\ &-1,-1,1,-1,1,-1,1,1,1,1,-1,-1,-1,1,0,0,0,-1,1,1,-1,1,1,-1,-1,1,1,-1,\\ &1,-1,1,1,1,1,1,1,-1,-1,1,1,-1,1,-1,1,1,1,1,1,1,-1,-1,1,1,-1,1,-1,1,\\ &-1,-1,-1,-1,-1,1,1,-1,-1,1,-1,1,-1,1,1,1,1\} \end{aligned} \tag{2.12}$$

Counting the number of non-zero elements in the STF and LTF sequences results in the values for N_{Field} for that specific field in Table 2.4 discussed before. These sequences for the HT-STF and HT-LTF fields in (2.11) and (2.12) respectively with the complex values are have their time domain representations defined through the discrete Fourier transform given in (2.8).

2.2.6 HT Signal Field

The transmitted signals preamble is followed by the HT Signal Field as can be seen in Figure 2.5. This field is used to carry information that is required to recover what is in the HT packet formats. HT-SIG is composed of two parts, HT-SIG1 and HT-SIG2, depicted in Figure 2.6. Each of the two parts consist of 24 bits divided into subparts. Each subpart defines a transmission specific property like the type of modulation used and the occupied channel bandwidth, which could be 20 or 40 MHz. In Table 2.5 the most remarkable fields within the HT-SIG field are discussed. The functions of the other fields are explained in more detail in [18, Ch. 20.3]. Before converting the HT-SIG field into the time domain, the two parts are first encoded, interleaved, mapped and have pilots inserted. Since the code rate $R = 1/2$, a stream of $48 \times 2 = 96$ complex numbers are generated which are subsequently divided into two groups of 48 complex numbers indicated by $d_{k,n}$ where $k = 0, 1, ..., 47$ and $n = 0, 1$.

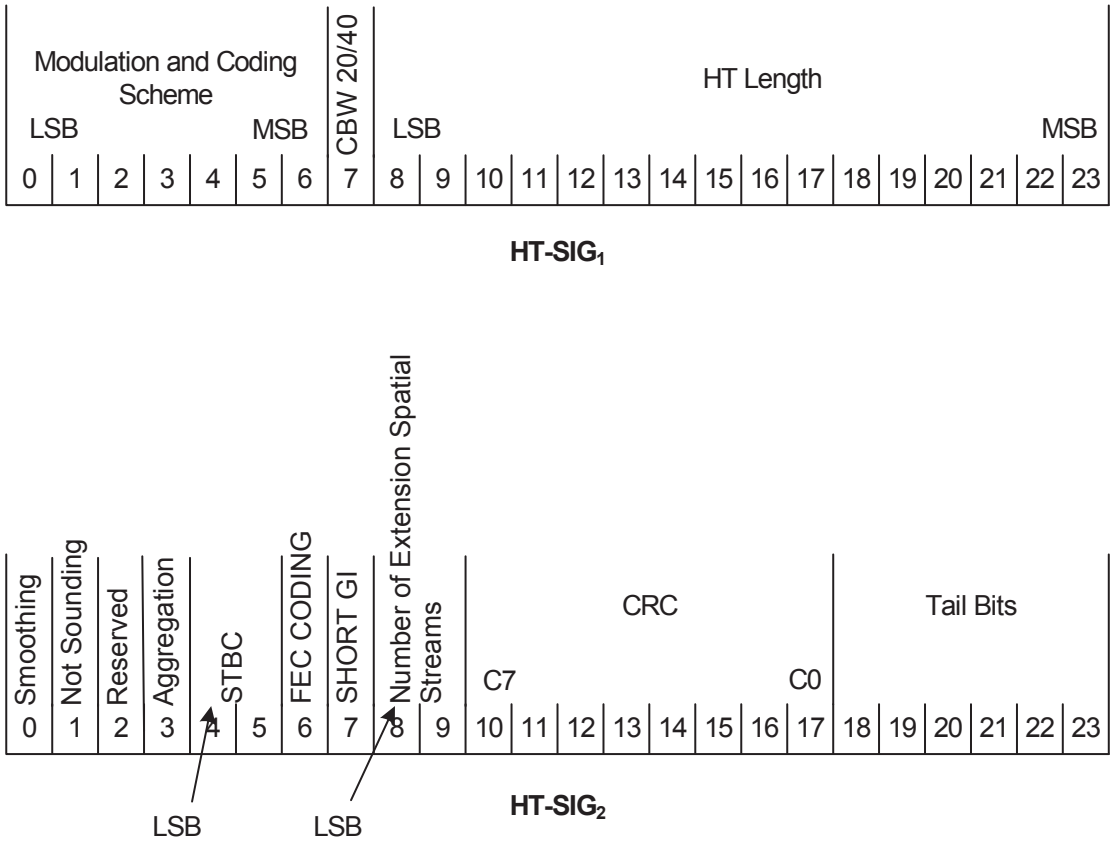

Figure 2.6: HT-SIG1 and HT-SIG2 [18]

2.2.7 HT-DATA Field

The main part of the message, the PSDU, which holds the actual data is enclosed in the DATA Field, that as can be seen from figure 2.5, is transmitted right after the HT-SIG field. Apart from the PSDU, the DATA field also includes the service field, pad bits and tail bits. The number of symbols in the DATA field varies, dependent on the amount of data that has to be sent and can be calculated using:

$$N_{SYM} = m_{STBC} \left\lceil \frac{8 \cdot \text{HT Length} + 16 + 6 \cdot N_{ES}}{m_{STBC} \cdot N_{DBPS}} \right\rceil \tag{2.13}$$

In this formula m_{STBC} can take the values '2' if STBC is used and '1' if not to make sure that the number of symbols is even if STBC is used, HT Length denotes the number of bytes in the PSDU discussed before and $\lceil x \rceil$ denotes the smallest integer greater than or equal to x. The service field, containing 16 all-zero bits, is used to initialize the scrambler that is used to scramble the bits from the DATA field. The six bits appended to the message form the tail bits and are required to return the convolutional encoder to the "zero state". Finally the pad bits added to the message, are to ensure that the length of the message is a multiple of N_{DBPS}. N_{DBPS} is the number of data bits per OFDM

symbol. Thus the amount of "zero" pad bits can be calculated as

$$N_{PAD} = (N_{SYM} \cdot N_{DBPS}) - (16 - 8 \times \text{HT Length} - 16 - 6N_{ES}) \tag{2.14}$$

For coding of the message, the high performing Low-Density Parity-Check (LDPC) codes for advanced channel coding are used. Furthermore puncturing and interleaving of the DATA field and the pilot insertion are performed according to the procedure described in [18, Ch. 20.3.11] and are not discussed here since they are beyond the scope of this work. As soon as the bits from the DATA field leave the interleaver (see Figure 2.4), they shall be mapped onto BPSK, QPSK, 16-QAM or 64-QAM constellation points according to Gray-coded constellations mappings, illustrated in figure 2.7. After the mappings N_{SS} streams of complex numbers exist denoted as $d_{k,l,n}$ where $k = 0, 1, ..., N_{SD}$, $l = 1, ..., N_{SS}$ and $n = 0, 1, ..., N_{SYM} - 1$ that are input to the STBC coder.

2.2.7.1 Space Time Block Coding

In case the number of space time streams, N_{STS} is greater than the number of spatial streams (N_{SS}), it means that STBC coding is applied. This subsection is devoted in how to map the SS streams onto STS streams through STBC coding. First of all the complex numbers in the streams arriving from the constellation mapper are denoted as $d_{k,l,2n}$ and $d_{k,l,2n+1}$ for the $(2n)^{\text{th}}$ and $(2n+1)^{\text{th}}$ OFDM symbol respectively. Then the spatial streams are mapped onto the space time streams according to the table in Figure 2.8. Next, as output of the STBC coder, the complex sequence $\widetilde{d}_{k,i,n}$ is obtained with $k = 0, 1, ..., N_{SD}$, $i = 1, ..., N_{STS}$ and $n = 0, 1, ..., N_{SYM} - 1$. In case the number of STS streams is equal to the number of SS streams, no space time block coding is applied and thus $\widetilde{d}_{k,i,n} = d_{k,l,n}$.

2.2.7.2 OFDM modulation and Spatial Mapping

Having obtained the several STS streams containing sequences of modulated complex numbers and after pilot insertion, the only thing that remains is to map the different STS streams onto the transmit chains and to transform the complex data sequence to a time domain signal following:

$$\begin{aligned} r_{Field}^{i_{TX}} =& \frac{1}{\sqrt{N_{STS} \cdot N_{Field}}} w_{T_{Field}}(t) \\ & \times \left\{ \sum_{k=-N_{SR}}^{N_{SR}} \sum_{i_{STS}=1}^{N_{STS}} [Q_k]_{i_{TX}, i_{STS}} X_k^{i_{STS}} e^{j2\pi k \Delta_F (t - T_{CS}^{i_{STS}})} \right\} \end{aligned} \tag{2.15}$$

In this formula $[Q_k]_{i_{TX}, i_{STS}}$ represents the element in the $(i_{TX})^{\text{th}}$ row and $(i_{STS})^{\text{th}}$ column of the $N_{TX} \times N_{STS}$ mapping matrix Q_k and T_{CS} is the cyclic shift period discussed before to prevent undesired beamforming. Q_k can be defined such that it can be applied for spatial mapping, where $Q_k = \mathbf{I}$ is the identity matrix. Q_k can be set to enable spatial expansion, for which $N_{STS} < N_{TX}$. In this case some of the STS streams are duplicated to form the signals on the transmit chains. Anothher option for Q_k is to enable beamforming for which knowledge about the channel at the receiver is essential.

These mapping methods together with the possible mapping matrices Q_k are described in more detail in [18, Ch. 20.3.11-12].

2.2.8 Channel Allocation: 2.4 GHz band and 5 GHz band

One of the demands for the new 802.11n standard is that it has to support operation in the 2.4 GHz band also, together with the operation in the 5 GHz band for which it is actually designed for. In the 2.4 GHz band 13 channels are available where the centre frequencies of each channel are spaced 5 MHz apart from each other implying there is room for 3 non-overlapping channels in the entire band. This gives the next relation between centre frequency f_{c_n} and channel number n:

$$f_{c_n} = 2407 + 5 \cdot n(MHz), \tag{2.16}$$

where $n = 1, 2, ..., 13$. However, since transmission is done through 40 MHz channels, only 2 non-overlapping channels are available in the 2.4 GHz band and operation in the 5 GHz band seems to offer more possibilities and space with respect to frequency availability. In the 5 GHz band the first centre frequency starts at 5000 MHz and this band provides frequency space for up to 200 channels all spaced 5 MHz apart. As a result the channel centre frequencies are given by

$$f_{c_n} = 5000 + 5 \cdot n(MHz), \tag{2.17}$$

where $n = 1, 2, ..., 200$. More than 20 non-overlapping channels are possible within this band.

2.2.9 Maximum Transmit Power and Transmit Spectrum Mask

The 802.11n standard has a maximum allowable output power that is the same as for the 802.11a/g standards, i.e. 100mW (in Europe). This means that in case multiple transmit chains are active, their total power should not exceed this limit. The transmit spectrum defined by the developers of the standard to stay within the spectrum regulations is illustrated in figure 2.9 for 40 MHz channels.

2.3 802.11n MAC Layer

Within the framework of interference, we need to understand how the wireless medium is shared in networks. The exact rules and specifications of how this works are defined in the 802.11n MAC specifications [18]. In this section we provide some main parts of these specifications and those parts that are of most interest to our work, e.g., multiple access protocols and medium sharing protocols, like CSMA and RTS/CTS mechanisms.

2.3.1 MAC functionality

The MAC layer has the important functions of association and re-association of a STA to an access point (AP) and roaming between different APs. Further, it controls authentication mechanisms, encryption, synchronization of STAs with regard to an AP

and power management. To provide multiple access the 802.11n MAC sublayer supports both the distributed coordination function (DCF) as the point coordinatio function (PCF). In addition to the older standars, also the hybrid coordination function (HCF) is supported. Allthough the three mechanisms are supported, the basic medium access protocol remains DCF in the 802.11n standard [13, 18]. Therefor we will only expain the functionality of the DCF mechanism.

2.3.2 DCF

The distributed coordination function offers asynchronous service based on the carrier sense multiple access with collision avoidance (CSMA/CA) mechanism in addition of a rondom backoff time. The operation of this mechanism with multiple STAs is illustrated in Figure 2.10. DIFS stands for DCF inter-frame spacing and denotes the mimimum waiting time before a STA can transmit its data. Before a STA transmits after having waited the DIFS period, it has to ensure that the medium is not used for a contention period that is based on a radom number generated by each STA each time it contends for the medium. The STA with the shortes contention period, is allowed to use the medium. Other STAs defer and have to go through the same process again. In case of unicast transmission within the CSMA/CA mechanism, the situation will be different as illustrated in Figure 2.11. Now the reception of a package is acknowledged by the receiver through an acknowledgement (ACK) and STAs need to wait for a short inter-frame spacing (SIFS) length in order to send short control messages, such as ACKs. So far we discussed the operation when all STAs in a service area can 'hear' each other.

When so called hidden nodes are foresoon, the network administrator can select an optional RTS/CTS mechanism, which is a virtual carrier sense mechanism that makes use of request to send (RTS) and clear to send (CTS) control packets. An RTS packet includes information containing the receiver of the data and the duration of the transmission time. This transmission duration is stored in each nodes net allocation vector (NAV) that receives the RTS and suchwise every node in the network knows for how long the medium will be busy. After receiving an RTS, the receiver transmits a CTS to inform the node that requested service from the medium that it can transmit and to inform all other nodes that the medium will be busy for a certain time interval. This operation is depicted in figure 2.12

2.4 Summary

From this chapter we understand how MIMO technique is used to increase data rates and ensure reliable data transfer through multiplexing and spatial diversity respectively. These properties are implemented in the 802.11n standard using space time block codes and spatial division multiplexing that decompose the transmission channel into parallel independent channels. The use of OFDM modulation ensures efficient use of the frequency spectrum. Through 64-QAM baseband modulation, a coding rate $R_c = 5/6$ and a short guard interval of 400ns, PHY layer data rates of 300 Mbit/s are achieved. Besides support of operation in the 2.4 GHz band, also operation in the 5 GHz band

is supported providing frequency bandwidth for more than 20 non-overlapping 40 MHz communication channels.

Further, we saw that the MAC ensures, through a carrier sense mechanism or an RTS/CTS mechanism, that stations within a certain range do not transmit when another station is transmitting, thus limiting interference caused by two stations transmitting at the same time.

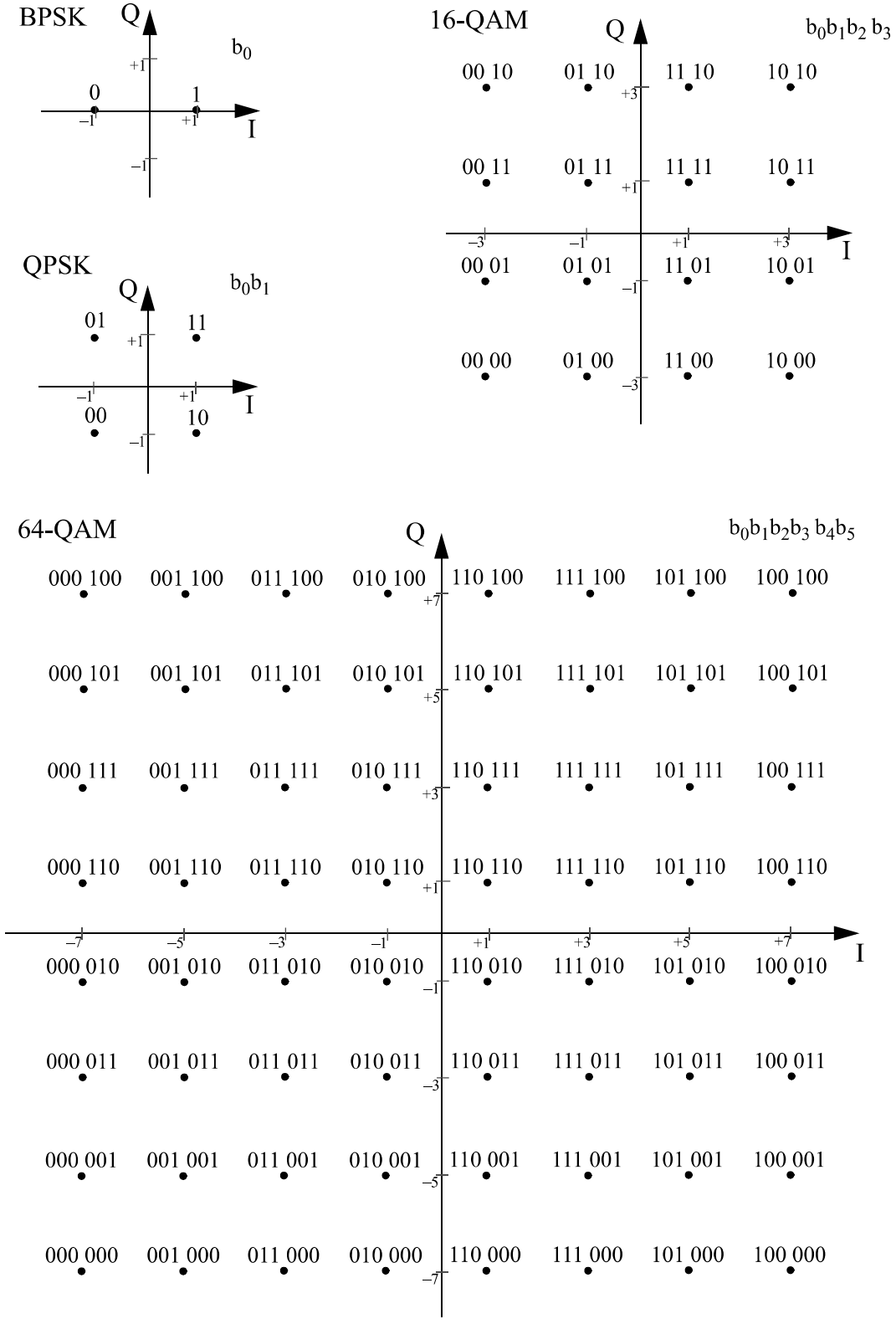

Figure 2.7: Gray-coded BPSK, QPSK, 16-QAM and 64-QAM constellation mappings [14]

N_{STS}	HT-SIG MCS field (bits 0-6 in HT-SIG$_1$)	N_{SS}	HT-SIG STBC field (bits 4–5 in HT-SIG$_2$)	i_{STS}	$\tilde{d}_{k,\,i,\,2m}$	$\tilde{d}_{k,\,i,\,2m+1}$
2	0-7	1	1	1	$d_{k,\,1,\,2m}$	$d_{k,\,1,\,2m+1}$
				2	$-d^{*}_{k,\,1,\,2m+1}$	$d^{*}_{k,\,1,\,2m}$
3	8-15, 33-38	2	1	1	$d_{k,\,1,\,2m}$	$d_{k,\,1,\,2m+1}$
				2	$-d^{*}_{k,\,1,\,2m+1}$	$d^{*}_{k,\,1,\,2m}$
				3	$d_{k,\,2,\,2m}$	$d_{k,\,2,\,2m+1}$
4	8-15	2	2	1	$d_{k,\,1,\,2m}$	$d_{k,\,1,\,2m+1}$
				2	$-d^{*}_{k,\,1,\,2m+1}$	$d^{*}_{k,\,1,\,2m}$
				3	$d_{k,\,2,\,2m}$	$d_{k,\,2,\,2m+1}$
				4	$-d^{*}_{k,\,2,\,2m+1}$	$d^{*}_{k,\,2,\,2m}$
4	16-23, 39, 41, 43, 46, 48, 50	3	1	1	$d_{k,\,1,\,2m}$	$d_{k,\,1,\,2m+1}$
				2	$-d^{*}_{k,\,1,\,2m+1}$	$d^{*}_{k,\,1,\,2m}$
				3	$d_{k,\,2,\,2m}$	$d_{k,\,2,\,2m+1}$
				4	$d_{k,\,3,\,2m}$	$d_{k,\,3,\,2m+1}$

Figure 2.8: STBC: mapping SS onto STS [18]

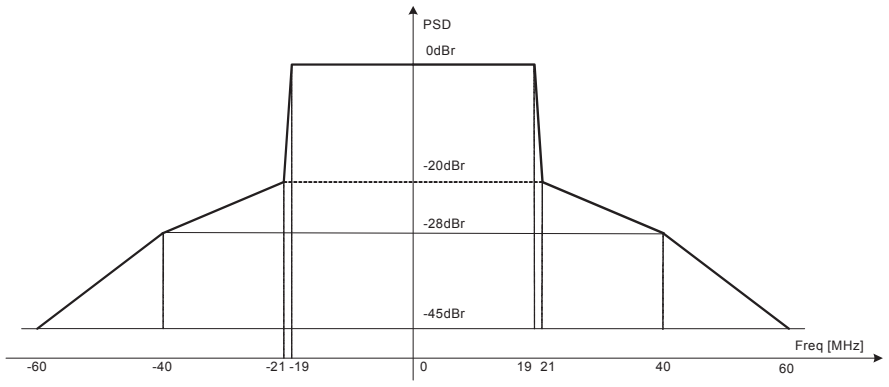

Figure 2.9: Transmit spectral mask for a 40 MHz operating channel [18]

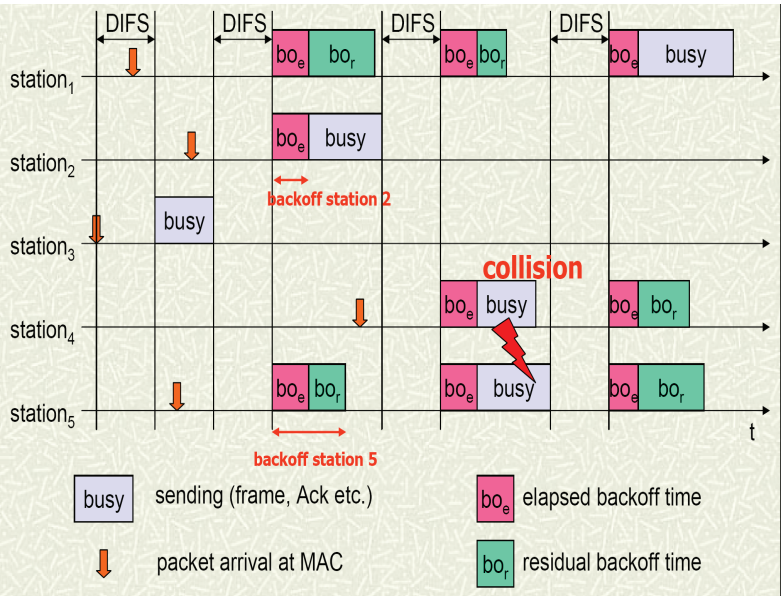

Figure 2.10: CSMA/CA operation with five STAs [34]

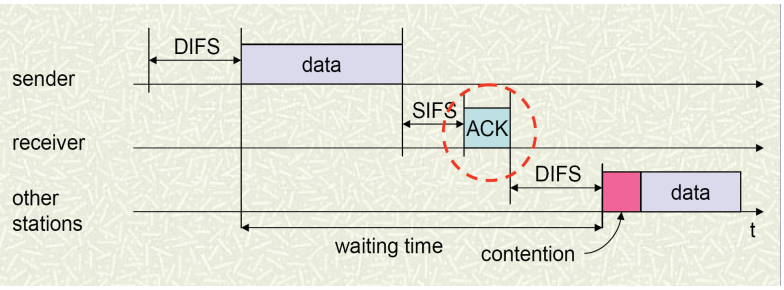

Figure 2.11: CSMA/CA operation for unicast data transfer [34]

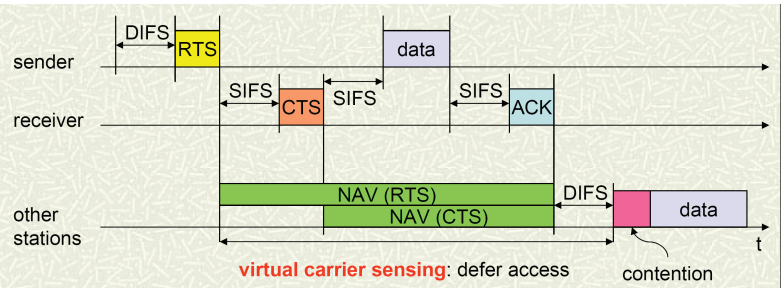

Figure 2.12: RTS/CTS mechanism [34]

3 Measurement Results

The new IEEE 802.11n standard supports operation in the license free 2.4 GHz frequency band. A disadvantage of this property is that the 2.4 GHz band is already very crowded due to the occupancy of IEEE 802.11b/g WLAN's, dect telephones, microwave ovens, bluetooth devices, etc. From the theoretical point of view (Chapter 4), we know that operation of these devices on the same frequency channels will force them to share the medium. Simply because of the fact that there is a limited number of non-overlapping channels. In this chapter we discuss the results obtained from measurements performed during real life medium sharing scenarios. In particular we focus on 802.11n networks when the medium has to be shared with other 802.11b/g/n networks. The throughput and the packet loss rate of transfers in networks is measured in the abscence and presence of another nearby located network to perceive the effect of medium sharing on them. New 802.11n devices are used in the form of routers and wireless adapters. Accomplishing this phase enables us to compare the obtained results with the interference analysis discussed in the next chapter. The first section gives on overview of the measurement locations and the various devices used with their specifications. Apart from having different measurement spots, also single transfers and multiple transfers simultaneously have to be distinguished. Multiple transfers have proved to reach much higher data rates than single transfers which we will explain further on in this chapter.

3.1 Measurements Overview

3.1.1 Locations

The measurements are performed in an office environment - a *KPN* building, called *TP6*, from here on referred to as KPN - and a home environment, i.e. an appartement on the 6th floor of a flat, from here on referred to as HOME . The different locations mean different electro magnetic properties that an EM signal is induced to resulting in different behaviours of the signals. A third place where measurements took place is an anechoic chamber at the 22nd floor of the EWI faculty of the TU Delft at *Ducat*, a division of the *IRCTR* group. Different measurement setups are used to measure the transfer throughputs for all kind of scenarios.

3.1.2 Measurement devices and Tools

In order to set up different interference scenarios and to measure different aspects indicating interference (e.g. throughput, PLR), we equipped ourselves with new 802.11n devices and already existing 802.11b/g devices. These are summed up in Table 3.1 together with relevant technical specifications. When this project started these were the routers and access points available with the 802.11n standard integrated based on draft

Device Name	**AP/STA**	**P_{TX} dBm**	**Nr. of** Antennas	**Chipset**	**Ethernet** Port
Linksys WAP4400N	AP	16	3	Marvel	Gigabit
Linksys WPC4400N	STA	16	2	Marvel	NA
Linksys WUSB300N	STA	14	2	Marvel	NA
Sitecom WL-183	AP	18	3	Ralink	100 Mbit
Sitecom WL-312	AP	18	2	Ralink	100 Mbit
Sitecom WL-182	STA	17	2	Ralink	NA
Sitecom WL-302	STA	17	2	Ralink	NA
Sweex LW300	AP	16	3	Ralink	100 Mbit
Sweex LW303	STA	14	2	Ralink	NA
Speedtouch 780i WL	AP	16	1	NA	100 Mbit

Table 3.1: Used networking devices with specifications. AP and STA stand for Access Point and wireless Station respectively.

2.0. Some of the specifications like the transmit power P_{TX} are needed later in this chapter. Besides the access points (AP) and wireless stations (STA) also computer

Name	Processor	RAM	Refer name
Acer Travelmate 8000	Intel Pentium M 1.6GHz	512 MB DDR	NB1
HP Pavillion ze5700	Mobile Intel P4 3.06GHz	512 MB DDR	NB2
Acer Aspire 9800	Intel Pentium M 1.73GHz	1024 MB DDR2	NB3
Acer Aspire 5020	AMD Turion 64ML-34 1.8 GHz	512 MB DDR	NB4
HP Desktop	Intel Pentium 4 2.93 GHz	1024 MB DDR2	DT1

Table 3.2: Different notebooks used with their specifications and how they are referred to.

hardware was needed, e.g. notebooks and desktop computers to provide the APs and STAs with data to transmit and receive wirelessly. These are denoted in Table 3.2 where also their processor type and RAM memory are specified. To be able to 'see' operation in the 2.4 GHz band which is the operation frequency band of the Access Points (AP) and wireless Stations (STA), we use a 2.4 GHz channel visualizing tool called *Chanalyzer 2.1.* This tool provides a real-time visualization of the 2.4 GHz frequency band, which is actually a frequency spectrum analyzer, that helps us to observe the operation in the 2.4 GHz band. A snapshot of this tool is illustrated in Figure 3.1. The signal amplitudes given in Figure 3.1 are measured by the aid of a 2.4 GHz spectrum analyzer, called *Wi-Spy v1* (Figure 3.2). This device is connected to the computer through a USB port and provides the *Chanalyzer* with the information it needs, i.e., the power of any EM signal per hertz in the 2.4 GHz band. In order to measure the throughput of transfers within a network a bandwidth monitoring tool called *Bandwidth Monitor* is used. As the name indicates, this tool monitors bandwidth usages of the computer it is installed on. Real-time downloads and uploads are displayed in ghraphical and numerical representations. A snapshot of this tool during an arbitrary transfer is shown in Figure 3.3.

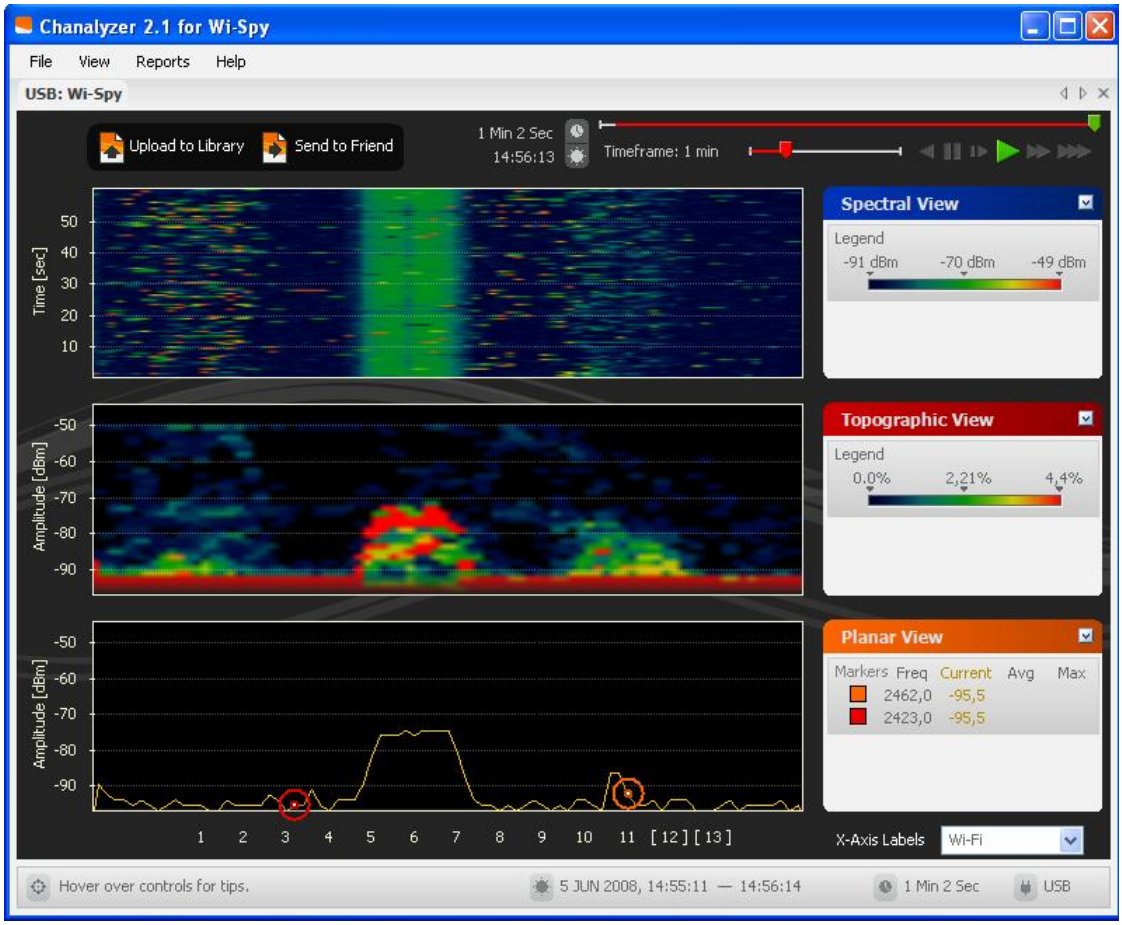

Figure 3.1: *Chanalyzer 2.1* snapshot showing the frequency spectrum of the 2.4 GHz channel

Figure 3.2: *Wi-Spy v1* USB dongle spectrum analyzer [4]

In order to obtain information about the performance during transfers, a tool called *Iperf* [3] is used. This tool gives back the number of packets lost, against the total number

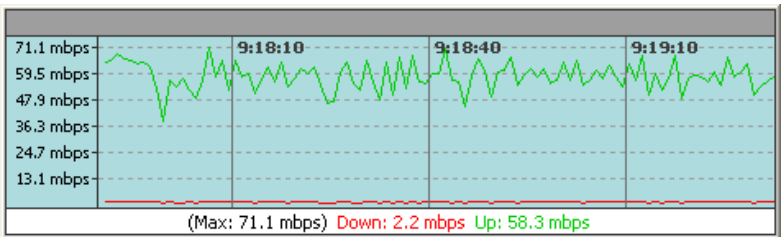

Figure 3.3: Snapshot of *Bandwidth Monitor* during a transfer

of packets supplied during a session. In fact, the packet loss ratio (PLR) is measured. Unfortunately, when we began our measurements, we believed that we were measuring the BER, but we dismissed that after our analysis, since *Iperf* counts the packet loss at the transport layer and bit errors should be measured at the PHY layer. Furthermore, we have to note that the origin of the packet losses is unknown. This might be due to e.g., collisions, signal degradation, noise, network routing or oversaturated links.

3.2 Throughput

When starting the measurements, first some scenarios were considered to gain an idea of the operation of the 802.11n standard in actual practice. The scenarios contained STA to STA transfers, AP to STA transfers and other relevant setups while measuring the transfer rates. These sceanarios are described in Appendix A together with their results.

3.2.1 Data rate or Throughput?

Data rate and throughput are terms to define the communication speed in a network. Often the terms are confused. The data rate is the physical data rate achieved at the physical layer of the OSI model. Due to overhead introduced by the higher layers, this maximum achieveble data rate reduces to a lower rate. At the transport layer, due to the operation of the TCP protocol [24], bandwidth is lost because of retransmissions and flow control resulting in lower transfer rates. The transfer rate that is achieved after all the error recovery mechanisms is called throughput. During the measurements data is transmitted through computers that operate under the operating system *MS Windows XP* where the TCP protocol is used. This means that we measure the throughput of a transfer and not the data rate.

3.2.2 Throughput with Interference

The throughput of transfers in networks is monitored while considering different scenarios. Distinction is made between 802.11b, 802.11g and 802.11n networks. The first measurements took place in Room 1 at KPN . A topographic view of the measurement spots at KPN is provided in Figure A.7. The APs and STAs of the two interfering networks are positioned as illustrated in Figure 3.5 where two different setups are considered. The networks are named NW1 and NW2 respectively and consist of

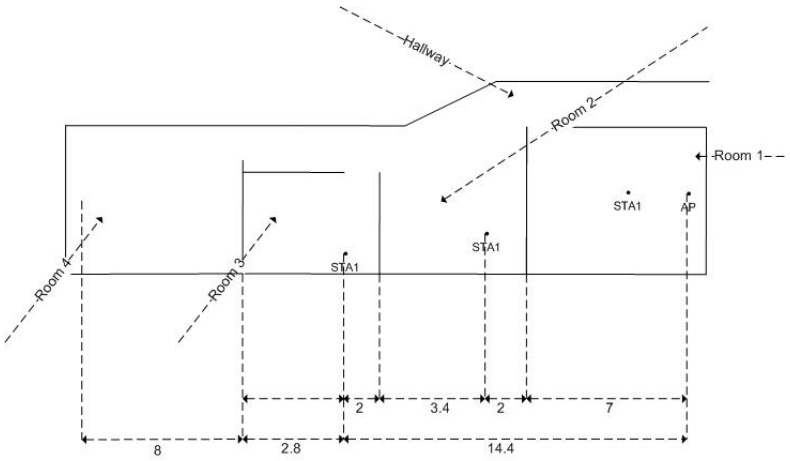

Figure 3.4: Geometry and dimensions in meters of the measurement spot at the KPN building.

- NW1: DT1 connected to Sweex LW300 as AP1 and Sweex LW303 connected to NB3 as STA1
- NW2: NB1 connected to Linksys WAP4400N as AP2 and Linksys WPC4400N connected to NB4 as STA2

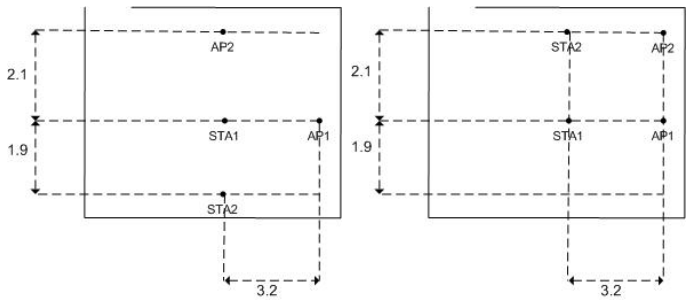

(a) Setup 1 (b) Setup 2

Figure 3.5: Measurement setups for monitoring the throughputs in two 802.11n networks in Room 1 (see Figure A.7)

The typical interference scenario is depicted in Figure 3.6, where we can see that two networks, NW1 and NW2, consisting of respectively AP1, STA1 and AP2, STA2, simultaneously make use of the wireless channel. The measurements are performed the following way. First data is transferred over NW1 for a time period of approximately 60 seconds while the throughput is being monitored. After this period simultaneously a second transfer will start at NW2 while the other transfer at NW1 is still taking place. At the same time the throughputs over both networks are being measured. This measurement is repeated five times and accordingly the 'reversed' process is also done: first sending data over NW2 and after approximately 60 seconds simultaneously start a transfer at NW1 while monitoring the throughputs of both networks and repeating

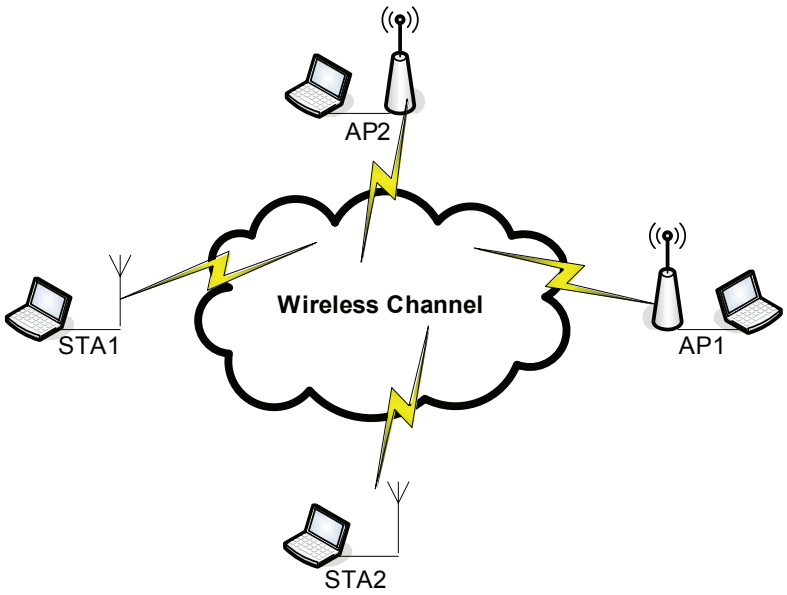

Figure 3.6: Typical Interference Scenario of two networks operating through the same wireless channel. NW1 consists of AP1 and STA1, NW2 consists of AP2 and STA2.

this for five times again. The transfers over both networks will have impact on the throughputs of each network and by processing the affected throughputs, something can be said about the interference between the networks in terms of throughput. These interference measurements are performed for two different setups depicted in Figure 3.5(a) and Figure 3.5(b). Measurements for the setup in Figure 3.5(b) are repeated, only with AP2 being Linksys WUSB300N in order to see its performance dissimilarities with respect to the WPC4400N adapter.

Figure 3.7 illustrates the resulting throughputs for the measurements using the first setup (Figure 3.5(a)). The plot of the throughput, indicated by R, is an average of the throughput values of 5 measurements. One can clearly see that immediately after the start of a second transfer at the other network the throughput of the already running transfer at the first network is affected and decreases as expected, because both networks operate at channel 13 of the WIFI band and need to share the available bandwidth. Clearly, the bandwidth is not equally divided among the two networks. Further, we should note that the sum of the throughputs of both networks equals the throughput when a single network operates.

Also remarkable is that NW2 remains transferring at a higher throughput than NW1 when the medium has to be shared with NW1. In fact, even when there is a transfer taking place at NW1 and at the same time a transfer starts at NW2, the throughput of the transfer in NW1 is almost entirely suppressed by the transfer of NW2. Obviously, NW2 uses the available bandwidth at channel 13 in a disproportional way. This appearance is due to some possible reasons, e.g. the AP and STA in NW2 are placed closer together than the one in NW1 or the antennas of LINKSYS AP and STA radiate with higher signal power. Searching for the reason, we tried to rearrange the positions of the networks with respect to each other and obtained the setup depicted in Figure 3.5(b). Again

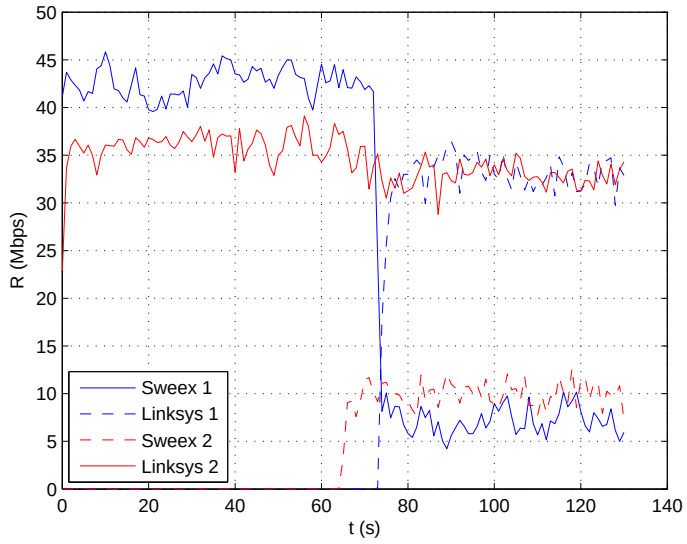

Figure 3.7: Average network throughputs measured for the setup in Figure 3.5(a) of NW1 and NW2 with no interference in the first 60 seconds and with interference over the last 60 seconds

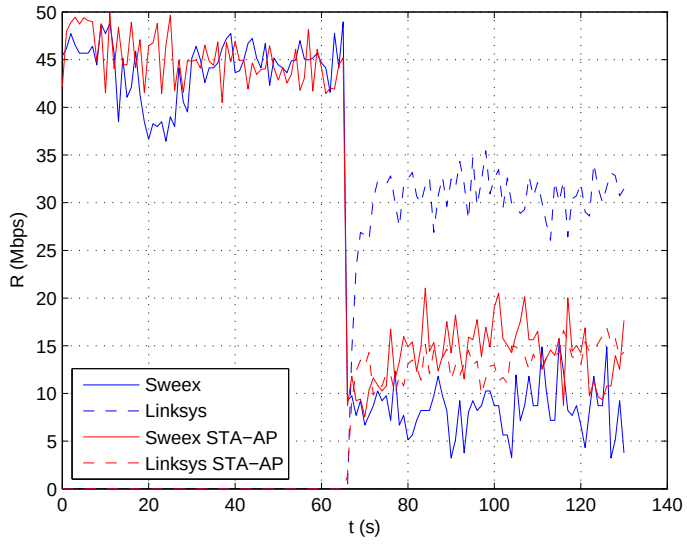

Figure 3.8: Average network throughputs measured for the setup in Figure 3.5(b) of NW1 and NW2 with no interference in the first 60 seconds and with interference over the last 60 seconds

we observe in 3.8 the same results as the previous setup, i.e., the throughput of both networks is affected and NW1 suffers more from medium sharing than NW2. Accordingly, the geometry of the measurement setup is not the reason for the unequal division of the available bandwidth. Looking at Table 3.1, we can see that the technical specifications of the APs of both networks are the same. However, STA1 in NW1 transmits with a lower

signal power than STA2 in NW2 and this might be the reason for the lower throughputs in NW1. In figure 3.9, the results are plotted of measurements, while using the LINKSYS WUSB300N USB dongle as STA2 in NW2. The results are very disappointing compared to the WPC4400N, most likely because of the lower transmit power of this device (see 3.1). In this case NW1 dominates the use of the available bandwidth. The maximum

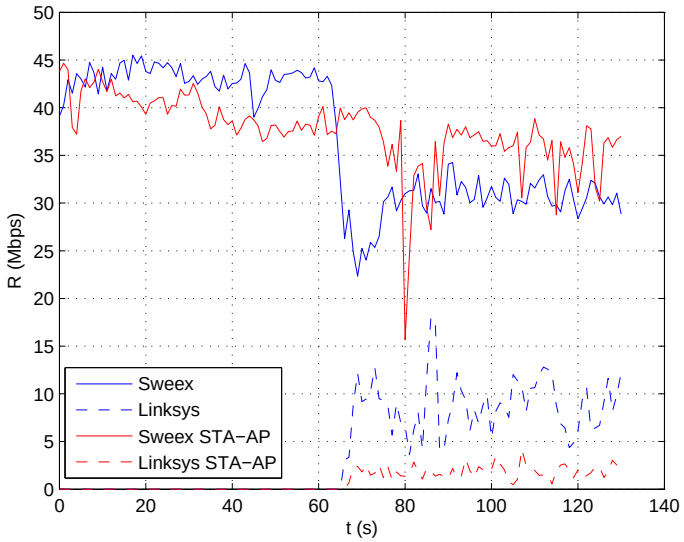

Figure 3.9: Average network throughputs measured for the setup in Figure 3.5(a) of NW1 and NW2 with no interference in the first 60 seconds and with interference over the last 60 seconds

throughput in all the graphs this far is 50 Mbit/s, while we expect at least throughput of half the maximum data rate, i.e., 150 Mbit/s. In the next section we will see how to obtain these higher throughputs.

3.3 Throughput Multiple Transfers

Somewhere in the middle of the measurement phase, a significant difference in the throughput was discovered, when transferring multiple files simultaneously. Much higher throughputs were achieved (A.16). Immediately the thoughts went to the TCP/IP protocol of the transport layer in the OSI model ([24]), that might put a boundary on the maximum transfer throughput at the physical layer by parameters such as the **Maximum Transfer Unit** (MTU) and the **TCP window size** ([24, 2]). Appendix A covers this issue and discusses the results of different scenarios related to the multiple transfers. In this section we will consider again interference scenarios, allthough this time we focus on multiple transfers simultaneously in a network.

3.3.1 KPN Office Environment

Also for multiple transfers different interference scenarios have been considered at KPN . So far we have seen that due to medium sharing the throughput of transfers within

a network decreases, but the some of the throughputs of each network equals approximately the maximum throughput provided by the medium. In this section the results for the throughput are discussed of medium sharing networks operating at their maximum capacity by means of multiple transfers. Also some methods are presented to reduce the effect of interference as much as possible by adjusting transmit powers or placing networks further away from each other.

3.3.1.1 Two Sitecom 802.11n networks

Throughputs are measured of transfers in a network while another transfer starts in a second network in an adjacent room. The two networks are referred to as NW1 and NW2 and they exist of the following:

- NW1: HP desktop connected to Sitecom 300N WL-312 as AP1 and Sitecom 300N WL-302 USB in NB3 as STA1 in Room 1
- NW2: NB1 connected to Sitecom 300N WL-183 as AP2 and Sitecom 300N WL-182 USB in NB4 as STA2 in Room 2

Three scenarios are tested, each of them having different WIFI channel occupations for NW2 while NW1 remains operating at WIFI channel 13. First three transfers are initiated at NW1 and at $t = 30$ s, NW2 starts transmitting with a single transfer and in the interval $30 < t < 40$ s, the second and third transfer in NW2 are also initiated. In Figure 3.10 we see the results for the scenario where the networks operate at two non-overlapping channels, i.e. 13 and 1 and the results are clear: there is no frequency overlap, thus no need to share the medium and no decrease in transfer throughput.

Figure 3.11 shows different and more disturbing results. NW2 now operates at channel 6 and when both networks simultaneously use the channel the throughputs drop dramatically, that is at least of one network.

The results of the third scenario where both networks operate at channel 13 are depicted in figure 3.12 and similar conlusions can be made as the second scenario, namely that due to the MAC mechanism NW1 and NW2 have to share the medium. We should note that in each plot, from $30 < t < 40$ seconds, we observe a sudden change in throughput which is caused by the start of a second and third file transfer performed during that interval. The reason that the available bandwidth is unequally distributed among the networks and NW2 consumes an over-proportional part of the bandwidth is because of the three antennas used in AP2 in NW2 in stead of two antennas used in AP1 in NW1. The three antennas in AP2 enable the network to transfer at higher throughputs than the other network. Further, we observe that the sum of the throughputs of both networks in case they share the medium, is $20.9 + 62.6 = 83.5$, which approximately equals the throughput of a single network when there is no sharing, indicating that the physical medium, that is, the channel, still provides the maximum achievable throughput. Since two networks contend for the use of the medium, the throughput has to be shared. This sharing of the medium is controlled by the MAC layer and the rules defined in the specifications of the MAC entity (Section 2.3) which ensures that the medium can only be used if the medium is free.

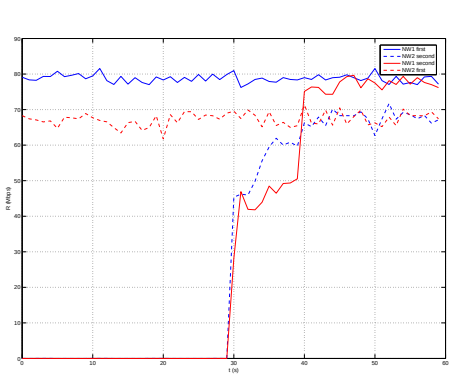

(a) Throughput

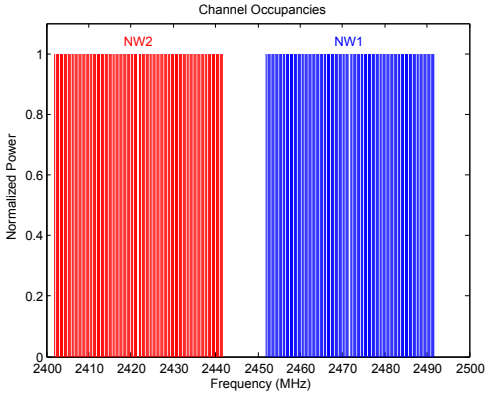

(b) NW1 Channel 13; NW2 Channel 1

Figure 3.10: Average network throughputs of interfering NW1 and NW2, occuping respectively channel 13 and 1 (see (b)).

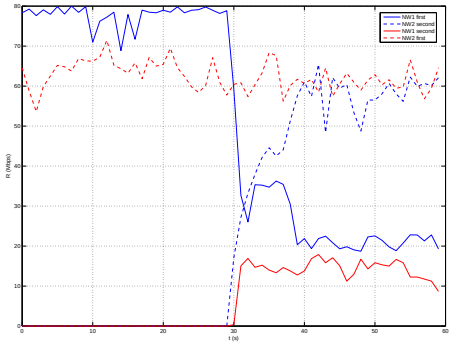

(a) Throughput

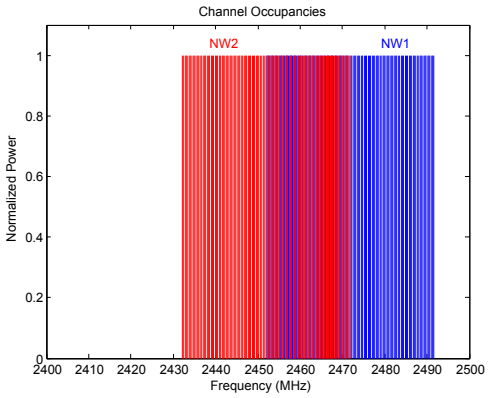

(b) NW1 Channel 13; NW2 Channel 6

Figure 3.11: Average network throughputs of interfering NW1 and NW2, occuping respectively channel 13 and 6 (see (b)). Throughput values of NW1 drop from a mean of 77.8 to 25.5 while NW2 starts transfering at a mean of 52.2. And NW2 values drop from a mean of 63.7 to 61.2 while NW1 transfers at a mean of 13.9. Values are in Mbit/s.

In order to get a better idea of how the throughput within NW1 and NW2 is affected, we define an expression for the performance of the networks in terms of throughput. Let us define the performance μ of a network as the ratio of the mean throughput in the presence of interference, $\widetilde{E}_{xy}$, to the mean throughput for transfers without interference, E_{xy}, where x and y can be n, g or b which represent respectively an 802.11n, 802.11g or 802.11b network. Then the performance of NW1 can be calculated as $\mu_1 = \widetilde{E}_{n_1n_2}/E_{n_1n_2} = 20.9/77.8 = 0.27$. Accordingly, the performance of NW2 will be $\mu_2 = \widetilde{E}_{n_2n_1}/E_{n_2n_1} = 57.9/67.3 = 0.86$. μ_1 tells us that medium sharing causes that NW1 only reaches to 27% of its normally achieved throughput. Likewise NW2 obtain

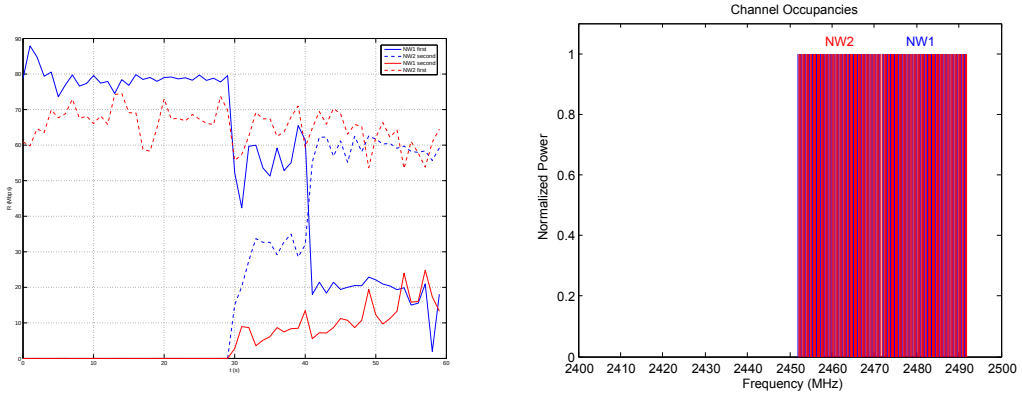

(a) Throughput

(b) NW1 Channel 13; NW2 Channel 13

Figure 3.12: Average network throughputs of interfering NW1 and NW2, both occuping channel 13 (see (b)). Throughput values of NW1 drop from a mean of 77.8 to 20.9 while NW2 transfers at a mean of 57.9. And NW2 values drop from a mean of 67.3 to 62.6 while NW1 starts transfering at a mean of 11.0. Values are in Mbit/s.

86% of its normally achieved throughput. If we take the sum of μ_1 and μ_2, we find out whether the medium still provides enough space to make the maximum throughputs for a network available. Consequently, we define the performance of an entire system, μ_{xy}, as the sum of μ_1 and μ_2 and know that for:

- $\mu_{xy} < 1$, medium sharing results in a total throughput of NW1 and NW2 that is less then the maximum throughput that the medium provides;
- $\mu_{xy} = 1$, medium sharing causes that the achieved throughput of the individual networks exactly match the maximum throughput that the medium provides;
- $\mu_{xy} > 1$, medium sharing enables a total throughput of NW1 and NW2 to be even more than the maximum throughput that the medium normally provides, which is quite unlikely, but indicates that the medium supports even higher throughputs than the maximum throughputs obtained by a single network.

Regarding the scenario of Figure 3.12, we find for the performance

$$\mu_{nn} = \mu_1 + \mu_2 = 0.27 + 0.86 = 1.13 \tag{3.1}$$

This value for the performance belongs to the third category described above and indicates that the medium is shared and allows even higher total throughputs when two networks make use of the medium simultaneously.

In order to provide a stochastic view of the obtained throughputs too, their Cumulative Distribution Functions (CDF) (see A.2.2) are included in figure 3.13 for the two networks when the medium is shared. In these graphs one can instantly see to which values the throughputs drop.

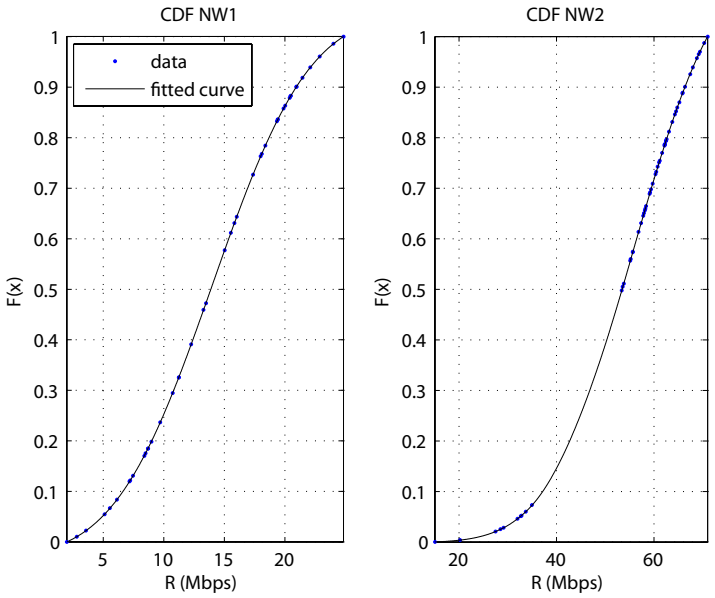

Figure 3.13: CDFs of the throughputs for the scenario considered in Figure 3.12 of the sharing SITECOM networks with mean throughputs of 13.9931 Mbit/s and 55.7277 Mbit/s for NW1 and NW2 respectively.

At this point we might wonder why the expected high data rates of 300 Mbit/s are not realized. We already figured out that not data rates are measured, but throughputs. This implies that due to overhead caused by the PHY layer header and preambles, the higher MAC layer, network layer and transport layer, the maximum rates of 300 Mbit/s at the physical layer cannot be reached. Based on the throughputs realized in 802.11g and 802.11b networks, which are 24 Mbit/s and 5 Mbit/s respectively, where the data rates are 54 Mbit/s and 11 Mbit/s respectively, we assume for this part of the work that an 802.11n network would realize a throughput of 50% of its data rate too, i.e., 150 Mbit/s. Still this does not explain the relatively low throughputs that are around 80 Mbit/s. We added in Figure 3.14 a scenario of an AP and a STA in a network along with the type of connection between the computers and the 802.11n router and 802.11n dongle and the communication rates. The USB dongle communicates with the notebook through a USB 2.0 connection which supports data rates up to 480 Mbit/s. Further, from Table 3.1 we find that the SITECOM routers that are used posses 100 Mbit ethernet ports indicating data rates of 100 Mbit/s. Accordingly, we have found the bottleneck in the communication system. The 100 Mbit ethernet ports do not allow higher transfer rates above 100 Mbit/s. Due to the dynamic behaviour of the channel this throughput decreases even more to approximately 80 Mbit/s that was obtained from the measurements.

The throughputs of interfering 802.11n with 802.11b/g networks are discussed in the subsections that follow.

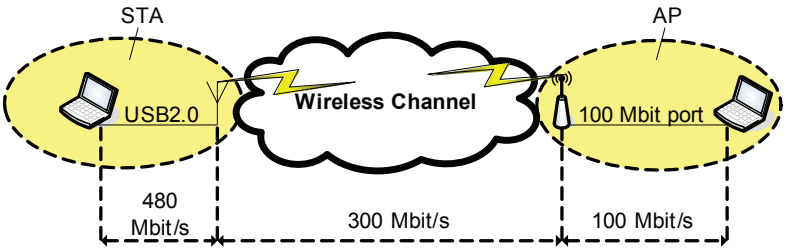

Figure 3.14: An 802.11n network with the type of connection between the devices and the communication data rates.

3.3.1.2 802.11b/g and 802.11n Medium Sharing

In the previous section the negative effects for the throughput of medium sharing 802.11n networks was proven. There was a substantial decrease in the throughput of the individual networks. We continue with the medium sharing results for 802.11b and 802.11g networks in the presence of nearby located 802.11n networks. For the 802.11b/g network - NW1 - a *Speedtouch 780i WL* modem is used, for which the desired standard 802.11b or 802.11g can be selected. The wireless STA is the *Intel Pro Wireless 2200BG Network* PC-card. For this PC-card also one of the standards 802.11b or 802.11g can be selected. The two medium sharing networks thus are defined as follows:

- NW1: HP desktop connected to Speedtouch 780i WL as AP1 and Intel Pro Wireless 2200BG Network PC-card in NB3 as STA1 in Room 1
- NW2: NB1 connected to Sitecom 300N WL-183 as AP2 and Sitecom 300N WL-182 USB in NB4 as STA2 in Room 2

The results for both 802.11g and 802.11b networks sharing the medium with an 802.11n network are in Figure 3.15. From Figure 3.15(a) we can determine the mean throughputs of the 802.11g and 802.11n networks. Then the performance of the entire system, when NW1 starts transfering first and NW2 begins transfering after $t = 30$ s, indicated by μ_{gn}, can be calculated according to the method described in Section 3.3.1.1, as:

$$\mu_{gn} = \mu_1 + \mu_2 = \frac{\widetilde{E}_{gn}}{E_{gn}} + \frac{\widetilde{E}_{ng}}{E_{ng}} = \frac{0.35}{17.0} + \frac{24.4}{50.9} = 0.02 + 0.48 = 0.50 \tag{3.2}$$

The outcome is very low and it indicates that the throughput allowed by the medium is not achieved and the medium sharing mechanism failes in this scenario. If we calculate the performance in case NW2 transfers first, then we yield

$$\mu_{ng} = \mu_2 + \mu_1 = \frac{\widetilde{E}_{ng}}{E_{ng}} + \frac{\widetilde{E}_{gn}}{E_{gn}} = \frac{23.7}{50.9} + \frac{0.20}{17.0} = 0.47 + 0.01 = 0.48, \tag{3.3}$$

which is again a low value, indicating that medium sharing is not performed as it should be. The outcomes of 3.2 and 3.3 show that the throughput of the 802.11g network degrades to approximately 1% of its unencumbered throughput as indicated by its μ.

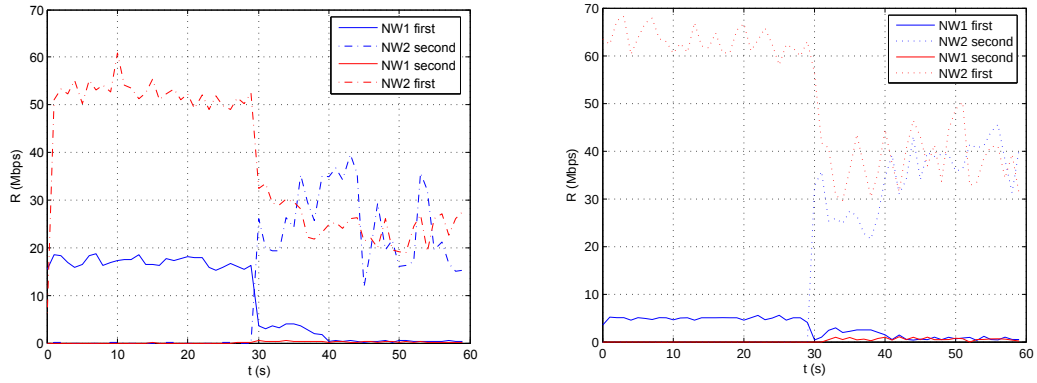

(a) 802.11g: NW1 throughputs drop from mean 17.0 to mean 0.35 Mbit/s, while NW2 transfers at a mean of 24.4 and NW2 throughputs drop from mean 50.9 to mean 23.7 Mbit/s, while NW1 transfers at a mean of 0.20

(b) 802.11b: NW1 throughputs drop from mean 4.9 to mean 0.77 Mbit/s, while NW2 transfers at a mean of 38.4 and NW2 throughputs drop from mean 62.6 to mean 39.1 Mbit/s, while NW1 transfers at a mean of 0.62

Figure 3.15: Network throughputs for 802.11g (a) and 802.11b (b) networks with an interfering 802.11n network transmitting at $T_{x_n} = 100\%$ of the maximum transmit power and located in Room 2.

From Figure 3.15(b) we can determine the mean throughputs of medium sharing 802.11b and 802.11n networks. Accordingly, the performance of the entire system, when NW1 begins transfering, μ_{bn}, can be calculated through:

$$\mu_{bn} = \mu_1 + \mu_2 = \frac{\widetilde{E}_{bn}}{E_{bn}} + \frac{\widetilde{E}_{nb}}{E_{nb}} = \frac{0.77}{4.9} + \frac{38.4}{62.6} = 0.16 + 0.61 = 0.77, \tag{3.4}$$

which is lower than 1 and indicates that the throughput allowed by the medium is not achieved and medium sharing is not performed properly. When NW2 begins transfering, the performance, μ_{nb}, will be

$$\mu_{nb} = \mu_2 + \mu_1 = \frac{\widetilde{E}_{nb}}{E_{nb}} + \frac{\widetilde{E}_{bn}}{E_{bn}} = \frac{39.1}{62.6} + \frac{0.62}{4.9} = 0.62 + 0.13 = 0.75, \tag{3.5}$$

wich is lower than 1 too and indicates that the medium sharing mechanism is not performed as it should be. Again we observe that the throughput of one of the networks, in this case the 802.11b network, degrades to approximately 15% of its unencumbered throughput

As we can see from the plots in Figure 3.15 and the system performances calculated in 3.1-3.5, all concerning networks show throughput degradation due to medium sharing. In particular, the 802.11b and 802.11g networks experience an over-proportional throughput degradation. The reason for this could be the Clear Channel Assesment (CCA) mechanism defined in the PHY layer specifications of the standards. CCA determines for a wireless device whether the medium is busy or idle and accordingly

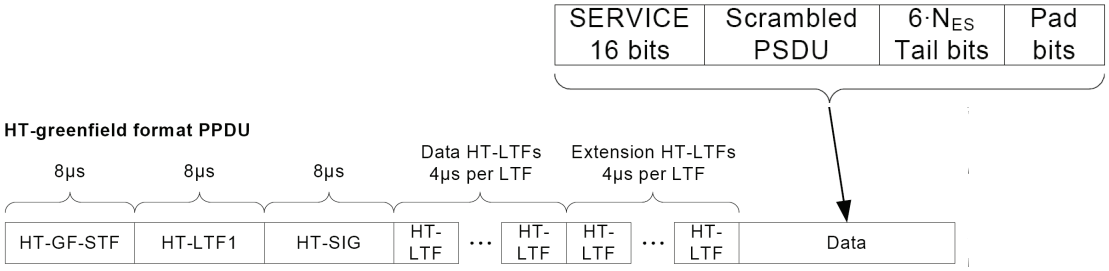

Figure 3.16: 802.11n PPDU format [18]

available to transmit data. We suspect that the devices with the particular standards we investigated, do not detect operation of devices based on any other standard, except their own standard. Consequently, we suspect that due to the failing CCA mechanisms, real interference occurs. A further analysis on this subject is given in Section 3.5.

Disproportional use of the medium Another reason for the fallbacks in throughput could be the medium sharing rules and disproportional use defined by the MAC layer specifications and the disproportional use of the medium by the various PHYs. We can explain this by the aid of Figure 3.17 and Figure 3.18 as follows. We have considered the operation in the MAC layer for the 802.11n, 802.11g and 802.11b network, where we assume unicast communication (Figure 2.11) and applying the CSMA/CA mechanism. For the 802.11n communication we assume the PPDU packets to be in HT Greenfield format as depicted in Figure 3.16, and if we take two spatial streams according to the measurements, it means that we can have two Data HT-LTFs and two Extension HT-LTFs, which are specified in [18, Ch. 20.3]. Accordingly, we can calculate the lenght of the PPDU packet as:

$$T_{PPDU} = T_{HT-GF-STF} + T_{HT-LTF1} + T_{HT-SIG} + 2T_{HT-DLTF} + 2T_{HT-ELTF} + T_{DATA}, \tag{3.6}$$

where $T_{HT-DLTF}$ and $T_{HT-ELTF}$ denote the lenghts of the Data HT-LTF fields and Extension HT-LTF fields respectively. The value for T_{DATA}, holding the length for the Data field, depends on the size of the MAC Protocol Data Unit (MPDU) packet determined in the MAC layer. According to the MAC layer specifications given by [18] this value lies between 1 and 7956 bytes. We assume the highest value and taking into account the 2 spatial streams in the 802.11n system, over each antenna packages existing of $7956/2 = 3978$ bytes are transmitted, which is equivalent to $3978 \times 8 = 31824$ bits. Previously, in Section 3.3.1.1, we clearified that the maximum throughput for a system based on the 802.11n standard, is 100 Mbit/s. The maximum data rate at the real wireless physical link is 300 Mbit/s. According to this, the duration of the Data field will be $\frac{31824}{300\times10^6} = 106\mu$s. Consequently we can fill in this value together with the durations of the other fields (Figure 3.16) in 3.6 to calculate the lenght of the PPDU packet. This yields:

$$T_{PPDU} = 8 + 8 + 8 + 2 \times 4 + 2 \times 4 + 106 = 146\mu\text{s} \tag{3.7}$$

According to this method we have also calculated the lengths of the PPDU packets for the 802.11g and 802.11b standard where we assume Data packets of respectively 4096 bytes [16] and 2304 bytes [15] equivalent to respectively $4096 \times 8 = 32768$ bits and 18432 bits. The preamble plus header length which are transmitted prior to the Data field, are determined for the 802.11g network at 20μs. Assuming a data rate of 54 Mbit/s, the length of the Data field will be $\frac{32768}{54\times10^6} = 607\mu$s. In total the duration of a transmitted 802.11g PPDU packet will be $20 + 607 = 627\mu$s. Likewise we calculate the

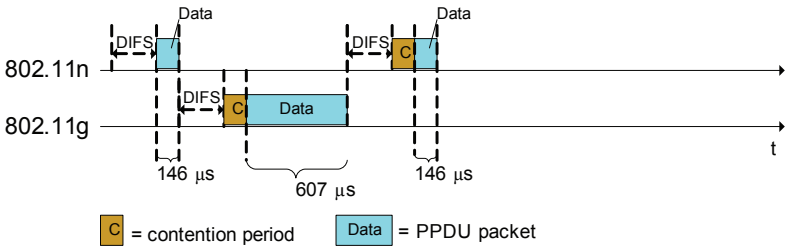

Figure 3.17: MAC packet lengths for 802.11n and 802.11g PPDUs.

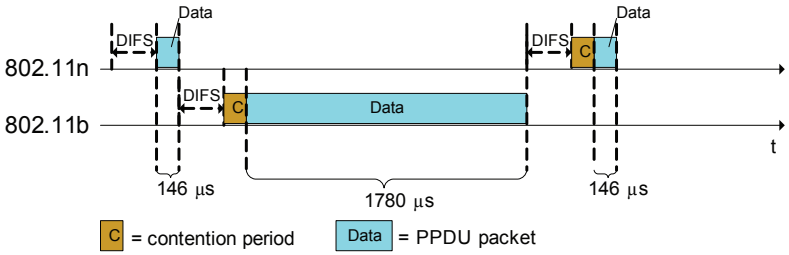

Figure 3.18: MAC packet lengths for 802.11n and 802.11b PPDUs.

length of an 802.11b PPDU packet, assuming a preamble plus header length of 96μs, a Data field packet consisting of 18432 bits and a data rate of 11 Mbit/s and yield $\frac{18432}{11\times10^6} + 96 \times 10^{-6} = 1.78$ms.

Obviously, older PHYs disproportionally use the medium. For instance, an 802.11b network that preserves much more time than the other two networks to use the medium for the transmission of a PPDU packet. As a consequense, the data rate of a medium sharing 802.11n network is negatively affected, since it has to wait longer between subsequent packets before the medium is idle again. The same holds when the medium is shared by an 802.11g and an 802.11n network. Since 802.11g PPDUs use the medium for a longer time, again the 802.11n network has to wait longer between subsequent packets, which degrades its data rate. Figure 3.17 and Figure 3.18 illustrate this event for an 802.11n network sharing the medium with respectively an 802.11g and 802.11b network.

A similar scenario exists when an 802.11n network consists of an AP and multiple STAs where the STAs are positioned at different distances from the AP. In Appendix A in Section A.1.1.2 the results for the throughput are depicted for 802.11n networks

where the STA is moved to locations further away from the AP. As a consequense the throughputs drop and accordingly, during the measurements we have seen that as the STA moves further away from the AP, the MCS index changes to a lower value, indicating lower data rates and thus longer PPDU packets. This means that the STA that is located at the greatest distance with respect to the AP, has the lowest data rate and thus the longest PPDU packets. The result is that the overall network throughput is being determined by the STA with the greatest distance to the AP and that network throughput is badly affected by this.

Transmit Power Reduced We have seen that throughputs of medium sharing 802.11b/g and 802.11n networks decrease because of medium sharing properties and probably different carrier detecting mechanisms defined in the CCA specifications of the different standards. In this paragraph we focus on reducing the medium sharing effects by adjusting the transmission power of an AP in such way that the influence to the other network is reduced. Theoretically decreasing the transmit power T_x causes the signal power at a certain distance d from the transmitter to be lower [19] and thus reducing the possible interference with a present second network. As can be

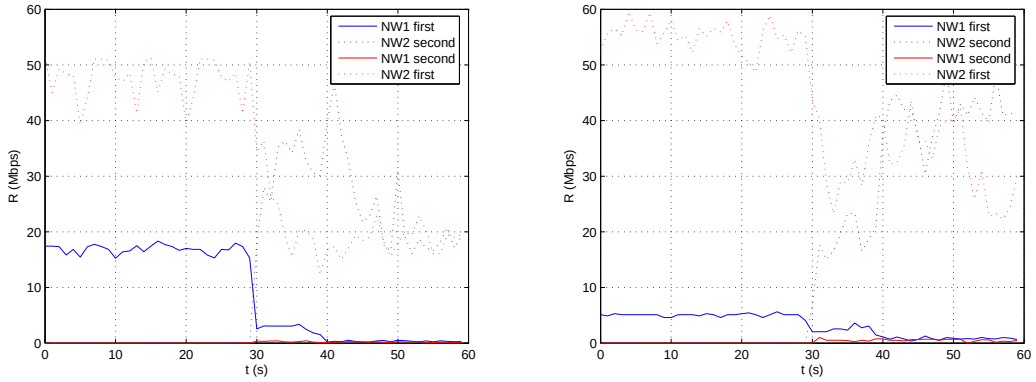

(a) 802.11g

(b) 802.11b

Figure 3.19: Network throughputs for 802.11g (a) and 802.11b (b) networks with an interfering 802.11n network transmitting at $T_{x_n} = 10\%$ of the maximum transmit power and located in Room 2.

seen from Figure 3.19, the results for the AP transmitting at 10% of its maximum transmit power are quite similar to the results for the AP transmitting at 100% of its transmit power depicted in Figure 3.15. We cannot determine the exact reason for this since we do not possess information about operation at the PHY layer. Further research should be executed to verify the correct operation of the CCA mechanisms.

Throughput of the operating networks is measured for even more scenarios. This includes scenarios with two STAs communicating through one AP, tranfers over different floors, etc. These scenarios are described in A.2.2 and are somehow related to

interference.

3.3.2 Home Environment

At HOME throughputs of 802.11n and 802.11g networks are measured while the medium has to be shared. The networks are defined as:

- NW1: 802.11g network with a LINKSYS -G router that is connented to a desktop with an Intel Pentium 4 3.2 GHz processor and512 MB RAM, together being AP1. The wireless station is NB1 with an Intel PRO/Wireless 2200BG Network Adapter integrated, serving as STA1. This network is located at HOME and operates at WIFI channel 11.
- NW2: SWEEX 300N router connected to NB4 as AP2 and the SWEEX WL-302 connected to NB3 as STA2. NW2 is positioned in the appartment next to HOME and operates in either channel 13 or channel 1.

The results of the measurements are in figure 3.20. The performance of the two interfering

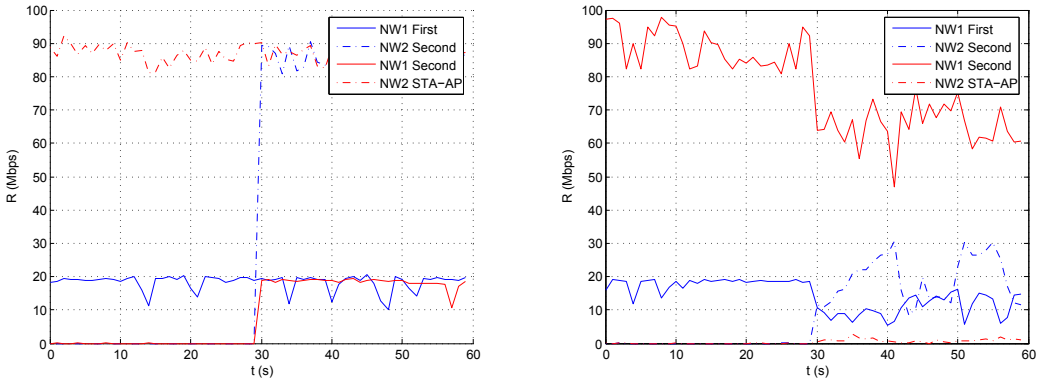

(a) NW2 at channel 1

(b) NW2 at channel 13

Figure 3.20: Average throughputs for NW1 and NW2 while sharing the medium. NW1 operates at WIFI channel 11 and NW2 at respectively channel 1 (a) and channel 13 (b)

networks with respect to throughput can be calculated according to the method defined in Section 3.3.1.1. For the performance of the system in Figure 3.20(b), when NW1 begins transfering, we find:

$$\mu_{gn} = \frac{10.8}{18.1} + \frac{19.8}{88.8} = 0.82 \tag{3.8}$$

When NW2 begins transfering we find for the performance:

$$\mu_{ng} = \frac{65.4}{88.8} + \frac{0.73}{18.1} = 0.78 \tag{3.9}$$

We can draw a similar conclusion as the measurements performed at KPN , i.e., because of medium sharing the network throughputs degrade and the CCA mechanisms of the particular standards seem to be incompatible.

3.4 Packet Loss Ratio (PLR)

So far we have seen how medium sharing can affect the throughput of a network. Particurly, when the CCA mechanisms are not compatible and probably interference takes place. However, the throughput is not the only parameter that can be used as a measure for the interference between two networks. In this part we are going to look at the PLR when the medium has to be shared. Again different scenarios with different networks are considered. Measuring the PLR requires a specific tool that operates over the UDP network protocol in stead of the TCP protocol. The reason for this is that the TCP protocol automatically recovers lost or erroneous packets through retransmission protocols which makes it impossible for the measurer to determine the amount of packets lost. The UDP protocol on the other hand does not care about packet errors or losses and makes it possible to determine the amount of packet losses on the receiver side. The origin of the packet losses is not known however. It could be due to noise introduced by the channel, packet collisions, signal degradation, network routing or oversaturated links. The tool used to perform the PLR measurements is called *Iperf* [3]. Earlier, we stated that the PLR gives back the ratio of the number of transmitted lost packets, against the total number of packets supplied during a transfer. In fact, we can define the PLR as:

$$\text{PLR} = \frac{\text{transmitted packets lost}}{\text{total supplied packets}} \tag{3.10}$$

3.4.1 802.11n without Medium Sharing

First some reference measurements are performed to obtain the PLR when the medium is used by only one network at a time. The devices used for this purpose are the SITECOM WL-183 AP and SITECOM WL-182 STA for the first setup and the SWEEX 300N AP and WL-302 STA for the second setup. The AP is being kept at a fixed location in Room 1, while the location of the STA changes from Room 1 to Room 2 and Room 3 (see figure 3.4) to have an indication of how the PLR behaves against the distance. The results are depicted in figure 3.21(a) and 3.21(b) for the SITECOM network and the SWEEX network respectively. We can vary the supply rate of data using *Iperf*, which sends at our desired supply rate at the transport layer. Obviously at the PHY layer, data is transferred at the maximum achievable data rate, and not at the supply rate that is bounded by the transport layer. Therefore, at low supply rates, the PHY layer has to wait transmitting between subsequent packets, simply because *Iperf* does not deliver data fast enough. From the graphs we can see that without sharing PLR < 0.003 for the SWEEX networks and for the SITECOM network even PLR < 0.001. The PLR increases as the supply rate, S, increases and obviously for greater distances (Room 3), the higher supply rates are not achievable. We know that based on the UDP protocol, a transmitter does not wait for acknowledgements from the receiver, but in stead, keeps transmitting regardless of whether a packet is received by the receiver or lost during transmissions. However, at the MAC layer still MPDUs that are transmitted, need to be acknowledged by the receiver. In case of packet loss, at the MAC layer, the transmission of MPDUs are not acknowledged by the receiver, which causes the MAC management entity to issue a lower rate command to the PHY layer. Consequently, the data rate is changed to a

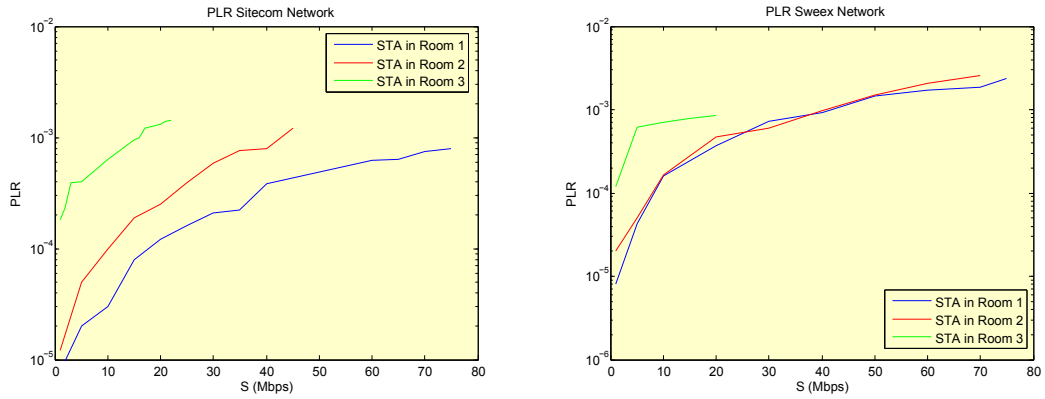

(a) SITECOM (b) SWEEX

Figure 3.21: PLRs plotted against supply rate S for SITECOM (a) and SWEEX (b) networks when the STA is located in Room 1, Room 2 and Room 3, respectively.

lower, more robust data rate. And as the supply rate at the transport layer increases during the measurements, the packets are not able to pass through the data link layer and get discarded. This happens when we increase the supply rate over the capacity of the medium. Generally, we can see from the plots, that as the supply rate increases, the PLR values gradually move towards an upper bound. When the distance between AP and STA increases, there is a fallback to a lower data rate, illustrated by the shifted plots for Room 2 and Room 3 in Figure 3.21(a).

From Figure 3.21(b) we can tell that for Room 2 the PLR values are almost equal to the PLR values measured for Room 1, indicating that the SWEEX system has not switched back to a lower data rate. However, for Room 3, it does switch back as shown by the shifted curve towards a higher PLR.

3.4.2 802.11n and 802.11n Medium Sharing

Consequently we proceed with the PLR in case of medium sharing. Our measurement setup consists of two 802.11n networks NW1 and NW2. During the first scenario both networks are SWEEX networks consisting of the 300N AP and the WL-302 STA. NW1 is placed in Room 1 and NW2 in Room 2 and the distance between the two networks is fixed at 10 m. NW2 transmits at the maximum capacity while the supply rate within NW1 is slowly increased. Subsequently, we perform the same measurement where we gradually increase the supply rate of the transfer in NW2, while NW1 is tranferring at its maximum supply rate. The results for the PLRs are shown in Figure 3.22 In case only NW1 is making use of the medium, the PLR increases with the supply rate as we also saw in the previous section. At maximum supply rate we find PLR < 0.004. When NW1 and NW2 operate simultaneously and the medium has to be shared, we can see from Figure 3.22 that the PLR grows to a value of PLR$= 0.1$. Clearly, the higher supply rates introduce higher PLR values. Since the networks are identical, i.e., both are SWEEX 802.11n networks, they show similar results.

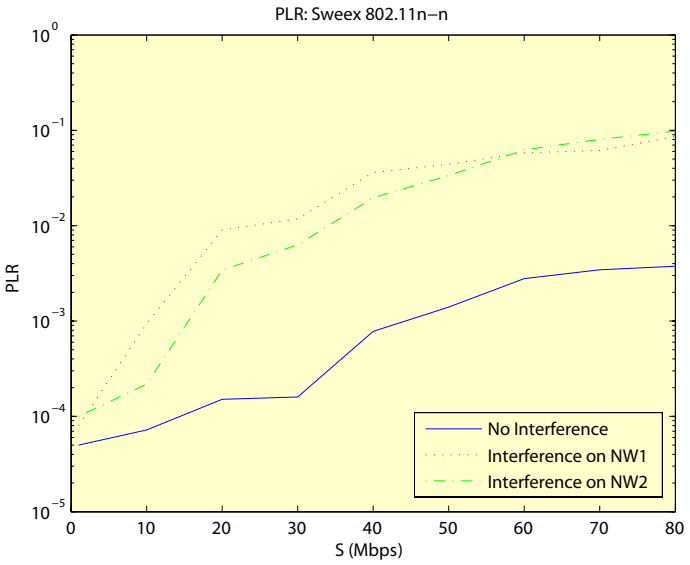

Figure 3.22: PLR values for two medium sharing 802.11n SWEEX networks against supply rate S

Subsequently, we try to further process the obtained results to retrieve information about the real throughput R through the networks of Figure 3.22. The PLR is the ratio of the number of packets lost relative to the total packets sent per unit of time, i.e. the supply rate. Hence the throughput is the difference of the supply rate and the loss rate. Table 3.3 provides an educated guess of the throughput in NW1 and NW2. If we take the ratio of the maximum derived throughput in Table 3.3 to the

S (Mbit/s)	**10**	**20**	**30**	**40**	**50**	**60**	**70**	**80**
PLR NW1	$9 \cdot 10^{-4}$	$9 \cdot 10^{-3}$	0.012	0.036	0.044	0.058	0.061	0.086
R NW1 (Mbit/s)	10	19.82	29.64	38.56	47.80	56.52	65.73	73.12
PLR NW2	$2 \cdot 10^{-4}$	$3 \cdot 10^{-3}$	$6 \cdot 10^{-3}$	0.020	0.033	0.058	0.081	0.10
R NW2 (Mbit/s)	10	19.94	29.82	39.2	48.35	56.52	64.33	72

Table 3.3: Retrieving the throughput R from the supply rate S using the PLR for 802.11n-802.11n scenario.

supply rate, we actually calculate μ_1 in 3.1. We find for the performance, μ_{1_P}, in NW1 $\mu_{1_P} = 73.12/80 = 0.91$. For NW2 we repeat this and find $\mu_{2_P} = 72/80 = 0.90$. The sum of μ_{1_P} and μ_{1_P} is much more than 1 which is quite unlikely to happen, indicating that something was not considered during the measurements. Most probably, we did not account for the throughput fallbacks in one of the networks caused by medium sharing. Furthermore, from the blue curve, we observe that at a supply rate of 80 Mbit/s the medium is not saturated yet, following from the relatively low PLRs.

To increase the integrity of our measurements, we also considered the PLRs in a scenario of two different 802.11n networks sharin the medium with each other. NW1

is again the SWEEX network in Room 1, and NW2 is this time the SITECOM network with WL-183 AP and WL-182 STA located in Room 2. Both networks operate at fixed positions. The supply rate in NW1 is gradually increased while the supply rate in NW2 is at its maximum. The results for the PLR are depicted in figure 3.23. Again we observe an increase of the PLR when the supply rate within the network increases. There is a similar behaviour as the PLR plots in Figure 3.22 and again we observe that at maximum supply rate, PLR < 0.1.

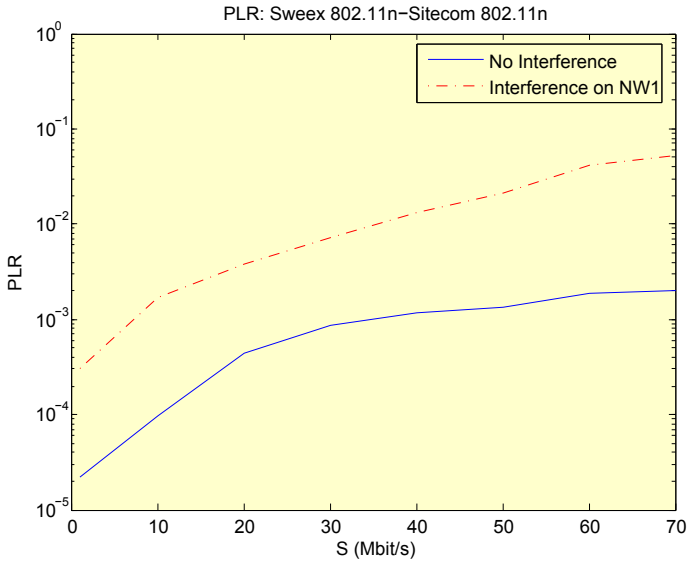

Figure 3.23: PLRs for medium sharing 802.11n SWEEX and SITECOM networks against supply rate S

3.4.3 802.11n and 802.11g Medium Sharing

Next we arrive at the part where is looked at the PLRs of 802.11n and 802.11g networks that need to share the medium. The two networks are defined as:

- NW1: Thomson Wireless-G AP and Intel Pro Wireless-G STA placed in Room 1
- NW2: SWEEX 300N AP and the WL-302 STA placed in Room 2

The results for the PLR are in figure 3.24. We measured the PLR in NW1 depicted in Figure 3.24 while increasing the supply rate in NW1 gradually and having the supply rate in NW2 at its maximum. The 802.11g network has a maximum supply rate of approximately 20 Mbit/s. We immediately notice that in NW1 a lot of packets are lost during transmission indicated by the high PLR values. The PLR increases up to 0.5. In Figure 3.24(b) we observe the PLR values of NW2 where the supply rate is increased gradually while NW1 is transfering at maximum supply rate. Also the 802.11n network shows higher PLRs for increasing supply rate and at maximum supply rate we find

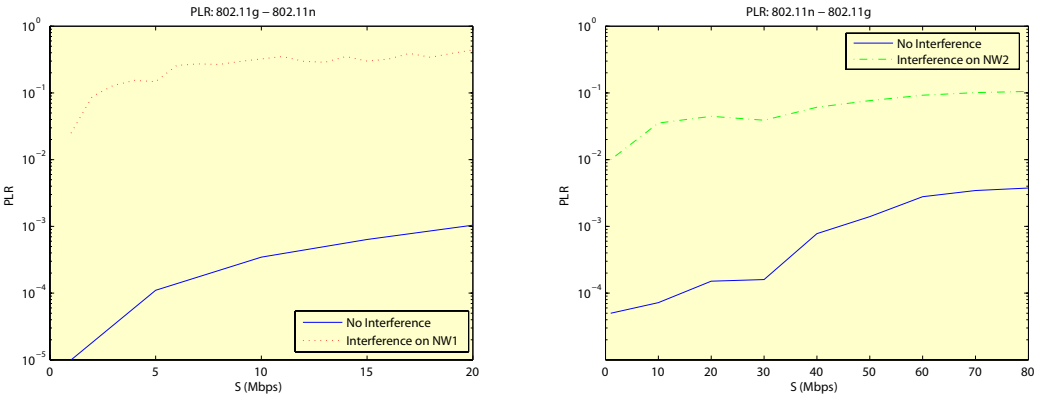

(a) 802.11g (b) 802.11n

Figure 3.24: PLRs for medium sharing 802.11g and 802.11n networks. In (a) the PLR is given for 802.11g against supply rate S. In (b) the same is shown for 802.11n.

PLR = 0.1 Processing the PLRs and the supply rates from Figure 3.24 according to the same method as in the 802.11n - 802.11n medium sharing scenario, leads to the results denoted in Table 3.4. Accordingly, we retrieve μ_{1_P} from Table 3.3, by taking the ratio

S (Mbit/s)	**10**	**20**	**30**	**40**	**50**	**60**	**70**	**80**
PLR NW1	0.323	0.441	NA	NA	NA	NA	NA	NA
R NW1 (Mbit/s)	6.77	11.18	NA	NA	NA	NA	6NA	NA
PLR NW2	0.035	0.045	0.039	0.061	0.077	0.092	0.101	0.105
R NW2 (Mbit/s)	9.65	19.10	28.83	37.56	46.15	54.48	62.93	71.6

Table 3.4: Retrieving the throughput R from the supply rate S using the PLR for 802.11g-802.11n scenario.

of the maximum throughput to the supply rate for NW1 as: $\mu_{1_P} = 11.18/20 = 0.56$. We do the same for NW2 and obtain: $\mu_{2_P} = 71.8/80 = 0.91$. Again, we note that at maximum supply rates, the medium is not saturated yet, resulting in the relatively high μ_{x_P}'s. Further on, in Section 3.6 we will see how the obtained values relate to the μ_{xy}'s calculated from the measured throughputs.

Since we consider two networks based on different standards (802.11n and 802.11g), it is plausible that the previously discussed CCA mechanism does not function properly. More on this issue is covered in Section 3.5.

3.4.4 802.11n and 802.11b Medium Sharing

The remaining scenario and yet not discussed is when there are two nearby located 802.11n and 802.11b networks that have to share the medium with each other. The two networks are defined as:

- NW1: Thomson Wireless-B AP and Intel Pro Wireless-B STA placed in Room 1

- NW2: SWEEX 300N AP and the WL-302 STA placed in Room 2

The outcomes of these measurements are presented in Figure 3.25 and again remarkable is that the performance of both networks in terms of PLR degrades as the supply rate of the considered networks increases. In Figure 3.25(a) the supply rate of NW1 increases, while NW2 is transfering at maximum supply rate. The 802.11b network has PLR values that increase to 0.5 in presence of the medium sharing NW2. In Figure 3.25(b) the supply rate of NW2 increases while NW1 is transfering at maximum supply rate. For the 802.11n network the PLR values increase to 0.3 as the supply rate of the system increases. Processing the PLRs and the supply rates from Figure 3.25 according to the method

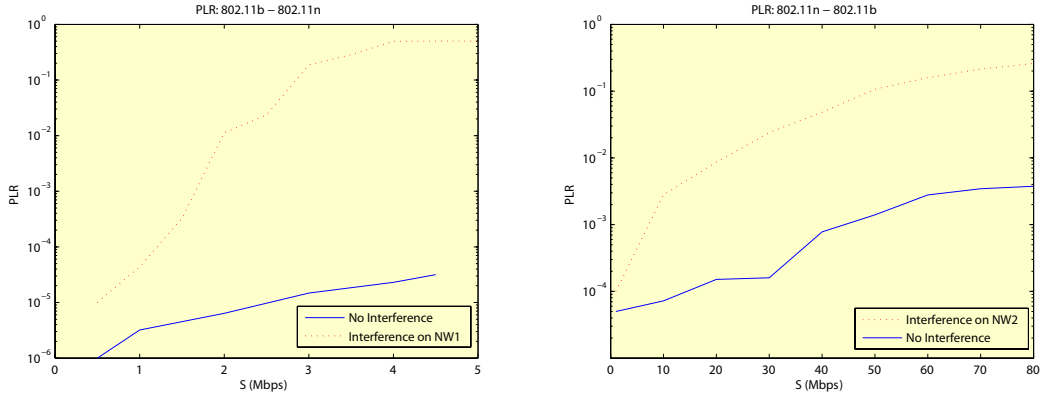

(a) 802.11b (b) 802.11n

Figure 3.25: PLRs for medium sharing 802.11b and 802.11n networks. In (a) the PLR is given for 802.11b against the supply rate S. In (b) the same is shown for 802.11n.

applied in the previous scenarios, leads to the results denoted in Table 3.5. Repeating

S NW1 (Mbit/s)	**1**	**2**	**3**	**4**	**5**	NA	NA	NA
PLR NW1	$4 \cdot 10^{-4}$	0.011	0.186	0.496	0.500	NA	NA	NA
R NW1 (Mbit/s)	1	1.98	2.44	2.02	2.5	NA	NA	NA
S NW2 (Mbit/s)	**10**	**20**	**30**	**40**	**50**	**60**	**70**	**80**
PLR NW2	0.003	0.009	0.024	0.048	0.107	0.159	0.214	0.260
R NW2 (Mbit/s)	10	19.82	29.28	38.08	44.65	50.46	55.02	59.20

Table 3.5: Retrieving the throughput R from the supply rate S using the PLR for 802.11g-802.11n scenario.

the method from the previous scenarios, we find from Table 3.5 $\mu_{1_P} = 2.5/5 = 0.5$ for NW1 and $\mu_{2_P} = 59.20/80 = 0.74$. Again, we see in Figure 3.25 that at maximum supply rates the medium is not saturated yet and similar conclusions can be drawn as in Section 3.4.2. Further on, in Section 3.6 we will see how these values relate to the μ_{xy}'s obtained from the throughputs.

Similarly as in the previous scenario, we face the fact that the two networks are operating based on different standards (802.11n and 802.11b) and there is a possibil-

ity that the manufactureres of the 802.11n and 802.11b devices, use a different CCA implementation, and the possible result of this is discussed in the next section.

3.5 CCA Mechanism

Explaining the growing PLR values when medium sharing takes place, requires knowledge about the Clear Channel Assesment (CCA) options, implemented in the wireless devices. The CCA mechanism is performed by a wireless device prior to transmission in order to find out whether the channel is clear to use or busy and thus unavailable. There are existing several methods to implement the CCA mechanism on a device and manufacturers can decide for themselves which they use. Unfortunately, information about the used CCA method is not published or kept confidential and we could not find the exact CCA specifications for the used devices. For the CCA mechanism, supported by the considered 802.11n and 802.11g standards, that are both based on the digital OFDM modulation technique, we refer the reader to [17, Ch. 18.4.8.4]. For the CCA mechanism supported by the 802.11b standard, that operates based on the DSSS modulation technique, we refer to [15]. Since we intend to explain our PLR results based on the CCA mechanisms, we briefly describe the possible CCA methods in the following.

- CCA 1: The CCA mechanism shall report a busy medium if any energy above a certain threshold is detected. This threshold is determined by the value stored in the Energy Detection (ED) parameter defined in [17, Ch. 18.4.8.4]
- CCA 2a: A busy medium is reported only upon detection of a DSSS signal.
- CCA 2b: The CCA mechanism will report a busy medium in case it senses a DSSS signal above a certain energy threshold ED.
- CCA 3a: Within the duration of a timer that is set to 3.65 ms the medium is sensing only for OFDM signals and a busy or idle medium shall be reported by the CCA depending on that.
- CCA 3b: A busy medium is reported in case an OFDM signal above the ED threshold is detected.

We divided the CCA methods in to three categories as can be seen above. The first category, indicated by **CCA 1**, is a general CCA method that can be selected in all three considered standards. The second category, indicated by **CCA 2**, describes the CCA methods that can be implemented in DSSS based systems. This would be in our case 802.11b. Finally, the third category, refered to as **CCA 3**, describes the plausible CCA methods for OFDM based systems.

Based on the CCA mechanisms we can probably explain the results from Figure 3.24 where we observe high PLR values for the 802.11g network when the 802.11n network is making use of the medium simultaneously. When the 802.11g network and 802.11n network use a different CCA mechanism, i.e., each one uses either CCA 1, CCA3a or CCA3b but not the same, it is possible that both networks cannot 'hear' each other, leading to real interference and explaining the high PLRs. This also clearifies the low

values for μ_{xy} found in Section 3.3.1.2 where medium sharing 802.11b/g and 802.11n networks result in low throughput values for particurly the 802.11b and 802.11g networks. Future work on which CCA mechanism are used exactly by the manufacturers of the used devices could clearify more about our suspicion.

Similarly, we can explain the high PLR values from Figure 3.25 for the medium sharing 802.11b and 802.11n networks by saying that different CCA mechanisms are used that are not compatible, causing that the two networks cannot 'hear' each other leading to packet collisions and indicating real interference.

3.6 Correlation Throughput and PLR

After having discussed the results from the throughput and PLR measurements, we are going to investigate in this section the correlation between the two. We have put all the results in Table 3.6 Previously, we stated that μ_{xy} values equal to and higher than 1

Scenario	$\mu_{\mathbf{xy}}$	**PLR**	$\mu_{\mathbf{1}}$	$\mu_{\mathbf{2}}$	$\mu_{\mathbf{1_P}}$	$\mu_{\mathbf{2_P}}$
802.11n - 802.11n	1.13	0.1	0.27	0.86	0.91	0.90
802.11n - 802.11g	0.48	0.11	0.47	0.01	NA	0.91
802.11g - 802.11n	0.50	0.5	0.02	0.48	0.56	NA
802.11n - 802.11b	0.75	0.3	0.62	0.13	NA	0.5
802.11b - 802.11n	0.77	0.5	0.16	0.61	0.5	NA

Table 3.6: Correlation between performance w.r.t. throughput (μ_{xy}) and performance with respect to PLR (μ_{x_P}) for different medium sharing scenarios.

indicate that medium sharing by two networks results in maximum throughputs provided by the medium and for $\mu_{xy} < 1$, medium sharing results into lower throughputs than the medium provides. In Table 3.6 we see in the first row that in case $\mu_{xy} > 1$, PLR = 0.1 is relatively low and with the exception of the second scenario, all $\mu_{xy} < 1$, correspond to higher PLR values. This observation strengthens our suspicion that more packet loss, indicated by the high PLR, leads to lower throughputs indicated by the low μ_{xy} values. We can see from Table 3.6 that this is the case for most of the scenarios were networks, based on different standards, with probably different CCA mechanism, need to share the medium. Further research should verify this and the outcomes of the second scenario, which we cannot explain.

3.7 Summary

In this chapter we discussed the measurements that were performed during this project and explained the results based on our theoretical knowledge. The measurements were performed at locations KPN , HOME and the unechoic chamber. Transfer throughputs and PLRs were measured and several types of scenarios were considered, e.g., STA to STA transfers, AP and STA communications, LOS transfers, measurements in a non-scattering and non-reflecting anechoic chamber, communication over multiple floors and most importantly for this work, interference scenarios consisting of two medium sharing

networks. Regarding the throughput different scenarios were considered containing 2 networks: NW1 and NW2. We defined the performance with respect to throughput, μ_{xy} as the ratio of the throughput in case of medium sharing, to the throughput when there is no medium sharing. Also, we measured the PLR for different scenarios. All the results are summarized in Table 3.7

Scenario	$\mu_{\mathbf{xy}}$	**PLR**	**Remarks**
802.11n - 802.11n	1.13	0.1	high μ_{xy} and low PLR
802.11n - 802.11g	0.48	0.11	low μ_{xy} and low PLR
802.11g - 802.11n	0.50	0.5	low μ_{xy} and high PLR
802.11n - 802.11b	0.75	0.3	low μ_{xy} and high PLR
802.11b - 802.11n	0.77	0.5	low μ_{xy} and high PLR

Table 3.7: Summary of $\mu_{\mathbf{xy}}$ and PLR.

From the results we can conclude that medium sharing causes reduction of the throughputs of all single networks considered. For the scenario with two 802.11n networks the medium still provides the maximum throughputs. We have seen that the unexpected low throughputs are caused by connections between wireless 802.11n devices and computer hardware. These connections introduce a bottleneck in the communication and limit the throughput to 100 Mbit/s. Further more, operation of the MAC protocol introduces delay in communication in case different PHY types make use of the same medium. Basically, the wireless connection with the slowest throughput, is the bottleneck in the communication. This includes an 802.11b connection, which generally has the lowest throughput of 11 Mbit/s, or a connection between a STA and AP of any WLAN at a distance that is large with respect to the distance of other STAs and the AP. Table 3.7 shows that all other scenarios result in lower throughputs than the throughput provided by the medium. We saw that this is a result of medium sharing and perhaps incompatible CCA mechanisms.

Regarding the PLR, we found that networks based on different standards that have to share the medium, have high PLR values as can be seen in the last three rows of Table 3.7. Different networks deploy different CCA implementations resulting in uncompatible CCA functionalities among the 802.11n, 802.11g and 802.11b networks. On account of this a lot of packet losses occurs, leading to the high PLR values from the measurements. Additionally, we tried to find a relation between μ_{xy} and PLR and saw that often a low value of μ_{xy} corresponds to a high value of PLR and vica versa. In order to count the number of lost packets during transfers, packets were transmitted over the UDP protocol in stead of the TCP protocol. Based on the results, we suspect that the throughput using the UDP protocol is higher, since packets are transmitted regardless of whether they are acknowledged by the receiver or not and thus retransmissions of lost packets are not carried out. We cannot confirm this though, due to the lack of time which stopped us from measuring with higher supply rates.

4 Interference Analysis

In order to achieve the objective of this work, i.e. studying and presenting the interference between nearby located and operating 802.11n and other 802.11b/g/n networks, an analytical interference model is derived in this chapter. The outcome of this chapter can help to verify and explain the results obtained from the measurements, discussed in the previous chapter. However, we should note that the measurements were all about transfer throughput and PLR, whereas our analysis will be based on the bit error rate of a communication system in the presence of interference. A further analysis should be carried out in order to compare the results with the results obtained from the measurements.

When modeling interference some preconditions need to be defined that depend on the technique and systems that are under consideration. The modulation for instance, can be digital or analog. In the case of 802.11n, digital modulation techniques like OFDM and QAM are used. The differences in interference effects of analog and digital modulation types can be found in [25, Ch. 3]. Other factors that influence the performance of a network due to interference are the specific modulation type, error correction, transmission power and network topology. The first two belong to the group where open loop interactions between two networks affect performance. More specifically, factors that mainly have influence on the network performance of which they are implemented [26, Ch. 3]. Transmission power and network topology belong to the group with closed loop interactions between interferring networks, i.e. factors that directly have effect on the other network's performance. The main focus in this analyis will be on the factors in the closed loop category.

4.1 Model Outline

The analysis will cover different inteference scenarios consisting of two nearby located 802.11n networks, an 802.11n and 802.11b system operating simueltaneously and an 802.11n system with an 802.11g system. The networks consist of an Access Point (AP) that is assumed to have a circle shaped range with radius R. Within this range a wireless station (STA) communicates through the wireless channel with the AP. At the same time another system with also an AP and STA operates in the close vicinity and the assumption is made that this AP has a range with radius R too. The fact that the systems are located close together, causes overlapping of the coverage areas of the APs which induces interference between the networks when both networks try to use the medium simultaneously. Normally, there would be a medium access mechanism, like the MAC protocol, that is integrated in the specifications of the IEEE 802.11 family and what is assumed to be the mechanism that prevents WLAN devices contending for the

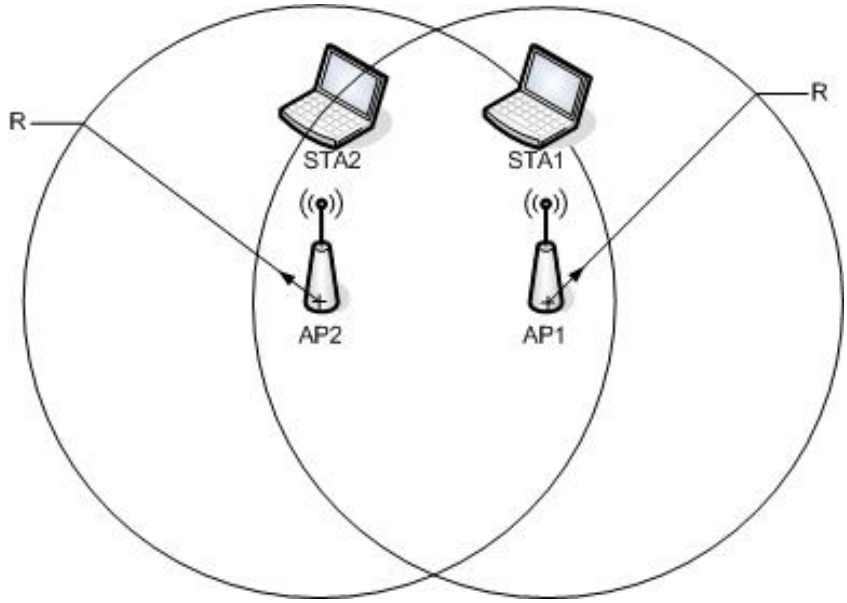

Figure 4.1: Interference scenario with 2 networks both consisting of an AP with radius R and a STA within the range of the AP

medium, to use the medium at the same time and cause interference. For the sake of simplicity though, we assume during our analysis that there is no such thing as a medium access mechanism, and the netwoks as defined before, are causing interference upon each other, because they start transmitting their data regardless of whether the medium is used or not. Future work can be performed continuing this analysis while incorporating the medium access functionalities.

The considered interference scenario is sketched in figure 4.1. The two networks are distinguished in such way that one of them - the so called VICTIM 's network - is experiencing interference from the other - the so called INTERFERER 's - network. For the model no distinguishment is made between transmitter TX_n and receiver RX_n for they are assumed to have symmetrical transmit and receive properties. Further more for the sake of simplicity other interferring sources are left out of the model. This scenario with the VICTIM 's and INTERFERER 's network is shown in figure 4.2. Between transmission and reception the signal will be influenced by the channel impulse response $h(t)$ and noise $n(t)$, also depicted in the figure and discussed further on in this chapter.

Allthough the 802.11n standard originally is intended to operate in the less crowded license free 5 GHz band, still operation in the 2.4 GHz band is mandatory and should be supported. The model that we derive assumes operation in the 2.4 GHz band which results in sharing the available bandwidth with other wireless systems, i.e. 802.11b and 802.11g networks. In our analysis, for each scenario only one other simultaneously operating network is present as a VICTIM or INTERFERER in the form of an 802.11b, 802.11g or 802.11n network. The 2.4 GHz frequency band is known to have 13 frequency channels (in Europe) with their center frequencies spaced 5 MHz apart from each other. However, 802.11b/g networks use an operation bandwidth of 20 MHz resulting in a

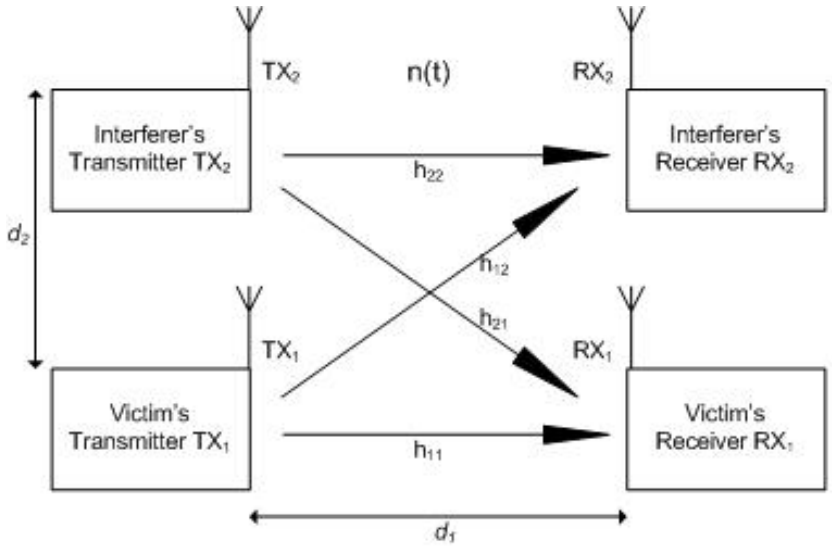

Figure 4.2: Interference model scenario with a VICTIM 's and INTERFERER 's network at distance d_2 both consisting of a transmitter TX and receiver RX at distance d_1. The channel impulse response parameters h_{mn} are also depicted.

maximum of three non-overlapping simultaneously used channels. For the case of 802.11n networks, even less non-overlapping channels are available, namely two, due to operation with 40 MHz bandwidth channels. Since our model covers only networks with 20 MHz or 40 MHz wide operating channels, the scenarios to be considered are of the form shown in figure 4.3:

- a scenario where the operating frequencies of the two systems do not overlap (4.3, left-hand side)
- a scenario with overlapping of the operating frequencies, referred to as interference (4.3, right-hand side)

Since we intend to derive an interference model, our focus in the remaining of this chapter will be on the second scenario where the operating channel frequencies overlap. Having selected the scenario with interference, we can look in more detail to two different forms of interference, from which their occurance mainly depends on the subcarrier frequency offsets of the networks that are considered. If we look at a simplified example of the frequency spectra in figure 4.3 and zoom in, we yield the spectrum depicted in figure 4.4, where we assume we have two simultaneously operating networks, both with 6 independent subcarriers that partially overlap in frequency causing interference to one another.

In this figure, the centre frequencies of the subcarriers that overlap have exactly the same value and are therefore independent with respect to each other, like the mutual subcurriers of a single system. But in another, more worse case, the subcarriers of the different systems differ slighty in their centre frequencies, causing more interference. This less desirable scenario is shown in figure 4.5. Normally, the systems based on the IEEE 802.11g/n standards operate in frequency channels with the same centre frequencies and

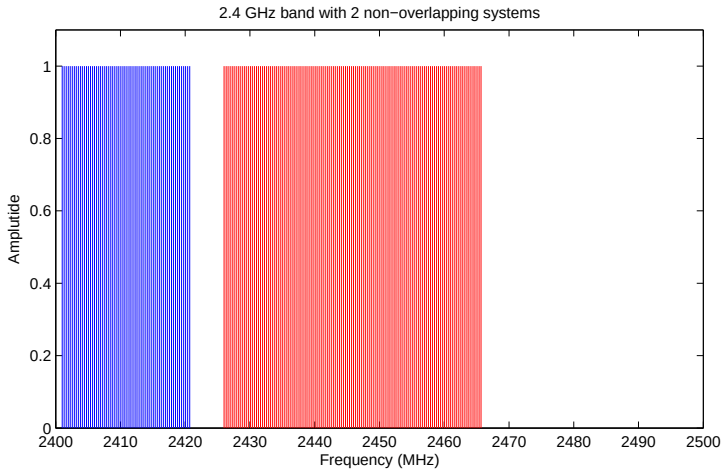

(a) Non-Overlap

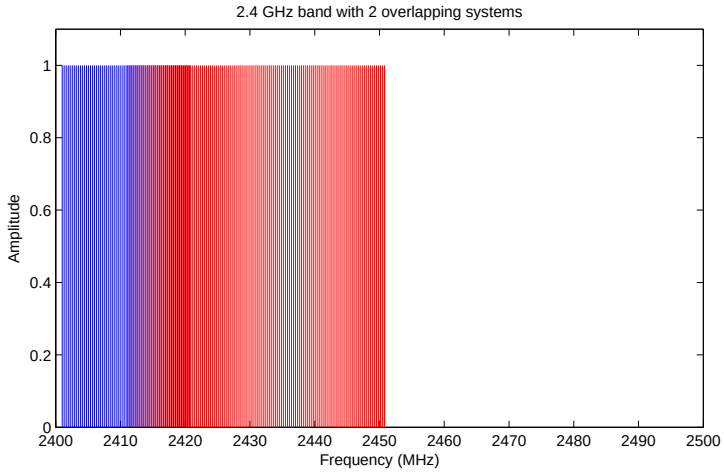

(b) Overlap

Figure 4.3: 2.4 GHz frequency band with a scenario where the 802.11n system (red) and other system (blue) do not overlap in the frequency domain (a) and the scenario where they do overlap (b), causing interference.

subcarrier spacings. But due to inaccuracies in the tuning oscillators in the transmitter and receiver of the networks and due to the Doppler shift, it might occur that there is a small frequency offset for the carrier frequencies causing a phase shift (denoted by Δ_f in the figure) between the subcarriers of the different systems. The remainder of this analysis is based on the former scenario shown in figure 4.4 where we make the general assumption that the subcarriers of the two systems are mutually independent.

In the remainder of this chapter, based on the assumptions we have made so far, we will try to obtain signal to interference ratios (SIR) and bit error rates (BER) for the different scenarios we cover.

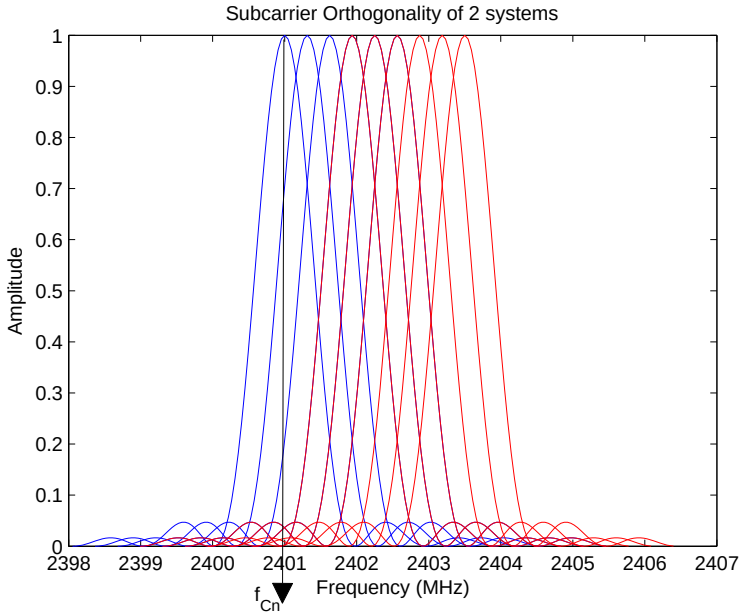

Figure 4.4: Simplified plot of 2 OFDM systems partially overlapping in frequency with their subcarriers being independent with respect to each other, i.e. the overlapping subcarrier centre frequencies f_{c_n} of the two systems are exactly the same.

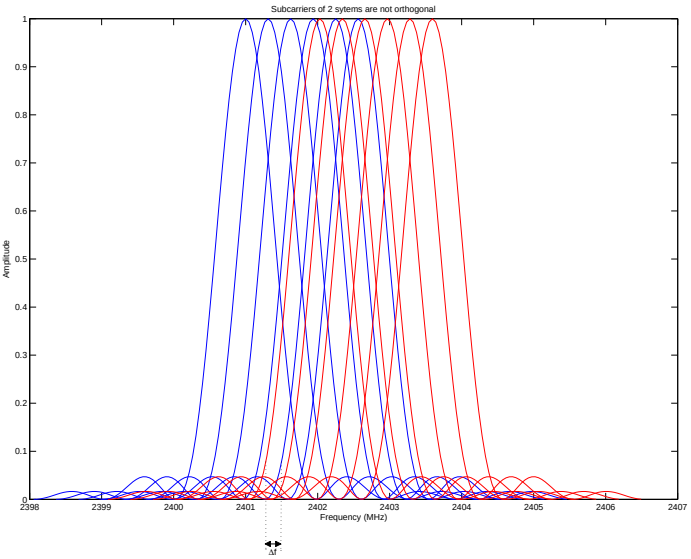

Figure 4.5: Simplified plot of 2 OFDM systems, but this time with non-orthogonal mutual subcarriers introducing a phase shift Δ_f between the overlapping subcarriers of the two systems.

4.2 Signal to Interference plus Noise Ratio

Having defined the different scenarios and their conditions in the previous section, we move on to obtain the signal to interference plus noise ratio (SINR), γ in this part. To do this we first need to define the signals associated with the networks under study, i.e., 802.11n, 802.11g and 802.11b, from here on denoted as N , G and B respectively. We start by giving the general OFDM-MIMO signal generated in an N network, which is of the form [9]

$$s_n(t) = \frac{1}{\sqrt{N^{Tone} N_{STS}}} \sum_{m}^{M} \sum_{i_{STS}}^{N_{STS}} \sum_{i=-\infty}^{\infty} Q_{i_{STS}} X_m(i) e^{j2\pi(f_0 + m\Delta_F)t} w(t), \tag{4.1}$$

where $X_m(i)$ is the i^{th} coefficients of a set of complex numbers on the m^{th} subcarrier representing data, pilot or training symbols specified in Chapter 2. $\frac{1}{\sqrt{N^{Tone} N_{STS}}}$ is a scaling factor to ensure that the total power of the time domain signal summed over all transmit chains has a maximum of 1. This factor depends on the number of space time streams (STS) N_{STS} and the number of tones per field N^{Tone} discussed in Chapter 2. The parameter Δ_F is the subcarrier frequency spacing determined at 312.5 KHz (40/128 MHz, [22]) and f_0 is the lowest carrier frequency, used to determine all other carrier frequencies through $f_m = f_0 + m\Delta_F$. $Q_{i_{STS}}$ is set to map the i_{STS} STS signals to the transmit chains of the MIMO system and finally $w(t)$ is a time-windowing function to set the boundaries of each frame. All these parameters are described in more detail in chapter 2. The transmitted OFDM signal in the G network is given by [26, Ch. 12]

$$s_g(t) = \sum_{m=0}^{M-1} \sum_{i=-\infty}^{\infty} b_m(i) \exp(j2\pi f_m t) p(t - iT), \tag{4.2}$$

where M stands for the number of subcarriers, $p(t)$ is the filter response of the transmitter that defines the time bounderies of each OFDM symbol and $b_m(i)$ is the set of complex numbers with the data. The signal transmitted in the B network, which is based on the direct sequence spread spectrum (DSSS) modulation technique is given by [26]

$$s_b(t) = x(t) s_c(t) \cos(2\pi f_c t), \tag{4.3}$$

where $x(t) = \sum_l s_l g(t - lT_s)$ is the baseband modulated (BPSK/QPSK) signal with $g(t)$ being a shaping pulse, T_s the symbol time and s_l the symbol transmitted over the lth symbol time, $s_c(t)$ is the DSSS spreading code [26, Ch. 13] and $\cos(2\pi f_c t)$ is the carrier. To define γ, the scenario depicted in figure 4.2 is used and the following five possible configurations are considered:

- γ_{nn}: SINR with N being VICTIM and N being INTERFERER
- γ_{ng}: SINR with N being VICTIM and G being INTERFERER
- γ_{nb}: SINR with N being VICTIM and B being INTERFERER
- γ_{gn}: SINR with G being VICTIM and N being INTERFERER

- γ_{bn}: SINR with B being VICTIM and N being INTERFERER

The wireless channel the EM signal is propagating through is modelled as an Addititive White Gaussian Noise channel (AWGN). Depending on which configurations is considered, indicated by γ_{xx} for The channel impulse response that follows dependent on the above given possibilities, then will be

- $h_{nn}(t)$: channel impulse response between N T_X and N R_X;
- $h_{gg}(t)$: channel impulse response between G T_X and G R_X;
- $h_{gn}(t)$: channel impulse response between G T_X and N R_X;
- $h_{ng}(t)$: channel impulse response between N T_X and G R_X;

for the interference between N and G networks, and

- $h_{nn}(t)$: channel impulse response between N T_X and N R_X;
- $h_{bb}(t)$: channel impulse response between B T_X and B R_X;
- $h_{bn}(t)$: channel impulse response between B T_X and N R_X;
- $h_{nb}(t)$: channel impulse response between N T_X and B R_X;

for the interference between N and B networks. First we start with the scenario where both VICTIM and INTERFERER are N networks. For the sake of simplicity we assume symmetrical geographic and electric conditions between the two networks and thus we can consider their reciprocal interference effects as identical. This enables us to calculate the SIR of one of them, which can be assumed to be equal for the other N network. Consequently, we will have at the receiver the signal of the form

$$\begin{aligned} r_{nn}(t) &= h_{nn}(t) * s_{n1}(t) + h_{nn}(t) * s_{n2}(t) + n(t) \\ &= h_{nn}(t) * [s_{n1}(t) + s_{n2}(t)] + n(t), \end{aligned} \tag{4.4}$$

where s_{n1} and s_{n2} are the transmitted signals from the VICTIM and INTERFERER respectively and $n(t)$ is the noise introduced by the channel which is assumed to be white Gaussian noise. Continuing with interference from a G network, we will detect a signal at the N receiver of the form

$$r_{ng}(t) = h_{nn}(t) * s_n(t) + h_{gn}(t) * s_g(t) + n(t) \tag{4.5}$$

Followed by the expression for the received signal in case B is the interfering source which is of the form

$$r_{nb}(t) = h_{nn}(t) * s_n(t) + h_{bn}(t) * s_b(t) + n(t) \tag{4.6}$$

In case G is the VICTIM 's network and N is the INTERFERER , the signal on the G receiver will be of the form

$$r_{gn}(t) = h_{gg}(t) * s_g(t) + h_{ng}(t) * s_n(t) + n(t) \tag{4.7}$$

In the final scenario B will VICTIM and N will be INTERFERER and the signal on the receiver will be:

$$r_{bn}(t) = h_{bb}(t) * s_b(t) + h_{nb}(t) * s_n(t) + n(t), \tag{4.8}$$

In [27, Ch. 5] a general method to derive the signal to interference ratio is discussed where by means of the Fourier transform the time domain signals are transformed to the frequency domain to derive the power spectral densities (PSD) and the power to interference ratios. We will apply the same method to derive the SIR's. The convolutions in the time domain in (4.4-4.8) change into multiplications when performing the Fourier transform on them, yielding the PSD's of the received signals. (4.4) then becomes

$$S_{nn}(f) = H_{nn}(f)[S_{n1}(f) + S_{n2}(f)] + N_n \tag{4.9}$$

(4.5) will transform into:

$$S_{ng}(f) = H_{nn}(f)S_n(f) + H_{gn}(f)S_g(f) + N_n, \tag{4.10}$$

and (4.6) will be of the form

$$S_{nb}(f) = H_{nn}(f)S_n(f) + H_{bn}(f)S_b(f) + N_n, \tag{4.11}$$

We continue with the PSD's of the received signals in case N is INTERFERER . For the G network we transform (4.7) and find

$$S_{gn}(f) = H_{gg}(f)S_g(f) + H_{ng}(f)S_n(f) + N_g, \tag{4.12}$$

Transforming (4.8) leads for the signal in the B network to

$$S_{bn}(f) = H_{bb}(f)S_b(f) + H_{nb}(f)S_n(f) + N_b, \tag{4.13}$$

For all the given PSD's we have used the property of the Fourier transform for a time domain signal, where

$$X(f) = \mathcal{F}[x(t)] = \int_{-\infty}^{\infty} [w(t)]e^{-j2\pi ft}dt \tag{4.14}$$

Further we note that N_n and N_g and N_b are the PSD's of the noises introduced by the channel and through the receivers of the N , G and B networks respectively. Consequently, by taking the area under the PSD functions, we can derive the normalized average powers [31, Ch. 6.2-4] of the desired signals at the receivers. Thus, at the N receiver - for all scenarios that N is VICTIM - we obtain the power of the N signal as:

$$P_n = \int_0^{\infty} |H_{nn}(f)|^2 S_{n1}(f)df \tag{4.15}$$

and the power of the signal from the INTERFERER at the N receiver as:

$$I_n = \int_0^{\infty} |H_{nn}(f)|^2 S_{n2}(f)df \tag{4.16}$$

for N ,

$$I_g = \int_0^\infty |H_{gn}(f)|^2 S_g(f) df \tag{4.17}$$

for G and

$$I_b = \int_0^\infty |H_{bn}(f)|^2 S_b(f) df \tag{4.18}$$

for B . With the derived signal powers of the concerned networks, we can define the signal to interference plus noise ratios γ_{nn}, γ_{ng} and γ_{nb} for respectively interference from an N , G and B network to the N network as [19, Ch. 6]:

$$\gamma_{nn} = \frac{P_n}{I_n + N_n B_n}, \tag{4.19}$$

where both VICTIM and INTERFERER are N networks. In case N is VICTIM and G is INTERFERER we yield

$$\gamma_{ng} = \frac{P_n}{I_g + N_n B_n}, \tag{4.20}$$

and when N is VICTIM and B is interferer we have

$$\gamma_{nb} = \frac{P_n}{I_b + N_n B_n}, \tag{4.21}$$

In (4.19-4.21 B_n is defined as the operating frequency bandwidth of the N network. The same method as described above can be applied to calculate the SINR's of the G and B networks. In order to do this for the G network, we have to repeat the steps from (4.12) on and accordingly calculate the power of the G signal at the G receiver as:

$$P_g = \int_0^\infty |H_{gg}(f)|^2 S_g(f) df \tag{4.22}$$

and the power of the N network being INTERFERER as:

$$I_n = \int_0^\infty |H_{ng}(f)|^2 S_n(f) df \tag{4.23}$$

which leads us directly to the SINR in the G network in case of an interfering N network, i.e.,:

$$\gamma_g = \frac{P_g}{I_n + N_g B_g}, \tag{4.24}$$

with B_g the bandwidth of the G network. We repeat this procedure for the B network and find the B signal power at its receiver as:

$$P_b = \int_0^\infty |H_{bb}(f)|^2 S_b(f) df \tag{4.25}$$

and the power of the N network being INTERFERER as:

$$I_n = \int_0^\infty |H_{nb}(f)|^2 S_n(f) df \tag{4.26}$$

This leads to an SINR in the B network with an interfering N network of:

$$\gamma_b = \frac{P_b}{I_n + N_b B_b}, \tag{4.27}$$

where B_b is the bandwidth of the B network.

4.3 Probability of Error

In this section we study the effects of interference between the related networks in terms of the probability of bit error. Since we have assumed there is no active medium access mechanism present, medium contending devices will transmit their data, even if the medium is busy. Consequently, signals of two simultaneously transmitting devices, will interfere, resulting in signal degradation such way that at the receiver the original bits forming the signal cannot be recovered anymore which leads to bit errors. Having said that, we find that the probability of error will deteriorate in the presence of interference. Therefore it will be a good measure of the interference effects impinged upon the observerd network. We try to calculate the probaility of error for the three networks that are considered: 802.11n (N), 802.11g (G) and 802.11b (B).

4.3.1 802.11n

For the N network it is required to calculate the BER for three different scenarios, i.e. for interference from another N network, a G network and a B network. The general form of a N signal is given by equation 4.1 in Section 4.2 and without loss of generality we can leave out the normalization factor and the time windowing function in this equation and yield

$$s_n(t) = \sum_{m=0}^{M-1} \sum_{i_{STS}=0}^{N_{STS}-1} \sum_{i=-\infty}^{\infty} Q_{i_{STS}} X_m(i) \exp(j2\pi f_m t) p(t - iT), \tag{4.28}$$

where $p(t)$ is the transmitter filter response. To calculate the BER we will use the approach as performed in [28] where the BER is calculated for an OFDM system experiencing interference from an Ultra Wideband system and apply this to our situation. When transmitted through the channel, $s_n(t)$ will be influenced by the channel impulse reponse

$$h(t) = \sum_{n=0}^{N-1} a_n \delta_(t - \tau_n) e^{j\theta_n}, \tag{4.29}$$

where a_n, τ_n, θ_n and N are the amplitude, time of arrival, phase of arrival and the number of multipath components of the channel impulse response respectively. This will cause the input at the receiver to have the form:

$$r_n(t) = s_n(t) * h(t) + n(t), \tag{4.30}$$

where $n(t)$ is noise added by the channel that is modelled as AWGN. By replacing $s_n(t)$ and $h(t)$ by equations 4.28 and 4.29 respectively, we get

$$\begin{aligned} r_n(t) = & \sum_{n'=0}^{N-1} \sum_{m=0}^{M-1} \sum_{i_{STS}=0}^{N_{STS}-1} \sum_{i=-\infty}^{\infty} Q_{i_{STS}} a_n X_m(i) e^{j2\pi f_m (t - iT - \tau_n - \tau_{STS}) + \theta_n} p(t - iT - \tau_n - \tau_{STS}) \\ & + n(t), \end{aligned} \tag{4.31}$$

where τ_{STS} is the delay at the receiver introduced by the associated STS stream. The decision device at the receiver is used to determine the values of the data modulated on a specific subcarrier. This is performed through the decision variable denoted as

$$z_k = \int_0^T r(t)p(t)e^{-j2\pi f_k t} \tag{4.32}$$

Thus, to retrieve the data on the k^{th} subcarrier, the equation for the decision variable z_k is set up as

$$\begin{aligned} z_k = & \sum_{n=0}^{N-1}\sum_{m=0}^{M-1}\sum_{i_{STS}=0}^{N_{STS}-1}\sum_{i=-\infty}^{\infty} Q_{i_{STS}} a_n X_m(i) e^{-j[2\pi f_m(iT+\tau_n+\tau_{STS})+\theta_n]} \\ & \int_0^T e^{j2\pi(f_m-f_k)t} p(t-iT-\tau_{n'}-\tau_{STS})p(t)dt + \int_0^T n(t)p(t)e^{-2\pi f_k t}dt \end{aligned} \tag{4.33}$$

Now if we want to find the desired signal, we can make use of the properties of the $p(t)$ funtion, with amplitude 1 and the indicated duration, to fill in the bounderies of the integrals in (4.33) and write it as

$$\begin{aligned} z_k = & \sum_{n=0}^{N-1}\sum_{m=0}^{M-1}\sum_{i_{STS}=0}^{N_{STS}-1} Q_{i_{STS}} a_n \Bigg\{ X_m(-1)\int_0^{\tau_n+\tau_{STS}} e^{j[2\pi(f_m-f_k)t-\Phi_{m,n}]}dt \\ & + X_m(0)\int_{\tau_n+\tau_{STS}}^{T} e^{j[2\pi(f_m-f_k)t-\Phi_{m,n}]}dt \Bigg\} + \int_0^T n(t)e^{-2\pi f_k t}dt, \end{aligned} \tag{4.34}$$

where we recognize the 0^{th} complex symbol $b_m(0)$ and its predecessor $b_m(-1)$ and where $\Phi_{m,n} = 2\pi f_m(\tau_n + \tau_{STS}) - \theta_n$. To seperate the data on the k^{th} subcarrier from the other subcarriers, we take $m = k$ and this equation can be written as

$$\begin{aligned} z_k = & \sum_{n=0}^{N-1}\sum_{i_{STS}=0}^{N_{STS}-1} Q_{i_{STS}} a_n \left\{ X_k(-1)\int_0^{\tau_n+\tau_{STS}} e^{j\Phi_{m,n}}dt + X_k(0)\int_{\tau_n+\tau_{STS}}^{T} e^{j\Phi_{m,n}}dt \right\} \\ & + \sum_{n=0}^{N-1}\sum_{m=0,m\neq k}^{M-1}\sum_{i_{STS}=0}^{N_{STS}-1} Q_{i_{STS}} a_n \Bigg\{ X_m(-1)\int_0^{\tau_n+\tau_{STS}} e^{j[2\pi(f_m-f_k)t-\Phi_{m,n}]}dt \\ & + X_m(0)\int_{\tau_n+\tau_{STS}}^{T} e^{j[2\pi(f_m-f_k)t-\Phi_{m,n}]}dt \Bigg\} + \int_0^T n(t)e^{-2\pi f_k t}dt \end{aligned} \tag{4.35}$$

Without loss of generality, we can assume the receiver is matched to the first component of the multipath received signal and the first STS stream. Hence we assume $\tau_0 = 0$, $\theta_0 = 0$ and $Q_0 = \mathbf{I}$ is the identity matrix, for which the decision variable will get the

form

$$\begin{aligned} z_k = a_0 X_k(0) T \\ &+ \sum_{n=1}^{N-1} \sum_{i_{STS}=1}^{N_{STS}-1} Q_{i_{STS}} a_n \left\{ X_k(-1) \int_0^{\tau_n+\tau_{STS}} e^{j\Phi_{m,n}} dt + X_k(0) \int_{\tau_n+\tau_{STS}}^{T} e^{j\Phi_{m,n}} dt \right\} \\ &+ \sum_{n=0}^{N-1} \sum_{m=0, m\neq k}^{M-1} \sum_{i_{STS}=0}^{N_{STS}-1} Q_{i_{STS}} a_n \Bigg\{ X_m(-1) \int_0^{\tau_n+\tau_{STS}} e^{j[2\pi(f_m-f_k)t-\Phi_{m,n}]} dt \\ &+ X_m(0) \int_{\tau_n+\tau_{STS}}^{T} e^{j[2\pi(f_m-f_k)t-\Phi_{m,n}]} dt \Bigg\} + \int_0^T n(t) e^{-2\pi f_k t} dt \end{aligned} \tag{4.36}$$

At this point we can distinguish 4 terms in equation 4.36, where for each one a certain cause can be assigned to. The first term is the desired signal, the second term exists of all other multipaths of the same k^{th} subcarrier, indicating inter symbol interference (ISI). The third term is recognized as inter carrier interference (ICI), because of the non-orthogonality between the subcarriers caused by the Doppler effect and the fourth term is due to noise. Having these terms assigned their causes to, we can rewrite 4.36 as

$$z_k = \text{desired signal} + \text{ISI} + \text{ICI} + w_k, \tag{4.37}$$

where

$$\text{desired signal} = a_0 X_k(0) T \tag{4.38}$$

with amplitude a_0 and signal duration T. Further more ISI is written as

$$\text{ISI} = \sum_{n=1}^{N-1} \sum_{i_{STS}=1}^{N_{STS}-1} Q_{i_{STS}} a_n \left\{ X_k(-1) \int_0^{\tau_n+\tau_{STS}} e^{j\Phi_{m,n}} dt + X_k(0) \int_{\tau_n+\tau_{STS}}^{T} e^{j\Phi_{m,n}} dt \right\}, \tag{4.39}$$

ICI is written as

$$\begin{aligned} \text{ICI} = + \sum_{n=0}^{N-1} \sum_{m=0, m\neq k}^{M-1} \sum_{i_{STS}=0}^{N_{STS}-1} Q_{i_{STS}} a_n \Bigg\{ X_m(-1) \int_0^{\tau_n+\tau_{STS}} e^{j[2\pi(f_m-f_k)t-\Phi_{m,n}]} dt \\ + X_m(0) \int_{\tau_n+\tau_{STS}}^{T} e^{j[2\pi(f_m-f_k)t-\Phi_{m,n}]} dt \Bigg\} \end{aligned} \tag{4.40}$$

and

$$w_k = \int_0^T n(t) e^{\frac{j2\pi kt}{T}} dt \tag{4.41}$$

representing the noise part of the signal. Additionally, we have to account for the interference from another N , G or B network too. For the time being we denote this interference as I and add it to (4.37) as:

$$z_k = \text{desired signal} + \text{ISI} + \text{ICI} + w_k + I, \tag{4.42}$$

To cope with the ISI, OFDM is tooled with a guard interval T_G which is added to the signal duration in the following way

$$T = T_G + T' \tag{4.43}$$

This leaves equation 4.37 as

$$z_k = \text{desired signal} + \text{ICI} + w_k + I \tag{4.44}$$

Next we would like to get rid of the ICI term by assumingthat the transmitter and receiver are equipped with ICI cancellation schemes proposed in [32],[33]. Hence (4.44) can be written as:

$$z_k = \text{desired signal} + w_k + I \tag{4.45}$$

If we take BPSK as our data modulation technique, then the decision variable in 4.45 has two outcomes $\in \{0, 1\}$ and the error probability P_e is computed by setting this outcome smaller than zero, assuming a 1 has been transmitted, i.e.

$$P_e = Prob(z_k < 0 | b_k = 1) \tag{4.46}$$

In [31, Ch. 7] we find that P_e can be calculated through

$$P_e = Q\left\{\sqrt{2\frac{E_b}{N_0}}\right\}, \tag{4.47}$$

where E_b is the energy per bit and in our case is $E_b = a_0^2 T/2$. Further, we also experience interference, thus in stead of only N_0, we should also account for interference for which we introduce the variance of the decision variable z_k given by:

$$\text{var}(z_k) = \text{var}(w_k) + \text{var}(I) \tag{4.48}$$

As the noise is modeled as a Gaussion process, it has mean zero and variance $N_0/2$ in our case being

$$\text{var}(w_k) = \frac{N_0(T - T_G)}{2} \tag{4.49}$$

Now we can write (4.47) as

$$P_e = Q\left\{\sqrt{\frac{a_0^2 T}{\text{var}(z_k)}}\right\}, \tag{4.50}$$

with $Q\{.\}$ the Q-function:

$$Q(x) = \int_x^\infty \frac{1}{\sqrt{2\pi}} e^{-x^2/2} dx \tag{4.51}$$

To calculate 4.51, we first need to define I, which is the power of the interfering source. This interfering source can be an N , G or B network depending on the concerned scenario. I is a function of its power spectral density PSD_I at the carrier frequency (2.4 GHz) and the bandwidth of the N network B_n. Furthermore I is determined by the path

loss rule [19]. Accordingly, in case N is INTERFERER , I will be I_n and can be written as:

$$\text{var}(I_n) = PSD_n B_n (\frac{d}{d_0})^{-\gamma_0} \tag{4.52}$$

If the interfering source is a G network, then I becomes I_g and will be of the form

$$\text{var}(I_g) = PSD_g B_n (\frac{d}{d_0})^{-\gamma_0} \tag{4.53}$$

And in case in INTERFERER $I = I_b$ and is written as:

$$\text{var}(I_b) = PSD_b B_n (\frac{d}{d_0})^{-\gamma_0}, \tag{4.54}$$

In (4.52-4.54 PSD_n, PSD_g and PSD_b are the PSD's of the signal powers in respectively the interfering N , G and B networks and d, d_0 and γ_0 are the distance between the N receiver and the interfering network, the reference distance and the path loss exponent, respectively. Eventually, since the signal's amplitude a_0 is a random variable, P_e should be averaged over the PDF of the fading $f_A(a_0)$ and we get

$$P_e = \int_0^\infty Q\left\{\sqrt{\frac{a_0^2 T}{\text{var}(z_k)}}\right\} f_A(a_0) da_0 \tag{4.55}$$

4.3.2 802.11g

In this part we look at the interference caused when an 802.11n and an 802.11g network are operating within each others range. The basic modulation scheme used in the 802.11g standard is Orthogonal Frequency-Division Multiplexing (OFDM) where data is modulated onto independent subcarriers that have no mutual interference because of their orthogonality. An OFDM signal formed as:

$$s_g(t) = \sum_{m=0}^{M-1} \sum_{i=-\infty}^{\infty} b_m(i) \exp(j2\pi f_m t) p(t - iT), \tag{4.56}$$

where M stands for the number of subcarriers and $p(t)$ is the filter response of the transmitter that defines the time bounderies of each OFDM symbol. After transmission, the signal will pass through the channel being affected by the channel impulse response given by (4.29) and result at the G receiver as the signal of the form:

$$r_g(t) = \sum_{n=0}^{N-1} \sum_{m=0}^{M-1} \sum_{i=-\infty}^{\infty} a_n b_m(i) e^{j[2\pi f_m (t - \tau_n - iT) + \theta_n]} p(t - iT - \tau_n) + n(t) \tag{4.57}$$

At the receiver the decision variable z_k is taken to gain the data associated with carrier f_k. Making use of the same method performed to calculate z_k in the previous part, we can set up the equation for the decision variable in this case as:

$$z_k = \text{desired signal} + w_k + I_n, \tag{4.58}$$

which is already the simplified equation with the ISI and ICI removed as explained in the previous part. I_n denotes the interference from an N network. Accordingly, the error probability can be written as

$$P_e = Q\left\{\sqrt{\frac{a_0^2 T}{\mathrm{var}(z_k)}}\right\}, \tag{4.59}$$

and the variance of z_k as

$$\mathrm{var}(z_k) = \mathrm{var}(w_k) + \mathrm{var}(I_n) \tag{4.60}$$

The noise we already determined in (4.51) and the calculation of the variance of I_n is done by means of the N 's network signal power spectral density PSD_n at the carrier frequency (2.4 GHz), the bandwidth of the 802.11g system B_G and again the path loss rule. Accordingly we have for this

$$\mathrm{var}(I_n) = PSD_n B_G (\frac{d}{d_0})^{-\gamma_0}, \tag{4.61}$$

At last the bit error probabilty is given by

$$P_e = \int_0^\infty Q\left\{\sqrt{\frac{a_0^2 T}{\mathrm{var}(z_k)}}\right\} f_A(a_0) da_0 \tag{4.62}$$

4.3.3 802.11b

This section covers the interference between an 802.11n and 802.11b network with respect to bit error probabilities. The 802.11b standard [15] uses direct-sequence spread spectrum (DSSS) modulation technique to cope with interference and to allow multiple users to share the bandwidth. Also complementary code keying (CCK) is used for this purpose but this analysis focuses only on the DSSS technique. A DSSS transmitted signal in 802.11b has the form

$$s_b(t) = x(t) s_c(t) \cos(2\pi f_c t), \tag{4.63}$$

where $x(t)$ is the baseband modulated signal and $s_c(t)$ the spreading code. This signal will be affected by the channel $h(t)$ defined in (4.29), also introducing interference $I(t)$ and AWGN $n(t)$. What follows as input at the receiver is given by

$$\begin{aligned} r_b(t) &= s_b(t) * h(t) + n(t) + I(t) \\ &= \sum_{n=0}^{N-1} a_n x(t-\tau_n) s_c(t-\tau_n) \cos(2\pi f_c t) + n(t) + I(t) \end{aligned} \tag{4.64}$$

After reception demodulation of the carrier takes place and then after synchronization, the spreading code $s_c(t-\tau_n)$ is used to despread the received signal, where τ_n accounts for the delay associated with the current multipath component. As described in more detail in [19, Ch. 13], the input to the matched filter after despreading is given by

$$\begin{aligned} \widehat{x}(t) = a_n &\left[([x(t) s_c(t) \cos(2\pi f_c t)] \star h(t)) s_c(t-\tau_n) cos(2\pi f_c t + \phi)\right] \\ &+ n(t) s_c(t-\tau_n) \cos(2\pi f_c t + \phi) \\ &+ I(t) s_c(t-\tau_n) \cos(2\pi f_c t + \phi), \end{aligned} \tag{4.65}$$

where ϕ is set for the phase of the receiver carrier to match to the carrier phase of the received signal. Assuming there is no multipath and the receiver ideally synchronizes with $\tau_n = 0$, i.e. $h(t) = \delta(t)$ and $\phi = 0$, (4.65) will reduce to

$$\begin{aligned}\widehat{x}(t) &= a_0 x(t) s_c^2(t) \cos^2(2\pi f_c t) + n(t) s_c(t) cos(2\pi f_c t) + I(t) s_c(t) cos(2\pi f_c t) \\ &= a_0 x(t) \cos^2(2\pi f_c t) + n(t) s_c(t) cos(2\pi f_c t) + I(t) s_c(t) cos(2\pi f_c t),\end{aligned} \tag{4.66}$$

since $s_c^2(t) = 1$. At the output of the matched filter over one symbol time T_s will be [19, Ch. 13]

$$\widehat{s_l} \approx a_0 s_l + n_l + I_{n_l}, \tag{4.67}$$

where s_l, n_l and I_{n_l} are the data, noise and interference from an N network respectively. (4.67) is input to the decision device where the decision variable z_l is used to determine the error probability given that the data is BPSK modulated. z_l is defined as

$$z_l = a_0 s_l + n_l + I_{n_l} \tag{4.68}$$

and the error probability P_e for the case the sampled signal is less then zero, given a 1 has been transmitted is given by (4.44). Assuming the decision variable is a Gaussian random variable, P_e becomes

$$P_e = Q\left\{\sqrt{\frac{a_0^2 T_s}{\text{var}(z_l)}}\right\}, \tag{4.69}$$

where the variance of z_l is given by

$$\text{var}(z_l) = \text{var}(n_l) + \text{var}(I_{n_l}), \tag{4.70}$$

where

$$\text{var}(n_l) = \frac{N_0 B_{DSSS}}{2}, \tag{4.71}$$

with B_{DSSS} as the bandwidth of the DSSS system and for the variance of I_{n_l} we derive a similar equation as for the N and G systems discussed previously, i.e.

$$\text{var}(I_{n_l}) = PSD_{I_n} B_{DSSS} (\frac{d}{d_0})^{-\gamma_0} \tag{4.72}$$

Finally for the error probability, according to the method discussed earlier, we find

$$P_e = \int_0^\infty Q\left\{\sqrt{\frac{a_0^2 T_s}{\text{var}(z_l)}}\right\} f_A(a_0) da_0 \tag{4.73}$$

Since with BPSK modulation a symbol consist of one bit only, the symbol time equals the bit time and for simplicity we can replace T_s by T and write (4.72) as

$$P_e = \int_0^\infty Q\left\{\sqrt{\frac{a_0^2 T}{\text{var}(z_l)}}\right\} f_A(a_0) da_0 \tag{4.74}$$

Parameter	N	G	B
N_{SD}: Number of data subcarriers	108	48	
N_{SP}: Number of pilot subcarriers	6	4	
N_{ST}: Total number of subcarriers	114	52	
Δ_F: Subcarrier frequency spacing	312.5 KHz	312.5 KHz	
T_{FFT}: FFT/IFFT period	3.2μs	3.2μs	
T_{GI}: Guard interval length	0.8μs	0.8μs	
T: OFDM symbol length	4μs	4μs	
B: Operating frequency bandwidth	40 MHz	20 MHz	20 MHz
G_p: DSSS Processing Gain			11
PSD: Power Spectral Density in W/Hz	3.125×10^{-9}	6.25×10^{-9}	4.55×10^{-10}

Table 4.1: Parameters for the different networks

4.3.4 BER Results

Having defined the BER equations in the previous sections for the different networks and scenarios, in this section the results of these derivations are presented in the form of graphs, obtained in *Matlab*. In order to draw these graphs, we first need to define the specific parameters associated with the different networks, e.g. operating bandwidth, number of subcarriers, symbol durations, etc. The values for these parameters are denoted in table 4.1. The value of the PSD in a B network denoted in Table 4.1 is determined by acquiring knowledge about the processing gain or spreading gain G_p of the DSSS system. From [26, Ch. 13] we learn that G_p is related to the bandwidth of the modulated (BPSK/QPSK) signal B and the bandwidth of the spreading code B_c through

$$G_p = \frac{B_c}{B} = \frac{R_{ch}}{R_s}, \tag{4.75}$$

where R_{ch} is the chip rate and R_s the symbol rate. With the knowledge that the chip rate of the spreading code is 11 million chips per second (Mcps) [15, Ch. 18.4], thus $R_{ch} = 11$ Mcps and assuming BPSK modulation where the data rate is equal to the symbol rate is 1 Mbps, the processing gain would be $G_p = \frac{11\times10^6}{1\times10^6} = 11$. Spreading the data signal by the spreading code, makes the bandwidth of the signal increase by a factor G_p and to ensure that the area under the PSD graph remains the same, thus $B * PSD = 100$mW, the height of the PSD is divided by G_p. This a new value for the PSD is attained which is much smaller and difficult to distinguish from noise. However, the use of QPSK as modulation technique to obtain 11 Mbps, determines the data rate at 11 Mbps and thus the symbol rate at 5.5 Mbps, leading to a processing gain of $11/5.5 = 2$. The measurements discussed in the previous chapter were performed at a data rate of 11 Mbps and according to this we assume the value of the processing gain to be $G_p = 2$ and the PSD to be $100\text{mW}/(20 \times 10^6 \times 2) = 2.5 \times 10^{-9}$W/Hz. The PSD values of signals in the three considered standards are denoted in tabel 4.1.

With the aid of the equations from the previous section, and the parameters defined in Table 4.1 the plots in Figure 4.6 and Figure 4.7 are made assuming two values of the pathloss exponent, namely $\gamma_0 = 3.0$ and $\gamma_0 = 3.5$ respectively. These values are based

on typical pathloss exponents for office environments given in [19, Ch. 2]. Instantly

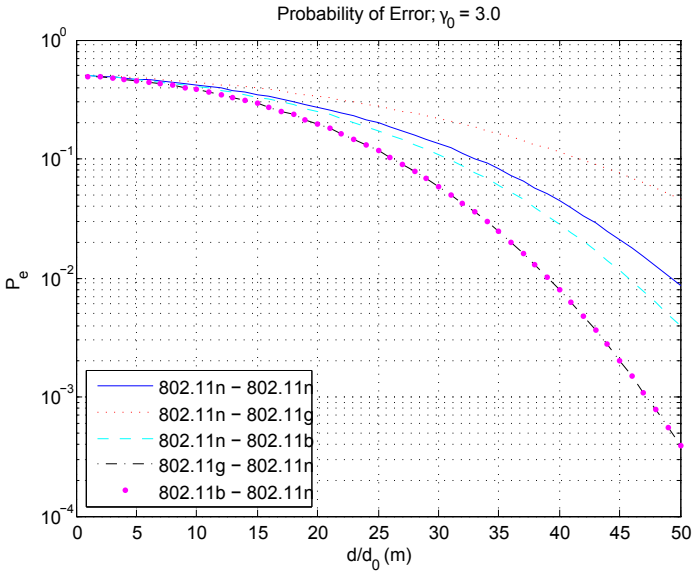

Figure 4.6: Plots of P_e against normalized distance d/d_0 for $\gamma_0 = 3.0$ and different interference scenarios

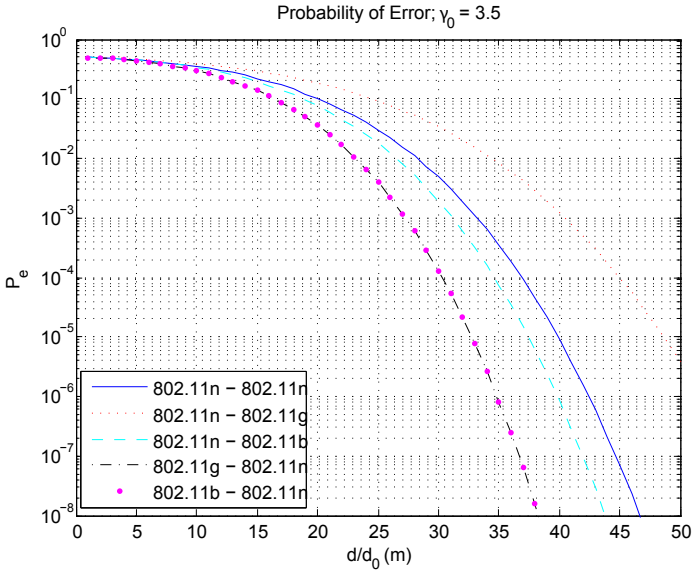

Figure 4.7: Plots of P_e against normalized distance d/d_0 for $\gamma_0 = 3.5$ and different interference scenarios

we can remark the great differences in the P_e for the different values of γ_0 which can be explained by the fact that a higher value of γ_0 results in a higher pathloss caused by the channel. This fact ensures that the impact of the interfering network at greater

distances is reduced and as a result smaller error probabilities are realized. Also we see in the plots that as the distance increases, the error probabilities of the G and B network, experiencing interference from N , decrease faster than the others. This is due to the PSD of the N signal which is relatively low, since the same power (100 mW [14]) is spread over a larger bandwidth, i.e. 40 MHz in stead of 20 MHz. The other reason is the relatively small operating bandwidths of the G and B networks. The highest BER comes from the scenario where the N network is interfered by the G network due to G 's highest PSD ($0.1W/16\text{MHz} = 6.25\text{nW/Hz}$) and the wider operating bandwidth (40 MHz) of the N network. Further, we see that the fourth and fifth scenario have exactly the same P_e plot, because their PSD's are equal and both experience interference from the same N network. Also we remark that when $\gamma_0 = 3.5$ and larger, in the worst case, the probability of error decreases to values smaller than 10^{-5} at $d/d_0 = 50$. Accordingly, we can say that for larger distances (beyond $d/d_0 = 50$), the channel may seem clear for assessment.

So far, the plots we have gained are based on the assumption that there is no fading, which means the attenuation factor $a_0 = 1$. However, to increase the accuracy of our results, this parameter should be modeled in order to take into account fading too. This is accomplished by modeling a_0 as a random variable and using the formula in (4.55). To analytically solve the integral in this equation would be a difficult and time consuming task. A numerical approach seems to be an easier and still accurate way to do this.

From the literature [29] we know that the definition af an integral of $f(x)$ over interval $[a, b]$ is given by

$$\int_a^b f(x)dx = \lim_{n\to\infty} \sum_{i=1}^{n} f(x_i^*)\delta x, \tag{4.76}$$

where the interval $[a, b]$ is divided into n subintervals and x_i^* are the sample points within these subintervals. The sum on the right-handside of this equation, i.e. $\sum_{i=1}^{n} f(x_i^*)\delta x$ is called the Riemann sum. The numerical method where the Riemann sum is used to approximate the total area under the graph incorporated in (4.55) is performed in *Matlab*. The source code for this is provided in Appendix B.1. Using this method the results as in Figure 4.8 and Figure 4.9 are obtained for pathloss exponents $\gamma_0 = 3.0$ and $\gamma_0 = 3.5$ respectively. The influence of the channel fading on the error probability is clear from the results. P_e still decreases as the distance increases, but with a much lower slope with respect to the cases without fading discussed before. Obviously, the fading by the channel results in higher bit error rates for greater distances. Again for lower values of the pathloss exponent, the results for P_e are higher. In the scheme with higher pathloss the influence from the other network is smaller at the considered network with the same reason as explained before. We should note though that at distances beyond 50 meters, the interference between two networks should be negligible as learned from the measurement discussed in the previous chapter. Basically, we can say that the fading introduces a too high bit error probability, knowing that without fading the results were not so dramatic. For now we continue our analysis based on this model, but we recommend for future work to consider other fading models too.

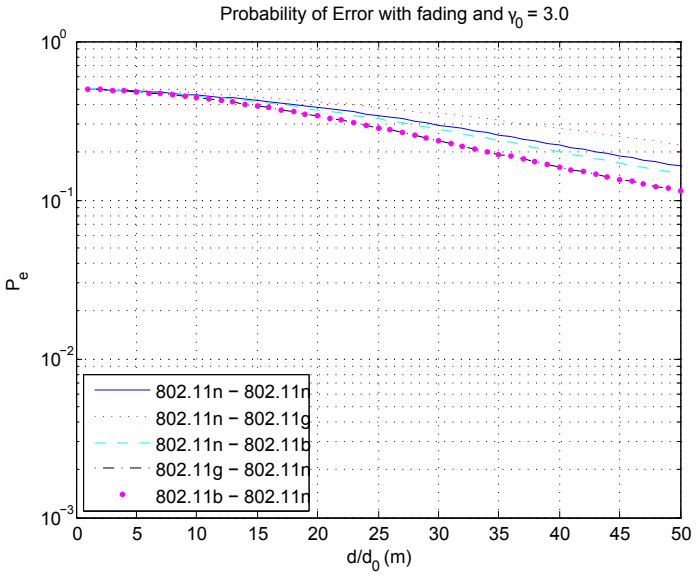

Figure 4.8: P_e against normalized distance d/d_0 for $\gamma_0 = 3.0$ with fading of the channel modeled as random variable for different interference scenarios

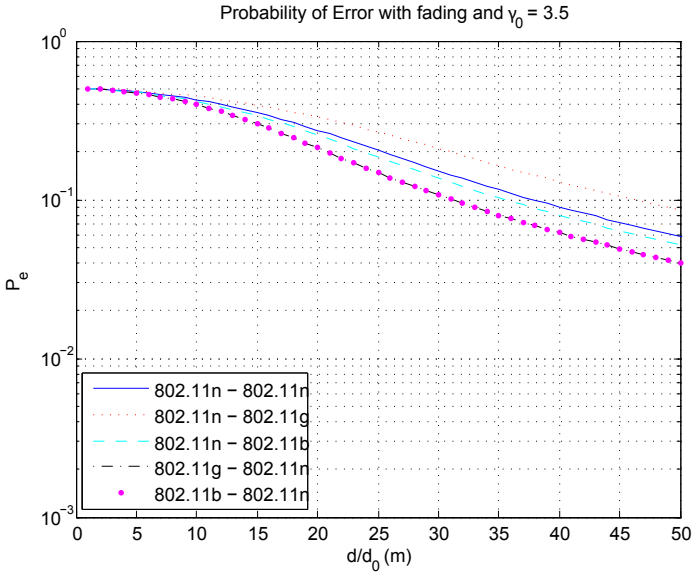

Figure 4.9: P_e against normalized distance d/d_0 for $\gamma_0 = 3.5$ with fading of the channel modeled as random variable for different interference scenarios

4.3.5 BER 64-QAM

Until now the BER was derived by assuming the data on the OFDM subcarriers is BPSK modulated. As a result the plots from the previous section were derived. In this part we will again derive results for the BER but now by assuming that the modulation type is 64-QAM (see chapter 2.2.7). This type of mapping is used to obtain the highest data

rate and therefore is frequently used. The 802.11b standard however, is not equipped with this modulation type and therefore it is left out from the further analysis. The probability of a symbol error for M-ary QAM is [30]

$$P_s = 2\left(1 - \frac{1}{\sqrt{M}}\right) Q\left\{\sqrt{\frac{3}{M-1}\frac{a_0^2 T_s}{\mathrm{var}(z)}}\right\} \tag{4.77}$$

Since we intend to derive the BER, this formula should be adjusted for the number of bits per symbol $k = N_{BPDS} =^2 \log M$ yielding

$$P_e = \frac{2}{k}\left(1 - \frac{1}{\sqrt{M}}\right) Q\left\{\sqrt{\frac{3k}{M-1}\frac{a_0^2 T_b}{\mathrm{var}(z)}}\right\}, \tag{4.78}$$

where now T_b, the bit time is used in stead of the symbol time T_s. Finally, in order to model the probability of bit error taking into account the fading a_0 too, we should average over the PDF of the fading and obtain

$$P_e = \frac{2}{k}\left(1 - \frac{1}{\sqrt{M}}\right) \int_0^\infty Q\left\{\sqrt{\frac{3k}{M-1}\frac{a_0^2 T_b}{\mathrm{var}(z)}}\right\} f_A(a_0) da_0 \tag{4.79}$$

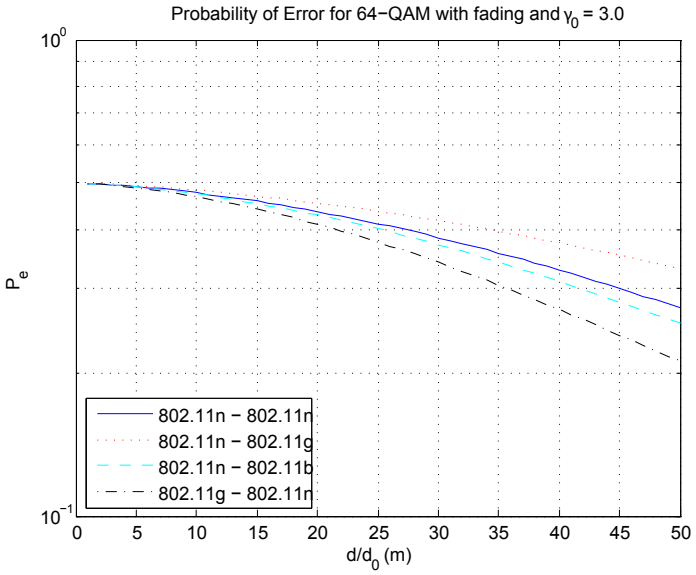

Figure 4.10: P_e for 64-QAM with pathloss exponent of 3.0

The results for 64-QAM using (4.79) are depicted in Figure 4.10 and Figure 4.11 for values of the pathloss exponent of respectively $\gamma_0 = 3.0$ and $\gamma_0 = 3.5$. It should be noted that 64-QAM modulation is more prone to errors due to its signal constellation [19, Ch. 5.3] and therefore has worse probability of error results. This fact can be easily gathered from the plots. As stated before, we would expect P_e to decrease faster with increasing distance, particularly for distances greater than 30 meters, when interference between

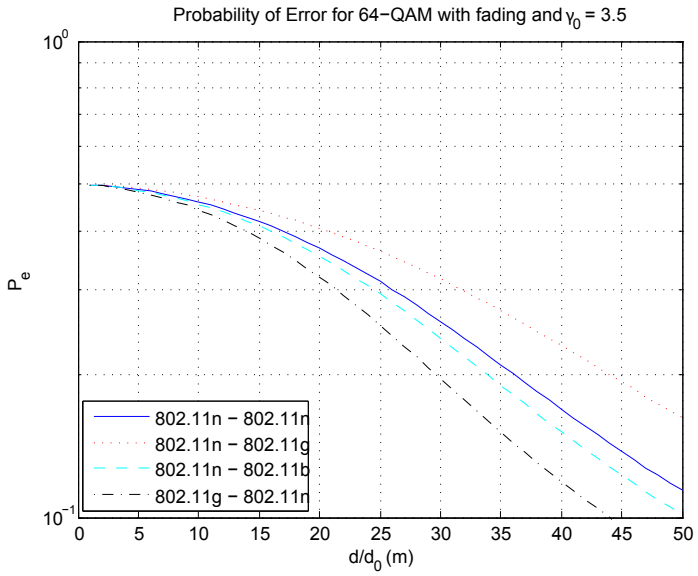

Figure 4.11: P_e for 64-QAM with pathloss exponent of 3.5

the networks should be much less. Future work can improve the channel model fading to acquire more proper results.

4.3.6 BER for MIMO systems

During the derivation of the P_e expression so far, we have considered the transmitted signal on the i^{th}_{TX} antenna and the signal on the i^{th}_{RX} receiver antenna only. Indeed, we considered a SISO system. During the measurements however, multiple transmitter antennas (three) and multiple receiver antennas (two) were present and active. The presence of these antennas enable an important feature of the MIMO technique integrated in the used routers. Spatial diversity makes it possible to transmit multiple copies of the same signal on different antennas increasing the probability that a signal is received at the receiver without an error, and thus reducing the probability of error. When an erroneous signal at the receiver cannot be recovered, it still is possible that a transmitted copy of this signal arrives at a different antenna at the receiver. This fact can explain the very low error probabilies obtained during the measurements and why they deviate so much from the analysis results. To be able to verify our presumption, we need to go one step deeper in our analysis. The results from the analysis were based on the assumption that the transmitter and receiver in a network operated with only one active antenna. In case there are more antennas, the capacity of the system increases (Section 2.1) due to a higher signal to interference plus noise ratio (SINR). For a SISO system we defined the SINR γ, in Section 4.2 as:

$$\gamma_{SISO} = \frac{P}{I + NB}, \tag{4.80}$$

where P is the power of the desired signal, I the power of the interfering signal and N the noise power. In case of a single input multi output (SIMO) sytem, the receiver uses

N_{RX} antennas resulting in N_{RX} different copies of the received signal with on average the same signal power. Combining these signals coherently, results in an $N_{RX} \times N_{RX} = N_{RX}^2$ increase in signal power at the receiver. Since N_{RX} receiver antennas exist, also N_{RX} interference plus noise sources are present. These signals add up incoherently resulting in an N-fold increase in interference plus noise power. For the SINR of the SIMO system it means the following:

$$\gamma_{SIMO} = \frac{N_{RX}^2 P}{N_{RX}(I + NB)} = N_{RX}\gamma_{SISO} \tag{4.81}$$

Accordingly, a multi input single output (MISO) system with N_{TX} transmit antennas and a single receiver antenna has an SINR given by:

$$\gamma_{SIMO} = \frac{N_{TX}^2 P}{N_{TX}(I + NB)} = N_{TX}\gamma_{SISO} \tag{4.82}$$

For a MIMO system, we have N_{TX} antennas at the transmitter and N_{TX} receive antennas. When coherently joining the N_{TX} transmitted copies of a signal at the receiver with N_{RX} antennas, an $N_{TX} \times N_{RX}$ increase of SINR is realized compared to the SISO sytem. The resulting equation for the SINR of the MIMO system is given by

$$\gamma_{MIMO} = \frac{N_{TX} N_{RX}^2 P}{N_{RX}(I + NB)} = N_{TX} N_{RX}\gamma_{SISO} \tag{4.83}$$

During the measurements the MIMO communication system consisted of three transmit antennas and two receive antennas, which leads in the most favourable case to an increase in SINR of a factor $3 \times 2 = 6$. In order to have a better comparison we need to account for this higher SINR value during our probability of error calculations. Earlier, in (4.79) the P_e is calculated based for an OFDM SISO sytem with 64-QAM modulated data. The SINR in this equation is given by the part in the Q-function under the square root sign, i.e.:

$$\gamma_{SISO} = \frac{3k}{M-1}\frac{a_0^2 T_b}{\mathrm{var}(z)} \tag{4.84}$$

To apply the SINR influence of MIMO to our model, we need to multiply (4.84) by $N_{TX}N_{RX}$ to yield

$$\gamma_{MIMO} = N_{TX} N_{RX}\frac{3k}{M-1}\frac{a_0^2 T_b}{\mathrm{var}(z)} \tag{4.85}$$

Finally, we fill this in (4.79) and find for the probability of error of an $N_{TX} \times N_{RX}$ MIMO system:

$$P_e = \frac{2}{k}\left(1 - \frac{1}{\sqrt{M}}\right)\int_0^\infty Q\left\{\sqrt{N_{TX} N_{RX}\frac{3k}{M-1}\frac{a_0^2 T_b}{\mathrm{var}(z)}}\right\} f_A(a_0)da_0 \tag{4.86}$$

Since MIMO is a feature within the 802.11n standard, we discard the scenarios were 802.11g and 802.11b based networks are VICTIM and continue with the results for the scenarios were an 802.11n network is VICTIM . Figures 4.12, 4.13 and 4.14 illustrate the

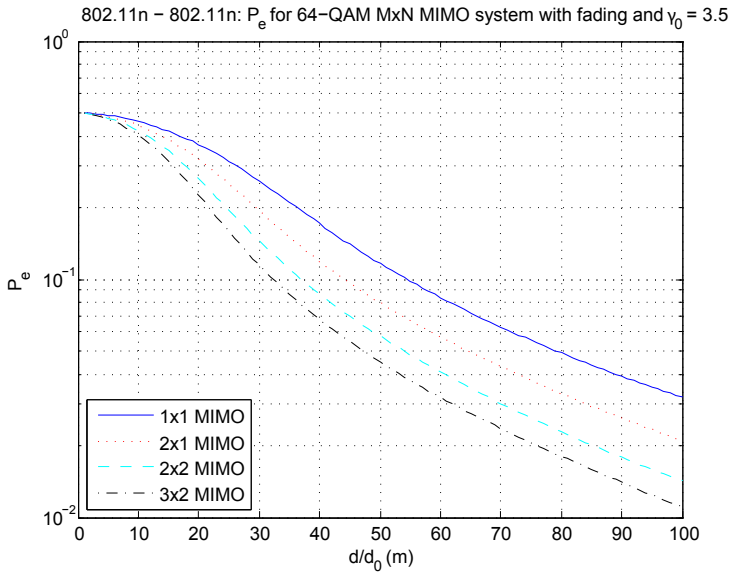

Figure 4.12: P_e for 802.11n - 801.11n scenario for 64-QAM MxN MIMO system with pathloss exponent of 3.5 and fading

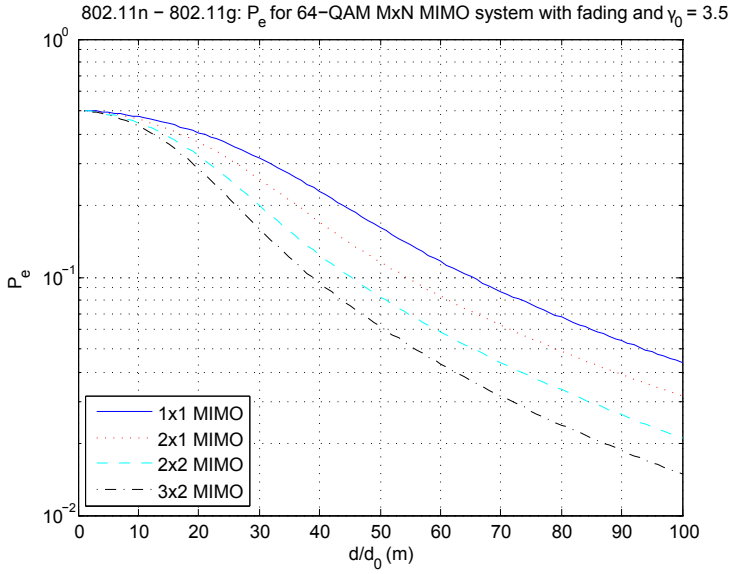

Figure 4.13: P_e for 802.11n - 801.11g scenario for 64-QAM MxN MIMO system with pathloss exponent of 3.5 and fading

P_e results for respectively the 802.11n - 802.11n, 802.11n - 802.11g and 802.11n - 802.11b scenarios. Different MIMO configurations are considered and generally it can be said that more advanced MIMO systems consisting of more antennas result in better probability of error characteristics. Obviously all figures show that a higher MIMO configuration leads to a faster decrease of P_e for all scenarios. We have increased the normalized distance up

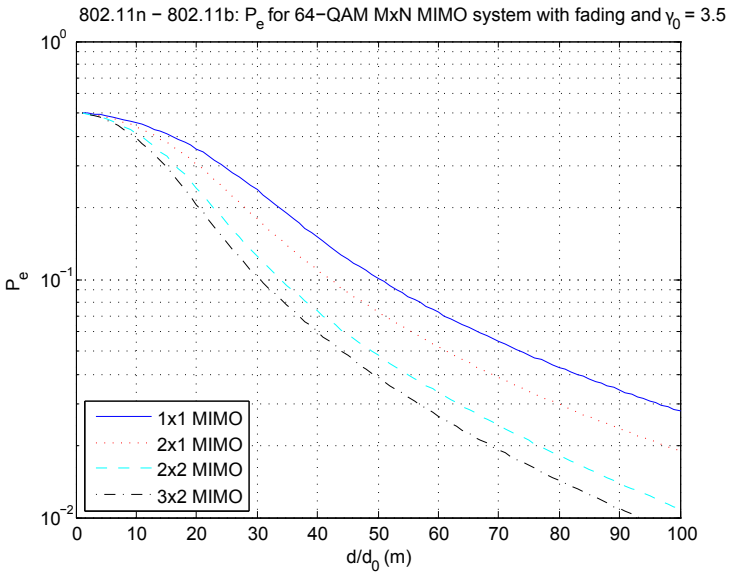

Figure 4.14: P_e for 802.11n - 801.11b scenario for 64-QAM MxN MIMO system with pathloss exponent of 3.5 and fading

to 100 meter to see if the two networks eventually do not influence each other no more, but as the plots show, P_e remains above 10^{-2} which is rather unlikely. We would expect that at distances beyond 30 meter, the probability of error would get very small. Again, future work should help to clearify this matter.

4.4 Summary

In this chapter we focused on deriving an interference model based on an interference analysis. We defined the scenarios and assumed that two 802.11b, -g or -n networks are operating near each other and cause interference to one another, given that no medium access mechanism (MAC) exists that ensures interference-free communication. We defined the signal to interference plus noise ratio as the ratio of the desired signal power to the signal power of the interfering network plus the noise. The results for the probability of error during transmissions within a network were obvious: an interfering source at close distance leads to high values of the probability of error in the order of 10^{-1} of the VICTIM 's network and as the distance to the interfering source increases, the probability of error will decrease. A higher pathloss exponant will lead to better probability of error results because more pathloss means a smaller value of the signal power of the interfering source. We saw that an enhanced modulation technique like 64-QAM has worse probability of error properties than BPSK/QPSK modulation in the presence of interference, because of its higher vulnerability to noise and interference effects. The increase in SINR, introduced by MIMO in 802.11n based devices, resulted in a decrease of the probability of error with values in the order of 10^{-2}. Still, the obtained values at distances above 50 m, were not small enough to guarantee succesfull

communication. We expect, based on our measurements (Chapter 3), that beyond 50 m, two operating networks do not have influence on each other and we suspect that the channel fading in our model has too much weight leading to poor probability of error results.

Overall, the calculated BER guarantees that no transfer is possible in case of interference, unless another mechanism is in place to prevent interference. The MAC has such mechanism as decribed in Section 2.3.

5 Conclusions

In this chapter we summarize the work done in this thesis. We mention our main contribution to the world of WLAN that we have accomplished and based on the conclusions we draw, we propose some ideas and recommendations for future work on this subject.

5.1 Summary

In Chapter 2 we discussed how MIMO technique is used to increase data rates and ensure reliable data transfer through multiplexing and spatial diversity respectively. These properties are implemented in the 802.11n standard using space time block codes and spatial division multiplexing which decomposes the transmission channel into parallel independent channels. The use of OFDM modulation ensures efficient use of the frequency spectrum. Through 64-QAM baseband modulation, a coding rate $R_c = 5/6$, a short guard interval and the employment of multiple spatial streams, PHY layer data rates up to 300 Mbit/s or 600 Mbit/s can be reached when using respectively a 2x2 or 4x4 MIMO system. Besides support of operation in the 2.4 GHz band, also operation in the 5 GHz band is provided offering frequency bandwidth as much as at least 20 non-overlapping 40 MHz channels. Further, we saw that by utilizing a carrier sense mechanism with or without the RTS/CTS extension, the MAC ensures that STAs within a certain range do not transmit in case they sense that the medium is used by other STAs, thus limiting interference caused by two stations transmitting at the same time.

Chapter 3 described the various measurement scenarios and setups that were realized during the measurement phase and the results were discussed and explained based on our theoretical knowledge. The measurements were performed at locations KPN , HOME and the unechoic chamber. Transfer throughputs and PLRs were measured and several types of scenarios were considered, e.g., STA to STA transfers, AP and STA communications, LOS transfers, measurements in a non-scattering and non-reflecting anechoic chamber, communication over multiple floors and most importantly for this work, interference scenarios consisting of two networks sharing the medium and creating interesting (interference) scenarios. We found out that the throughput and PLR in a network deviate significantly when the medium has to be shared.

From the results we concluded that medium sharing causes reduction of the throughputs of all single networks considered in order not to lead to interference. For the scenario with two 802.11n networks the medium still provides the maximum throughputs but the individual throughputs per network are lower. We have seen that the unexpected low throughputs are caused by connections between wireless 802.11n devices and computer hardware. These connections introduce a bottleneck in the

communication and limit the throughput to 100 Mbit/s. Further more, operation of the MAC protocol introduces delay in communication in case different PHY types make use of the same medium. Basically, the wireless connection with the slowest throughput, is the bottleneck in the communication. Obviously in our case, there is the 802.11b connection, which has the lowest maximum data rate of 11 Mbit/s. But generally each connection, whether it is based on the 802.11b, 802.11g or 802.11n standard, can cause this bottleneck, if due to bad channel conditions, the data rates are forced to drop to very low values. Another reason for delay in a network can be caused by a connection between a STA and an AP of any WLAN, spaced too far apart with respect to other STAs to that same AP. The longer distance leads to a longer occupancy of the medium causing lower throughputs for the entire network. Further, we learned that medium sharing of networks based on different standards leads to lower throughputs (Table 3.7) than provided by the medium due to probably incompatible CCA mechanisms. Regarding the PLR, we found that medium sharing networks based on different standards, have high PLR values (Table 3.7). We suspect that this is due to different networks deploying different CCA implementations resulting in uncompatible CCA functionalities among the 802.11n, 802.11g and 802.11b networks. Indeed, the networks imping interference upon each other. On account of this, a lot of packet losses occur, leading to the high PLR values from the measurements. Additionally, we saw that in general, low values of the throughput, correspond to high values of the PLR and vica versa. In other words: more lost packets means that less packets will arrive, leading to a lower throughput. In order to count the number of lost packets during transfers, packets were transmitted over the UDP protocol in stead of the TCP protocol. Based on the results, we suspect that the throughput using the UDP protocol is higher. We cannot confirm this though, due to the lack of time which stopped us from measuring with higher supply rates.

In Chapter 4 we have carried out an analysis based on interference. We assumed the interference scenarios as two 802.11b, -g or -n networks operating near each other and cause interference to one another, given that no medium access mechanism (MAC) exists that ensures interference-free communication. We defined the signal to interference plus noise ratio as the ratio of the desired signal power to the signal power of the interfering network plus the noise. The results for the probability of error during transmissions within a network were obvious: an interfering source at close distance leads to high values of the probability of error in the order of 10^{-1} of the VICTIM 's network and as the distance to the interfering source increases, the probability of error will decrease. A higher pathloss exponant will lead to better probability of error results because more pathloss means a smaller value of the signal power of the interfering source. We saw that an enhanced modulation technique like 64-QAM has worse probability of error properties than BPSK/QPSK modulation in the presence of interference, because of its higher vulnerability to noise and interference effects. The increase in SINR, introduced by MIMO in 802.11n based devices, resulted in a decrease of the probability of error with values in the order of 10^{-2}. We suspect that the channel fading in our model has too much weight leading to poor probability of error results. Overall, the calculated BER guarantees that no transfer is possible in case of interference, unless another mechanism

is in place to prevent interference. The MAC has such mechanism as decribed in Section 2.3.

5.2 Main Contributions

Within the framework of this work, that is interference between near located 802.11n, 802.11g and 802.11b networks, measurements were performed and an interference analysis was carried out. We have seen how the throughput within a single network is affected when the medium has to be shared with other networks. Particurly, medium sharing networks based on different standards, e.g., 802.11n and 802.11b or 802.11g networks, showed dramatic throughput fallbacks. We pointed out that:

- Data rate within an 802.11n network is limited by the maximum supported data rate of the slowest connection between transmitter and receiver. In our case the 100 Mbit/s ethernet port between the computer and the wireless router was the bottleneck in the communication.

- The available bandwidth has to be divided among the medium sharing networks that need to use the wireless medium. Parameters, like the number of antennas and the channel environment, cause certain networks to over-proportionally occupy the medium, resulting in even worse throughput performances of other simultaneously operating networks. More antennas leads to a better gain from multipath fading and a more scattering environment ensures more reflections, both leading to higher throughputs.

- In case devices from the same or within different networks, have operation, based on different standards, the maximum throughput of a transfer within these networks is limited by the devices that operate according to the standard with the lowest data rates. An 802.11n transmitter has to wait longer between subsequent packets when an 802.11b transmitter with larger packet durations occupies the medium, causing lower throughputs for the 802.11n network. Similary, a bad wireless link with poor communication properties, introduces a bottleneck in an entire network, because it switches back to a lower data rate and thus occupies the medium for a longer time.

- Networks including an AP and multiple STAs have a limited throughput caused by the STA that has the largest distance with respect to the AP. As the distance increases, the data rate of a wireless link drops according to the fallback to a lower MCS configuration. Other STAs at shorter distances now experience lower throughputs because of the delay caused by the packets with longer durations coming from the STA that is placed the farthest away from the AP.

- Medium sharing networks based on different standards most probably deploy different CCA mechanisms leading to interference between the networks. As a result the maximum throughput provided by the medium, is not achieved and both networks transfer at lower throughputs.

By measuring the PLR during transfers, we experienced that this parameter grows dramatically when two networks induce interference upon each other. Interference occurs when the networks are based on different standards, e.g. 802.11n and 802.11b/g networks. We managed to explain this by taking into account the CCA specifications. Most probably the different standards deploy different CCA functionalities. The operation of the CCA mechanism that determines whether the channel is idle or busy, depends on the type of standard and even more, the type of signal. Detection can be based on an OFDM or DSSS signal or any signal above a certain threshold. This explains the high packet losses found during the measurements in 802.11b and 802.11g networks, that do not recognize and acknowledge signals from 802.11n networks and blindly transmit their packets regardless of occupation of the medium by 802.11n networks.

Our analysis on interference confirmed that without a controlling medium access mechanism, two simultaneously operating networks induce interference upon each other leading to high BER values when the networks operate in close vicinity. Proper communication at theoretically advertised high rates then, is hard to realize.

5.3 Recommendations for Future Work

This work provided us with a detailed view in medium sharing and interference effects of IEEE 802.11b/g/n WLANs using the medium simultaneously. Yet, there still remain scenarios which are not discussed that are recommendended in this section for future work. In this section we provide general recommendations in this field, but also recommendations that are particurlarly of more concern and interest for Telecom company KPN .

5.3.1 General Recommendations

This subsection discusses general recommendations.

5.3.1.1 Comparison Measurements and Analysis

The most important point of discussion for future work is probably the comparison of the obtained measurement results to the results of the analysis, which due to the lack of time was not performed in this project. Interesting would be how the obtained PLR values during measurements would relate to an interference model based on PLR. Since our interference model was based on the BER, a translation from BER to PLR is needed to enable the comparison. One could use the theorem provided in [35], that the probability that a packet error occurs corresponds to the probability that one bit error occurs within the packet and suchway convert BER values to PLR values.

5.3.1.2 PHY Layer Data Rates

Measuring the throughput within interfering networks was of main importance during our work. However, gaining knowledge about the real data rate at the PHY layer is also interesting. Unfortunately, during our work devices measuring the PHY data rate were

not available. Future work based on measuring the PHY data rate, might lead to better material for the analysis to compare with.

5.3.1.3 Beamforming

As being one of the advanced features of MIMO communication, beamforming can contribute to increase a signal's amplitude transmitted in a VICTIM network, while the power of the signal coming from the INTERFERER network remains the same. This way the SINR in the VICTIM network is increased, leading to lower probability of bit errors in this network. This is a subject that is definitely worth to study.

5.3.1.4 Multiple Interfering Sources

In our work we considered two simultanously operating networks resulting in interference. In practice multiple interfering networks can be present leading to even worse scenarios for the performance of the networks. As an extension to our analysis, scenarios with multiple interfering sources can be considered and simulations and measurements on the performance of the networks can be performed based on them.

5.3.1.5 CCA Standardization

This recommendation is primarily addressed to the developers of the WLAN standards and is related to the CCA mechanism. Further standardization of this property to sense the status of the medium would definetely be in favour of medium sharing capabilities of WLANs. In stead of the option to detect only signals originating from other similar WLANs, the developers could also choose to support only the CCA method that is able to detect any signal above a certain predefined threshold, to ensure the medium is really unused.

5.3.1.6 802.11n vs Ultra Wideband (UWB)

As one of the major competitors to 802.11n, UWB is also struggling to survive in the world of wireless communication, providing services with 100 Mbit/s data rate in the 2.4 GHz band where interference with possible 802.11n devices is inevitable. In [12] a method is proposed to reduce interference effects between 802.11n and UWB networks, but more research should be carried out on this topic to determine which technique shows best performance while making use of the bandwidth most efficiently.

5.3.1.7 Fading

During our analysis we assumed the channel to be a Rayleigh fading model based on random fading. Future work could be devoted to an analysis considering a Rician or Nagakami fading model. Particurly Nagakami fading should be considered since it better describes the fading of wireless channels.

5.3.2 Recommendations related to KPN

This subsection covers the recommendations that could be of most interest to KPN.

5.3.2.1 Transmit Power

It is recommended not to transmit at maximum strength when there is no need for. Our measurements proved that at 10% of the maximum transmit power of APs, 802.11n networks still provide performance with high throughputs. By applying this solution, not only interference with respect to other networks is reduced, but also less energy is consumed, which is favourable for future paradigm: "Green Communicatons".

5.3.2.2 Homogeneous Networks

To ensure the support of the highest available troughputs and lowest BERs, it could be of value to deploy networks with devices that all have the same standard implemented. Our thesis pointed out that devices based on older standards that support lower data rates, serve as a bottleneck in the throughput of the entire network.

5.3.2.3 Distribution of STAs over the APs coverage area

In a network that contains an AP and multiple STAs, the maximum time delay in the network is determined by the STA that has the largest distance to the AP. By distributing the STAs in such way that the distances to the AP are just about equal, the additional delay introduced by the farthest positioned STA is taken care of and consequently the throughput within the network is not affected. Therefore, it is recommended that all the STAs are positioned at equal distances with respect to the AP.

5.3.2.4 Channel Occupany Detector

By informing WLAN users about freeware like 'Netstumbler' [5], users can detect which WIFI channels are occupied and where in the frequency spectrum is the least occupancy. 'Netstumbler' enables them to do this. As a result there will be less overlapping networks, thus less bandwidth sharing and therefore advertised maximum throughputs can be maintained. It is recommended to add freeware like 'Netstumbler' to the installation packet of WLAN users or at least inform them about it.

Bibliography

[1] http://grouper.ieee.org/groups/802/11/Reports/tgn_update.htm

[2] http://www.psc.edu/networking/projects/tcptune

[3] http://www.noc.ucf.edu/Tools/Iperf/default.htm

[4] http://www.metageek.net

[5] http://www.netstumbler.com/

[6] http://support.microsoft.com/kb/314053

[7] http://support.microsoft.com/kb/283165

[8] C.E. Shannon, "A mathematical theory of communication", Bell System Tech. J., pp. 379-423, 623-56, 1948

[9] Lorincz, J.; Begusic, Physical layer analysis of emerging IEEE 802.11n WLAN standard, Advanced Communication Technology, 2006. ICACT 2006. The 8th International Conference, Volume 1, 20-22 Feb. 2006 Page(s):6 pp

[10] T. Paul, T. Ogunfunmi, "Wireless LAN comes of age: Understanding the IEEE 802.11n Amendment", IEEE Circuits and Systems Magazine, 2008

[11] M. Petrova, L. Wu, P. Mhnen, J. Riihijrvi, "Interference measurements on performance degredation between colocated IEEE 802.11g/n and IEEE 802.15.4 networks", Networking 2007, ICN '07. Sixth International Conference, April 2007, Page(s):93-93

[12] A. Rajeswaranm, Gyouhwan Kim, R. Negi, N. Sai Shankar, "Interference Handling in UWB Versus 802.11n Networks", Communications, 2007. ICC '07. IEEE International Conference, June 2007, Page(s):4710 - 4715

[13] ANSI/IEEE Std 802.11, Part 11 Wireless Lan Medium Access control (MAC) and Physical Layer (PHY) Specifications, IEEE, 1999

[14] IEEE Std 802.11a, Part 11 Wireless Lan Medium Access control (MAC) and Physical Layer (PHY) Specifications: High Speed Physical Layer in the 5 GHZ Band, IEEE, 1999

[15] IEEE Std 802.11b, "Part 11: Wireless LAN Medium Access Control (MAC) and Physical Layer (PHY) specifications: Higher-Speed Physical Layer Extension in the 2.4 GHz Band", IEEE, 1999

[16] IEEE Std 802.11g, "Part 11: Wireless LAN Medium Access Control (MAC) and Physical Layer (PHY) specifications Amendment 4: Further Higher Data Rate Extension in the 2.4 GHz Band", IEEE, 2003

[17] IEEE Std 802.11-2007, "Wireless LAN Medium Access Control (MAC) and Physical Layer (PHY) specifications", IEEE, 2007

[18] IEEE P802.11n/D4.00, "Part 11: Wireless LAN Medium Access Control (MAC) and Physical Layer (PHY) specifications Amendment 5: Enhancements For Higher Throughput", IEEE, March 2008

[19] A. Goldsmith, "Wireless Communications", Cambridge University Press, Cambridge, 2005

[20] E. Biglieri, "MIMO Wireless Communications",Cambridge University Press, Cambridge, 2007

[21] H. Nikookar, "Advanced Topics in Digital Wireless Communications", International Research Center for Telecommunications Transmission and Radar (IRCTR) - Delft University of Technology, Delft, 2004

[22] S. Coffey, A. Kashar, A. Stephens, Joint Proposal: High Throughput Extension to the 802.11 Standard: PHY, 2006

[23] L. H. Hemming, "Electromagnetic Anechoic Chambers: A Fundamental Design and Specification Guide Door" , IEEE Electromagnetic Compatibility Society, IEEE Antennas and Propagation Society, Wiley Interscience, 2002

[24] J. Casad, "TCP-IP in 24 Hours", Sams Publishing, 2004

[25] P. Stavroulakis, "Interference Analysis and Reduction for Wireless Systems", Artech House, 2003

[26] N. Golmie, "Coexistence in Wireless Networks: Challenges and System-Level Solutions in the Unlicensed Bands", Cambridge University Press, 2006

[27] H. Nikookar, R. Prasad, "Introduction to Ultra Wideband for Wireless Communications", Springer Netherlands, 2008

[28] H. Nikookar, R. Prasad, "Optimal Waveform Design for Multicarrier Transmission through a Multipath Channel", Vehicular Technology Conference, 1997 IEEE 47th Page(s):1812 - 1816 vol.3, 1997

[29] J. Stewart, "Calculus Early Transcendetals 5th edition", McMaster University, Brooks/Cole-Thomson Learning, 2003

[30] J. G. Proakis, "Digital Communications, 4th Edition", McGraw-Hill Book Co., 1995

[31] L. W. Couch II, "Digital and Analog Communication Systems, sixth edition", Prentice-Hall, 2001

[32] Yuping Zhao, S. G. Haggman, "BER Analysis of OFDM Communication Systems with Intercarrier Interference", Communication Technology Proceedings, 1998

[33] Zhang Jianhua, H. Rohling, Zhang Ping, "Analysis of ICI Cancellation Scheme in OFDM Systems with Phase Noise", Broadcasting, IEEE Transactions, 2004

[34] J. H. Schiller, "Mobile Communications, 2nd Edition", Pearson Education Limited, 2003

[35] B. Han, S. Lee, "Efficient Packet Error Rate Estimation in Wireless Networks", Testbeds and Research Infrastructure for the Development of Networks and Communities, TridentCom 3rd International Conference, 2007

Abbreviations

ACK - Acknowledgement fg
AGC - Automatic Gain Control
AP - Access Point
CCA - Clear Channel Assesment
CCK - Complementary Code Keying
CSI - Channel State Information
CSIT - CSI at the Transmitter
DCF - Distributed Coordination Function
DIFS - DCF Inter-Frame Spacing
DSSS - Direct Sequence Spread Spectrum
FEC - Forward Error Correcting
GU - Guard Interval
HCF - Hybrid Coordination Function
HT - High Throughput
ISM - Industrial Scientific and Medical band
LOS - Line Of Sight
LSB - Least Significant Bit
MCS - Modulation and Coding Scheme
MIMO - Multiple Input Multiple Output
MISO - Multiple Input Single Output
MPDU - MAC Protocol Data Unit
PER - Packet Error Rate
PHY - Physical Layer
PLCP - Physical Layer Convergence Protocol
PMD - Physical Medium Depenent
PPDU - PLCP Protocol Data Unit
PSDU - PHY Sublayer service Data Units
PCF - Point Coordination Function
SIFS - Short Inter-Frame Spacing
SIMO - Single Input Multiple Output
SISO - Single Input Single Output
SS - Spatial Stream
STS - Space Time Stream
STA - Station

List of Major Symbols

$\mathbf{H}$	-	$N \times M$ MIMO channel matrix
$\mathbf{\Sigma}$	-	$N \times M$ diagonal matrix with singular values of $\mathbf{H}$
P_{TX}	-	Transmit power
R	-	Throughput
S	-	Suplly rate
μ_{xy}	-	Performance with respect to throughput of a system consisting of 2 networks x and y
γ	-	Signal to interference plus noise ratio
h_{xy}	-	Channel impulse response between transmitter x and receiver y
P	-	Desired signal power
I	-	Interferer's signal power
N	-	Noise power
z_k	-	Decision variable for the k^{th} subcarrier
a_n	-	Ampitude of h_{xy} for the n^{th} multipath component
τ_n	-	Time of arrival of h_{xy} for the n^{th} multipath component
θ_n	-	Phase of arrival of h_{xy} for the n^{th} multipath component
P_e	-	Probability of bit error
γ_0	-	Path loss exponent
E_b	-	Energy per bit
G_p	-	Spreading gain of a DSSS system

Other Measurement Scenarios A

A.1 Single Transfers

This section provides the results of the single-file transfers of which the data rates have been measured. Single-file transfers imply that in order to measure the data rate of a data transfer, what was an objective of the thesis, the data that was transmitted existed of a single file. Later in this chapter we will see what happens if multiple files are transmitted simultaneously. The measurements discussed in this section are performed at KPN , HOME and the anechoic chamber.

A.1.1 KPN Office Environment

The *Device Competence Center* (DCC) is a department within *KPN* on the first floor of a nine storeys high building. It is a division where tests are performed on different customer products like *Digitenne* and *Interactive TV*. Herefore the place is full of (wireless) modems, transmitting and receiving data wirelessly equipped with the 802.11g standard. Measuring the throughput of 802.11n networks in such a place gives a good indication of the effects of 802.11g modems on this throughput. Different configurations are tested and the results are denoted in the following subsections.

A.1.1.1 STA to STA Transmission

The first measurements are performed according to the measurement setup depicted in figure A.1 where data transfer is taking place between one wireless station STA1 and another wireless station STA2. These stations are *Acer* notebooks equipped with *Sweex USB 2.0 Adapters 300 MBPS* and as their names indicate, they should be able to acquire data rates of 300 Mbit/s. During data transfers from one station to the other, the transfer throughput is measured by the aid of the *Performance* tool on Microsoft XP. Simultaneously the 2.4 GHz WLAN channel is being observed using software called *Channelyzer 2.1* (see figure 3.1) together with a *Wi-Spy* USB dongle that measures the frequency channel. In figure A.2 the data throughput of an arbitrary transfer of data between the 2 stations is depicted for a period of $t = 100$ seconds and a distance of 3 meter between the antennas, representing the average throughput between any 2 of these stations in such a setup.

From this graph it can be seen that the average received byte/s is approximately 2.9×10^6 which equals a throughput of 23.2 Mbit/s, not even near the high throughputs that are expected in an 802.11n network. This can be explained by the fact that the Sweex wireless adapters cannot operate in the 802.11n mode without an access point. Besides,

these adapters are only equipped with one antenna and thus can never satisfy the MIMO requirements of 802.11n of having at least 2 antennas at the transmitter and receiver to increase transmission rates.

A.1.1.2 AP and STA Data Transfer

For the next measurements the configuration as depicted in figure A.3 is used where data is transmitted from one notebook, wired to a SWEEX router acting as an AP, to another notebook with a emphSweex wireless adapter, being the wireless station STA1 and the other way around. For these data transmissions the router settings as can be seen in figure A.4 were used.

An interesting point to mention is the operation in the **GF** (Green Field) mode only which means only High Throughput packets are transmitted and received. More information about these packets and this mode can be found in [22]. In Section 3.3.1.2 we have showed how to calculate the length of these packets. Another point is the wireless frequency channel where the data transfer takes place which is channel 13. This choice has been made because channel 13 has proved to be a non-crowded channel at this location, and thus can be used as a good reference. The **MCS** (Modulation and Coding Scheme) is set to 15 [22, App. A] to reach the highest supported data rate of 300 Mbit/s.

During the transfer the throughput is measured by a more advanced program called "*Bandwidth Monitor*". With this software data from different measurements can be stored and processed in *Matlab*, and consequently be compared with each other. The results of these measurements are depicted in figure A.5 where the transmitter and receiver where placed 1.5 meter apart and space-time channel fluctuations could not be avoided due to people moving around in the building and in and out the room.

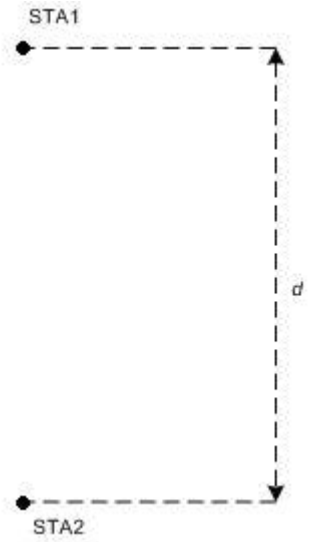

Figure A.1: Measurement setup with two wireless stations placed a distance d from each other

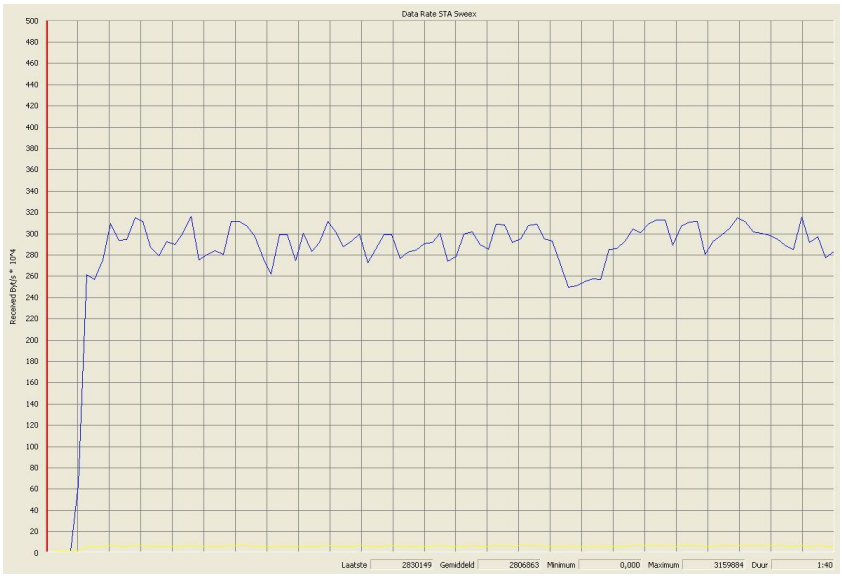

Figure A.2: Throughput for transmission between two wireless *Sweex stations*

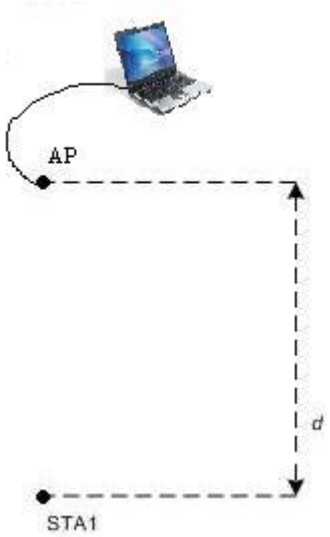

Figure A.3: Measurement setup with data transfer between an AP and STA1

The average downlink (AP to STA1 throughput) followed from these measurements is 40.4 Mbit/s and the average uplink (STA1 to AP throughput) is 37.0 Mbit/s, two values lying not too far from each other. Already an increase compared to the throughput of the transfer between the two SWEEX wireless adapters but still not near the theoretically expected 300 Mbit/s data rate at the PHY layer. The graph in figure A.5 shows large fluctuations in time caused by the dynamic character of the channel. As one can see, even the movement of people in the room effects the throughput of the transfer, because with every change in the channel parameters, the MIMO transmitter and receiver need to calculate new and appropriate channel matrix parameters in order to reach to the

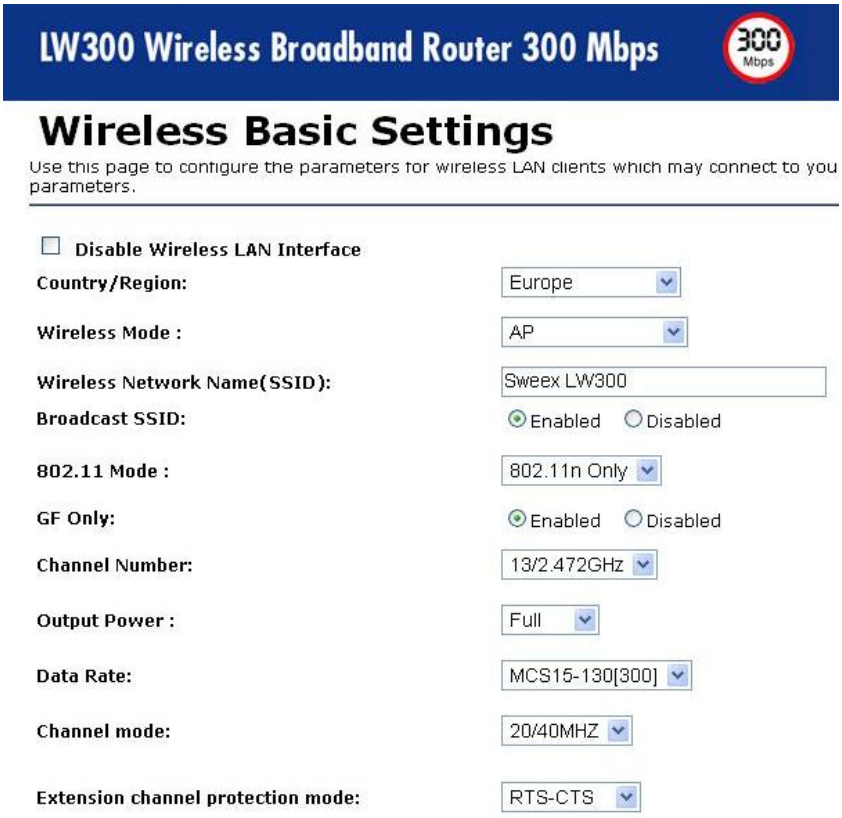

Figure A.4: SWEEX wireless router settings

optimal transfer conditions.
In addition the frequency spectrum of the channel is illustrated in figure A.6 to show the effect of the IEEE802.11n network transfer on the 2.4 GHz channel. The transfer occupies 20 MHz of the channel with the center frequency lying at WIFI channel 13, but also an additional lower 20 MHz introduced by the 802.11n standard to reach higher throughputs. As long as both the AP and the STA1 stay in the same room with dimensions 7×5 meter, the results are comparable to those in figure A.5, but as soon as the the AP and STA1 are in different rooms seperated by a wall, throughputs will drop as one can find out further on in this text. In figure A.7 the geometry and dimensions of the rooms in which the measurements take place are depicted with the location of the AP and the various locations of the STA1. Again data is transferred from the AP to the STA1 and vica versa, five times for every configuration and the throughputs are recorded. These records are processed and for every configuration the average rates are calculated over the five different measurements resulting in the graphs depicted in figure A.8. Immediately one can see that the transfer rate drops dramatically when moving to an adjacent room or a room even further which indicates the fact that signal power drops or the bit error rate increases when going through walls resulting in lower throughputs. Also remarkable is that the throughputs of transfers from STA1 to AP decrease faster than the throughputs of transfers from AP to STA1 when moving to other rooms. Knowing the AP has 3

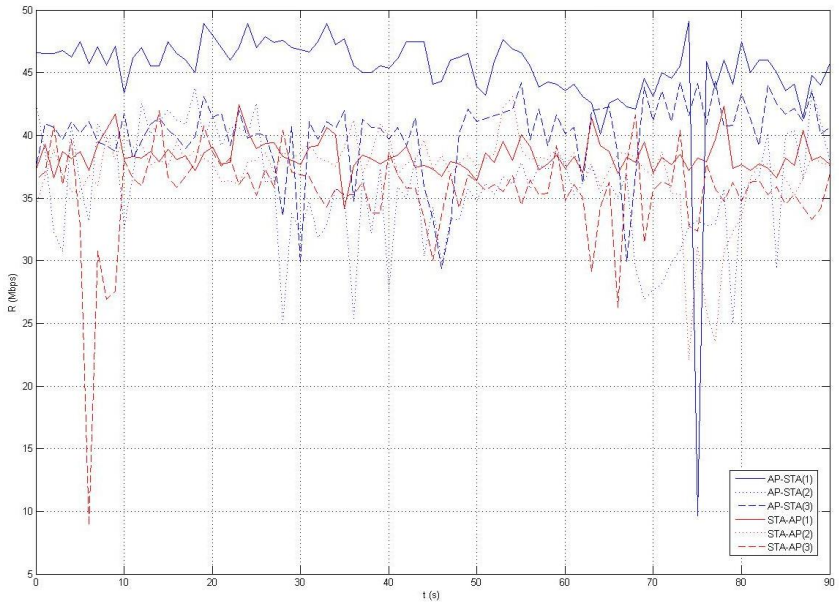

Figure A.5: Throughput for data transfer between SWEEX AP and STA1 in the same room placed 1.5 meter apart

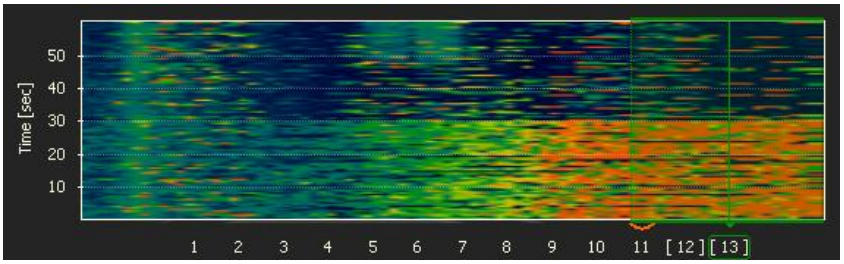

Figure A.6: 2.4 GHz frequency spectrum when starting a 802.11n file transfer at WIFI channel 13, with at the vertical axis the time (s) and at the horizontal axis the wifi channel numbers.

antennas and the STA1 has 2 (automatically configured), the reason for the lower rates for transmissions from AP - STA1 could be found here but from the literature [21] it is known that having an $M \times N$ or $N \times M$ MIMO system should make no difference for the capacity or the throughput. Future research should make this more clear.

A.1.1.3 Other Scenarios

Untill now a first glimp of the performance of the SWEEX router with respect to throughput has been revealed. In this paragraph the results of other various scenarios are discussed. These scenarios frequently occur in real life and therefore are analyzed.

Line-of-sight data transfer The first type of measurement that has been performed is data transfer from an AP to STA1 with a permanent line-of-sight (LOS) connection while increasing the distance between AP and STA1 for every measurement. Purpose of

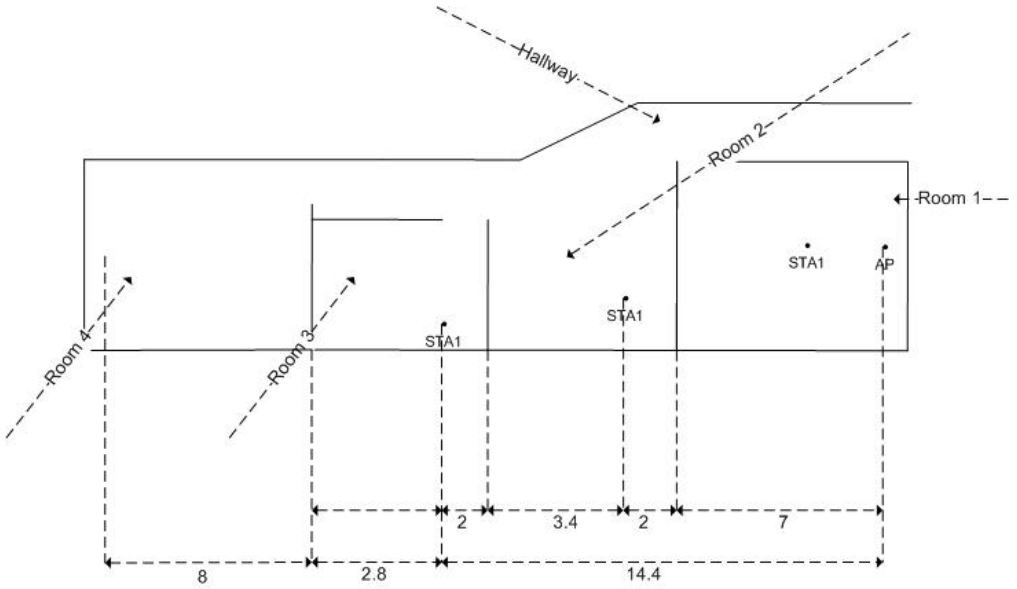

Figure A.7: Geometry and dimensions in meters of the measurement spot at the KPN building.

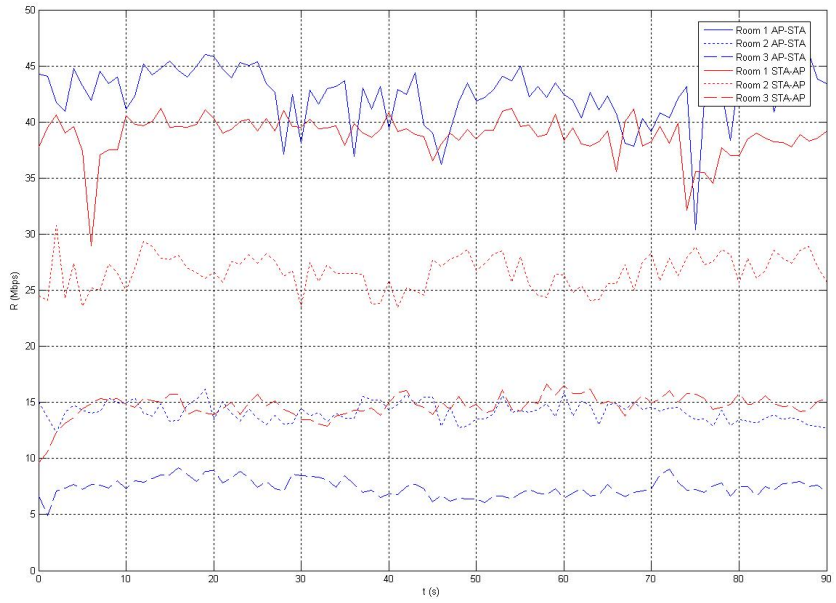

Figure A.8: Average throughputs in KPN Office Environment with Sweex AP and STA1 at different places w.r.t. each other. The mean values over time for the six different configurations are 42.4, 14.1 and 7.4 Mbit/s for the AP - STA1 transfers respectively and 38.8, 26.6 and 14.7 Mbit/s for the STA1 - AP transfers respectively.

this is to find out the range of the AP or STA in which there is a reliable link for data transfer. Again data is transferred from one notebook via the AP to STA1 and vica versa five times for each distance up to 30 meter and the average results are depicted in figure A.9.

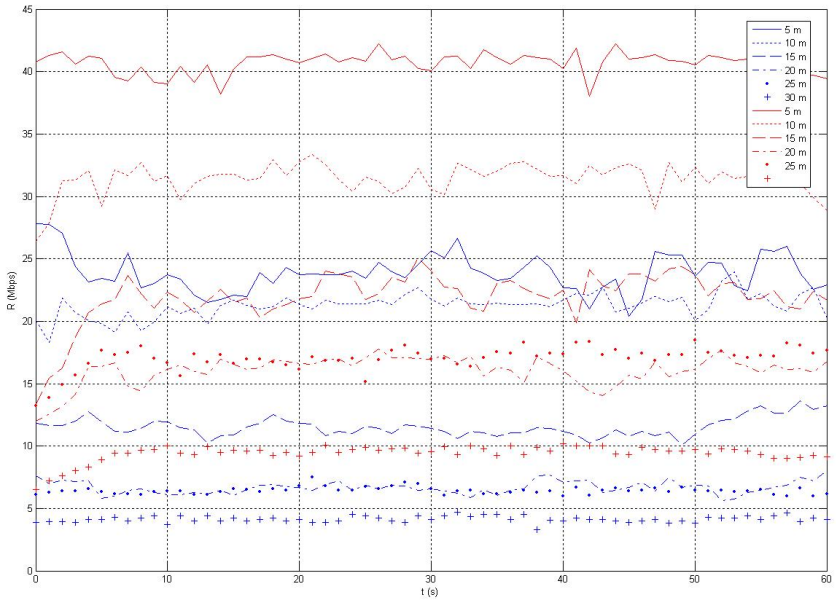

Figure A.9: Average throughputs for data transfers in the KPN hallway with permanent LOS connection with in blue the AP - STA1 transmission and in red the STA1 - AP transmissions and the mean values over time for the different distances are 40.6676, 31.3824, 21.9564, 16.0500, 17.0342, 9.4162 Mbit/s and 23.8728, 21.2664, 11.5319, 6.6773, 6.4174 and 4.1396 Mbit/s respectively.

As expected the throughput decreases as the AP and STA1 move further away form each other. Beyond the 30 meters the quality of the wireless link is not good enough to still have a reliable data transfer. Again the throughputs of the transmissions from STA1 to AP are higher than the transmissions from AP to STA1.

Influence of electronics in notebook This paragraph discusses the results of the measurements performed while transferring data between a SWEEX AP and STA where first a USB wire between the wireless adapter and the notebook is connented and in the other case not and thus the adaptar being immediately connected to the notebook. The results have to point out whether the electronics within the notebook effect the throughput or not. From figure A.11 where each graph is an average of 6 different measurements, it is obviously clear that having no wire between the wireless adapter and the notebook does not result in significant differences in throughput. Knowing this allowes for the future measurements to be performed with the wireless adapter being directly connected to the notebook without wire, because there are no real clues of either of the cases resulting in higher throughputs.

Influence of type of notebook While measuring it soon became obvious that the type of notebook used for transmitting and receiving data, has influence on the throughput. Therefore measurements were performed consisting of data transfers from a SWEEX AP to a SWEEX wireless STA connected to a different notebook every setup. From this it will be clear how the type of notebook used, influences the throughput. The type of

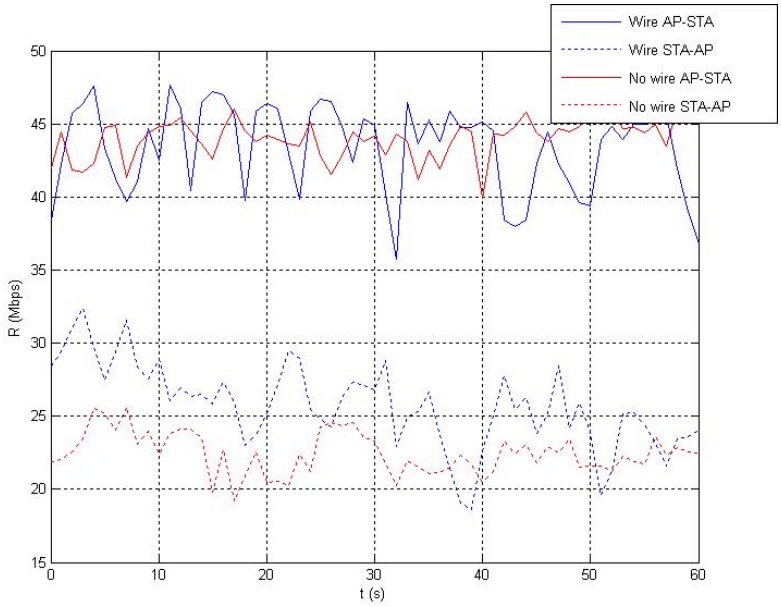

Figure A.10: Average throughputs for transfers between AP and STA with/without a USB wire between the notebook and the wireless adapter. The AP to STA transfers have a mean value of 43.4 Mbit/s and 44.0 Mbit/s for having or having not a wire respectively.

Name	Processor	RAM	Refer name
Acer Travelmate 8000	Intel Pentium M 1.6GHz	512 MB DDR	NB1
HP Pavillion ze5700	Mobile Intel P4 3.06GHz	512 MB DDR	NB2
Acer Aspire 9800	Intel Pentium M 1.73GHz	1024 MB DDR2	NB3
Acer Aspire 5020	AMD Turion 64ML-34 1.8 GHz	512 MB DDR	NB4
HP Desktop	Intel Pentium 4 2.93 GHz	1024 MB DDR2	DT1

Table A.1: Different notebooks used with their specifications and how they are referred to.

notebooks and their specifications are in Table A.1. The graph in figure A.11 confirms the prediction that different notebooks show dissimilar rates. One might think the processor speed or the RAM memory have something to do with the variying throughputs but the tests with different processer speeds and RAM capacities point out otherwise. From these tests the decision is made to discard NB2 from the measurements because its RAM is too small, degrading the rates too much.

A.1.2 Home Environment

In a place like HOME where there are a lots of housekeepings in a multiple storeys flat, nowadays the existance of many active wireless networks is a fact. In this part results are demonstrated of measurements done in such an environment for various scenarios and two networks SWEEX and LINKSYS are considered.

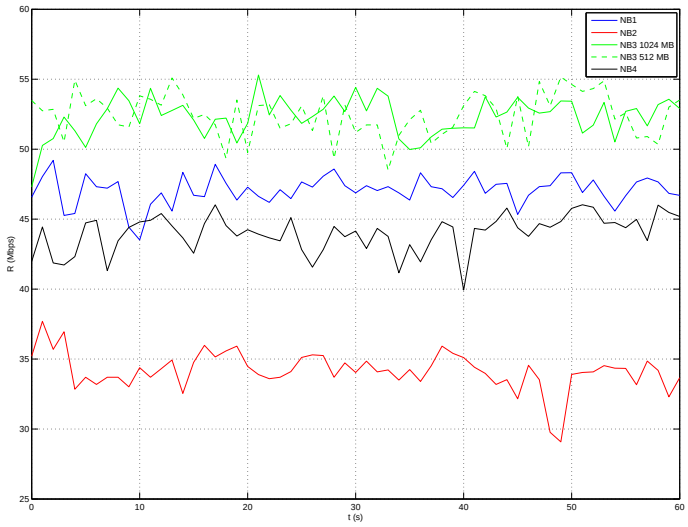

Figure A.11: Average rates with STA in Room 1 (see A.7 for transfers with different notebooks equipped with the SWEEX wireless adapter. Colors blue, red, green and black represent rates for NB1, NB2, NB3 and NB4 respectively Blue = NB1; Red =NB2; Green = NB3; Black = NB4

The average throughputs of transfers in a SWEEX network are presented in figure A.12. The STA is placed in different rooms and as expected the rates drop when moving further away from the AP. The same measurements were performed with the LINKSYS

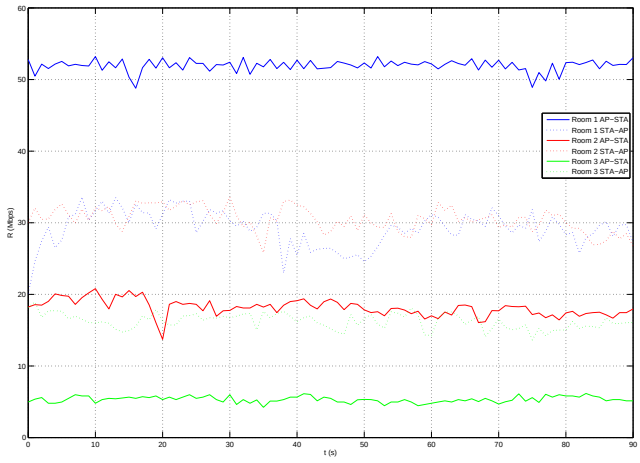

Figure A.12: Average rates for transfers between SWEEX AP and STA. Room 1 is same room as the AP stands, Room 2 is the adjacent room and Room 3 is the farrest room for which the distance from AP to STA is the maximum.

network and the results are in figure A.13.

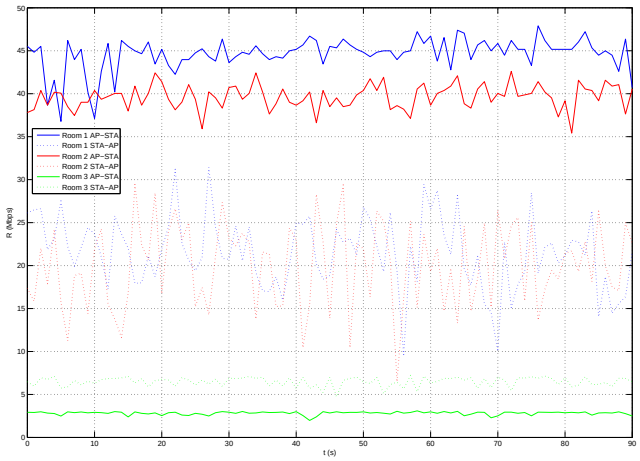

Figure A.13: Average rates for transfers between LINKSYS AP and STA. Room 1 is same room as the AP stands, Room 2 is the adjacent room and Room 3 is the room for which the distance from AP to STA is the maximum.

A.1.3 Anechoic Chamber

Although MIMO technique, used in 802.11n, makes use of the multipath character of the channel with reflections and scattering, it is still interesting to know how the standard operates in an environment with neglegible reflection and thus no multipath. Such an environment can be realised in an anechoic chamber: a room constructed in a way that inside the room there is no influence from radio signals outside the chamber and electromagnetic signals induced in the chamber are absorbed by the therefore specially constructed walls with pyramids (figure A.14(b). A detailed study about anechoic chambers can be found in [23]. In figure A.14 pictures of the chamber are illustrated.

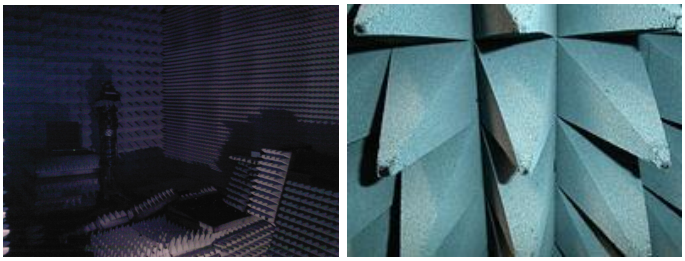

(a) Measurement place (b) Pyramid walls

Figure A.14: Anechoic chamber

The Anechoic Chamber measurements were carried out at the *Ducat* room of the *IRCTR* department at *TU Delft*. They were performed with SWEEX and SITECOM APs and STAs. The results are plotted in the graph of figure A.15. The SWEEX throughputs are around the 15 Mbit/s which is much lower than 42 Mbit/s derived before. Thus the

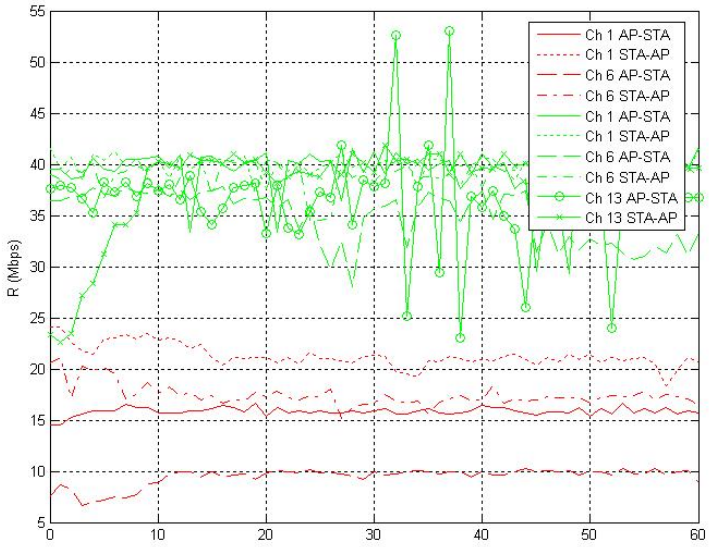

Figure A.15: Average throughputs against time (s) for transfers in an anechoic room: the red plots represent the SWEEX network values and the green plots represent the SITECOM network values.

effect on the throughput of having no reflections is proved by this graph. The SITECOM network shows higher rates, i.e. around the 37.5 Mbit/s. However, when blocking the LOS path in the middle of a transfer, the throughput drops to values as low as in the SITECOM network. This means the SITECOM AP has a very strong LOS component.

A.2 Multiple Transfers

In this section we discuss the reason why multiple simultaneous transmissions in a network result in higher throughputs. We also consider different measurement scenarios with multiple transmissions.

A.2.1 TCP window size and MTU

The TCP window size is a parameter set to avoid congestion in the network and to achieve flow control in such way that data is sent and received reliably. This window size is a predefined number of packets that can be transmitted without having received an acknoledgement from the receiver yet. The bottleneck in the throughput of the network introduced by the **Round Trip Time** (RTT) between transmitter and receiver is then avoided. The RTT puts a limit on the transfer rate because packets that have been sent and received succesfully need to be acknoledged by the receiver causing time delay in the communication. Measuring the RTT can simply be done by pinging the IP address of the receiver at the transmitter side. In the setup of figure A.3, the average RTT for a distance $d = 3$ meter, when sending a packet of 32 bytes is measured and determined

at 2 ms. This means that the maximum allowed bit rate by the transport layer is $\frac{32\times8}{2\cdot10^{-3}} = 128$ kbit/s. In order to reach a throughput of at least 100 Mbit/s, a minimum value for the TCP window of $100 \cdot 10^6/128 \cdot 10^3 \sim 782$ bits. The default window size in *Windows XP* operating system is 8 kbyte [6], which is equivalent to 8192 bits, This value is higher than the calculated minimum value of the TCP window size of 782, which is required. Thus we can conclude that the maximum throughput per file transfer could not be bounded by this parameter. The MTU is defined as the maximum packet size that can be transmitted for a layer in a network. A large MTU size results in higher bandwidth efficiency but on the other hand the channel will be occupied for a longer time. Besides, a too large MTU size might degrade the throughput because packet loss or errors in the packet cause retransmissions of bigger packets resulting in higher delays. Thus a good trade of has to be made. The default MTU size in Windows XP is 1480 bytes [7]. The routers used in the measurements have a default MTU size of 1492 bytes. Further research is needed to find out why in *Windows XP* the throughput of single file transfers is limited.

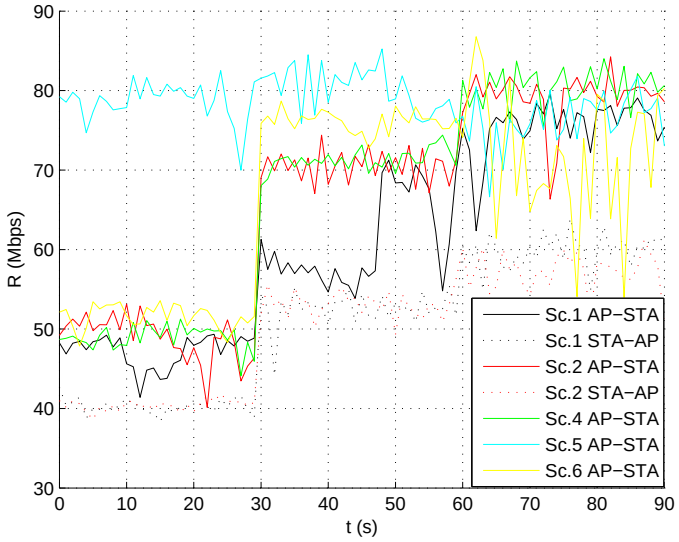

Figure A.16: Average rates for various values of the TCP window size and the MTU defined in table A.2 for the SWEEX network. Distinctions is also made between a single transfer for $0t <= 30$, two simultaneous file transfers for $31 \leq t \leq 60$ and three simultaneous file transfers for $61 \leq t \leq 90$ except for shenario 5 which is three file transfers for the whole 90 seconds.

Although theoretically the TCP window size under default circumstances could not influence the throughput, still it is interesting to do some measurement tests with various window sizes and MTU values. The results for the SWEEX network are in figure A.16 and for the SITECOM network in figure A.17. When the window size is too small like in scenario three in figure A.16 data communication is not possible at all and when it is too large like in scenario 6 the throughput is not optimal. For the SITECOM network the communication is not even possible and therefore has been left out of the graph in figure A.17. The rest of the scenarios in the SWEEX network do not show much variance and

Scenario	TCP Window	MTU XP	MTU router
1	2^{16}	1480	1492
2	2^{16}	1480	1400
3	2^{0}	1480	1400
4	2^{32}	2272	1400
5	2^{32}	12000	1400
6	2^{20}	1492	1492

Table A.2: Various values for the TCP window size and the MTU for multiple scenarios. The values are in bytes and K and G stand for kilo and giga respectively.

the SITECOM network operates best for window sizes of 1 Mbyte.

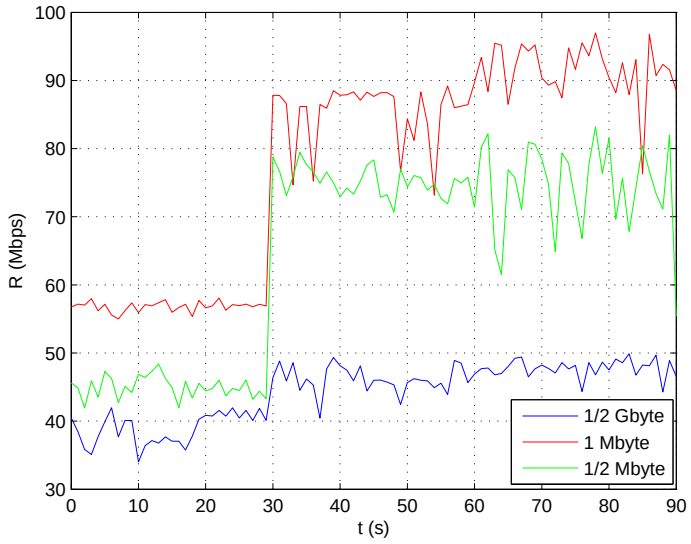

Figure A.17: Average rates for various values of the TCP window size for the SITECOM network. The MTU is set to the default value of 1492 bytes, because other values did not show improvements in the throughput. Again like in figure A.16 single and multiple file transfers are distinguished.

A.2.2 Operating system XP or Vista

Testing the theory of whether Windows XP as operating system would limit the throughput of a transfer and thus of one 802.11n communication link could be done by performing measurements under another operating system, e.g. *Windows Vista*. The results are in figure A.18 and obviously having one, two or three file transfers running simultaneously has no visible effect on the throughput. Knowing this confirms the declaration that Windows XP somehow limits the throughput of a transfer and only can achieve higher rates

when setting up multiple wireless links. When looking in more detail at this issue, it turns out that there exists a difference in the TCP window size settings between XP and Vista. The TCP window size discussed before, is set by default to 64 kbyte and larger window sizes can only be achieved when systems support **RFC 1323**, a TCP extension for high performance. Then by window scaling the window size can be increased to a maximum of 1073741823 bytes, which has to be done manually. In Vista however, window scaling is applied automatically as soon as the system detects RTT values greater than 1 ms. This phenomenon might be the reason why Vista achieves higher rates, but then again as explained before, the TCP window size in XP could never limit the throughput and even when enabling window scaling and setting the window size to a larger value did not help to increase the throughput.

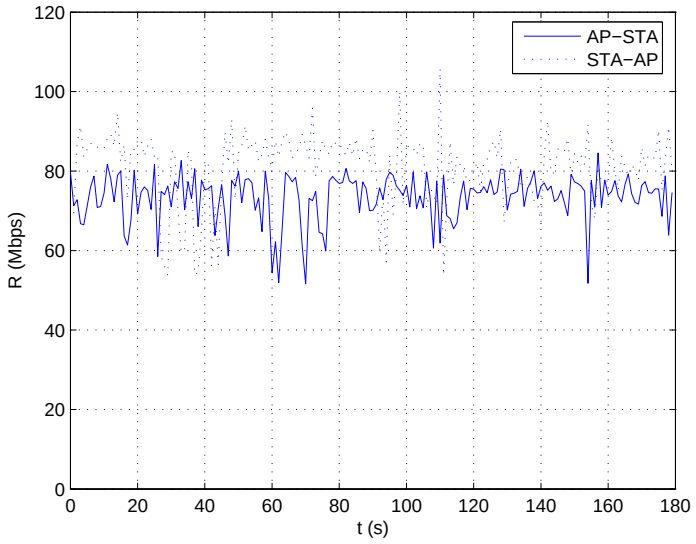

Figure A.18: Data rates for transfers of 1, 2 and 3 files simultaneously under Vista OS for the periods $0 \leq t \leq 60$, $61 \leq t \leq 120$ and $121 \leq t \leq 180$. The mean values of these periods are 73.5 Mbit/s , 72.1 Mbit/s and 74.7 Mbit/s for the AP to STA transfers respectively and 79.7 Mbit/s, 82.4 Mbit/s and 81.0 Mbit/s for the STA to AP transfers respectively.

In addition, in order to look at the throughput from another view, the probability density function (PDF) and the cumulative density function (CDF) of it rate are made available and depicted in figure A.19. The PDF is obtained by processing the data with the Gaussian function

$$f(x) = \frac{1}{\sigma\sqrt{2\pi}} e^{-\frac{(x-\mu)^2}{2\sigma^2}} \tag{A.1}$$

,where μ is the mean and σ is the standard deviation of the normal distribution. Fitting the elements of equation A.1 on a smooth line gives a plot with the normal distrubution. Consequently, integrating this function yields the CDF, i.e.

$$F(x) = \int_{-\infty}^{x} f(u)\, du \tag{A.2}$$

and fitting the elements of this function on a line results in the smooth CDF of figure A.19.

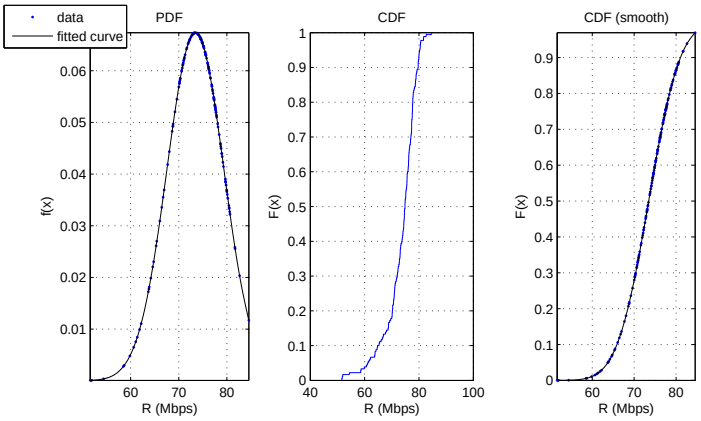

Figure A.19: PDF (left), CDF (middle) and 'smooth' CDF (right) of the throughputs under *MS Vista* with $\mu = 73.4621$ Mbit/s and $\sigma = 5.9221$

Multiple stations The next point of interest is the behaviour of the transfer rate when multiple wireless STA's are connected to the same AP. Both STA's intent to download or upload data from the network and therefore use the same frequency band, since the AP can only be assigned one WIFI channel for operation. Results are in figures A.21 and A.22 for different positions of the STA's (A.20). The AP is the SITECOM router that gets its data by NB1 and the STA's are the WL-302 connected to NB3, being STA1 and STA2 respectively.

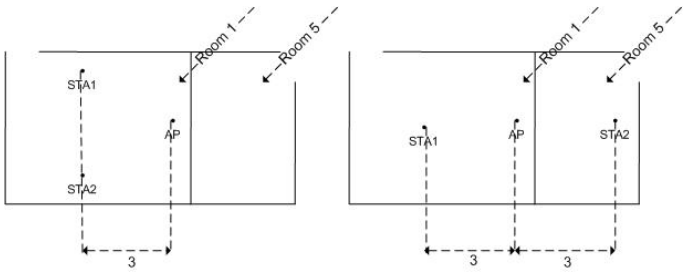

(a) Setup 1 (b) Setup 2

Figure A.20: Setups for the measurements with two STAs and one AP. Dimensions are in meters.

Other scenarios This section considers a view scenarios that occur frequently in real life like APs and STAs being on different floors of an appartment or the influence of a network to another network on a different floor.

Different floors In practice it often occurs that people like to have still connection to their AP even when they are on floor above or under the AP with their wireless

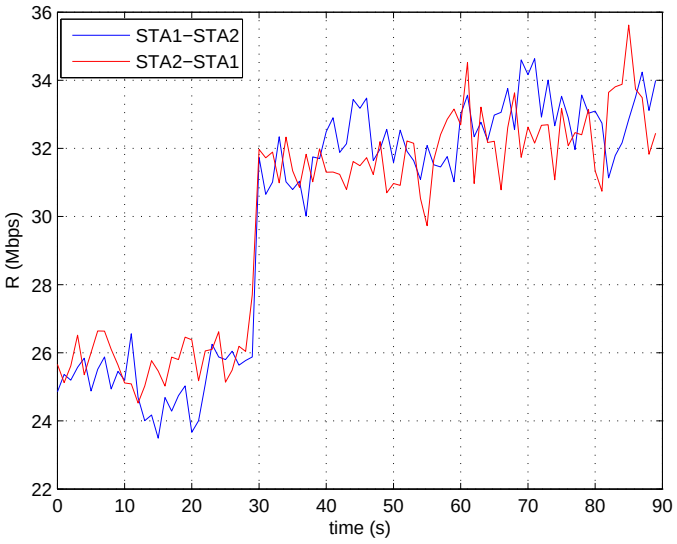

Figure A.21: Average throughputs of transfers between two STAs via an AP.

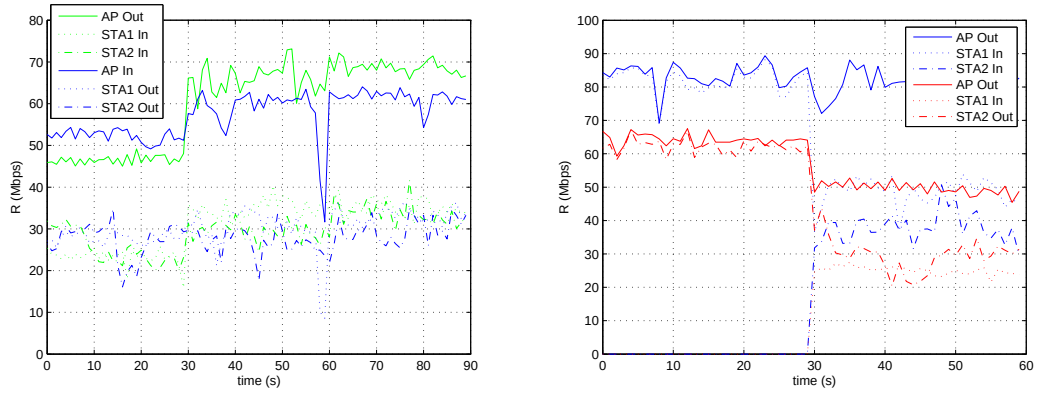

(a) Setup 1

(b) Setup 2

Figure A.22: Average throughputs with two STAs and one AP. Three periods are considered: $0 \leq t \leq 30$, $31 \leq t \leq 60$ and $61 \leq t \leq 90$ for respectively one, two and three simultaneous transfers.

station. However, this desire brings along a negative part too because the network could interfere with a co-existing network on the upper or lower floor. Some test have been done providing the throughputs of transfers where a STA is on a different floor with respect to the AP. SWEEX and SITECOM networks are tested. The results are in figure A.23.

"Exposed terminal" Another test has been done with two 802.11n networks transferring data at the same time. Only now AP2 of NW2 is placed at the edge of the range

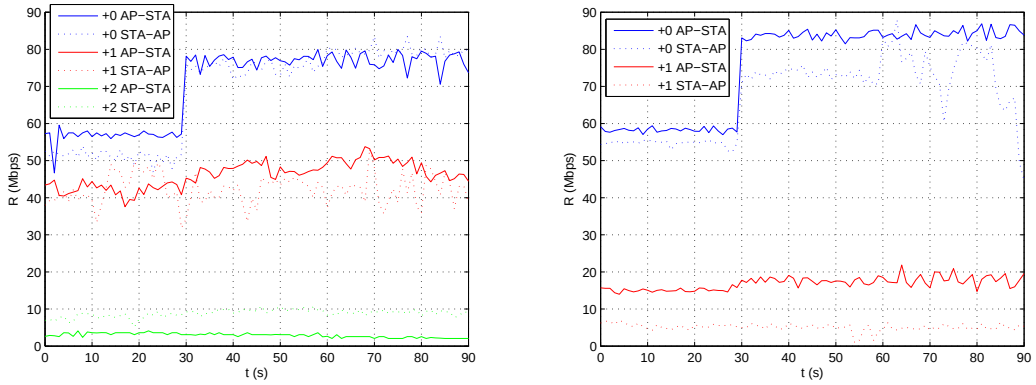

(a) SWEEX (b) SITECOM

Figure A.23: Average throughputs for transfers where STA and AP are at the same floor (+0), one floor apart (+1) and two floors apart (+2). Three periods are considered: $0 \leq t \leq 30$, $31 \leq t \leq 60$ and $61 \leq t \leq 90$ for respectively one, two and three simultaneous transfers.

of AP1 in NW1 and STA2 is positioned even outside the range of AP1 to simulate the exposed terminal problem in a way. Offcourse this would not be a legitimate exposed terminal problem because the involved nodes are in two independent networks, meaning they are not synchronized. Synchronization is a condition when hidden and exposed terminal problems are to be solved. The results are in figure A.24. Both networks operate at WIFI channel 13.

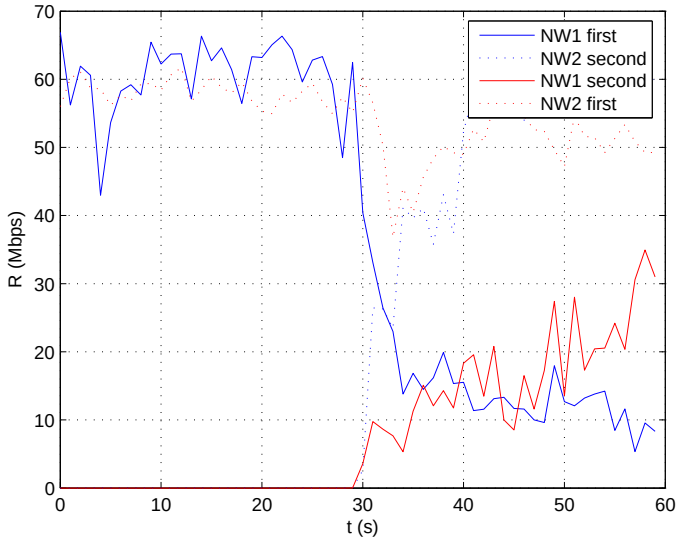

Figure A.24: Average throughputs for simultaneous transfers of two 802.11n networks positioned that way that the two access points are at each others maximum range. The intention is to imitate the exposed terminal problem.

Selected *Matlab* source codes B

B.1 Riemann Sum

Here we present the *Matlab* code for approximating the integral for the P_e calculation making use of the Riemann sum.

```
int_start =.01;                     % left integral boundary
int_end =1;                         % right integral boundary
int_length = int_end - int_start;   % total integration interval
delta = 0.0001;                     % integration stepsize <= 0.0001
points = (int_length)/delta;        % # of integration points


a = rand(points*5,1);               % create enough random variables
a = int_start + a*int_length;       % map the variables on the interval
                                    % given by int_start and int_end
F = hist(a,points);                 % make a histogram of the outcome
F = F./sum(F);                      % and calculate the probability of
                                    % each occurance (PDF of a)
    for d= 1:50                     % distance
        r = 0;                      % Riemann sum r
        cnt =0;                     % PDF index
        % Riemann sum of prob(d,a_0,scenario)*F(cnt) where prob(.) = P_e
        for a_0 = int_start:delta:1-delta
            cnt = cnt+1;
            r=r+prob(d,a_0,scenario)*F(cnt);
    end
    y(d) = r;                       % save the result in y for distance [1,30]
```

B.2 P_e calculation for different MCS parameters

Here we present a part of the *Matlab* code where P_e is calculated for different MCS parameters. The part where the fading is included was already given in Appendix B.1

```
%% Deriving P_e for different modulation types where
%% M is given for considered M-ary modulation and R is increasing throughput
```

```
k = log2(M);                    % k = 2log(M) is bits per symbol
d/d_0 = 10;                     % normalized fixed distance

R_c = 3/4;                      % code rate
N_SD = 108;                     % # of data subcarriers
N_BPSC = k;                     % coded bits per subcarrier
N_SS = 2;                       % spatial streams
A = N_SD*R_c*N_BPSC*N_SS*1e-6;  % all the parameters multiplied

v_z = v_w + v_n_n;              % v_z = var(z) given in (4.48)
                                % v_w = var(w) given in (4.49)
                                % v_n_n = var(I) given in (4.52)

P_e = (2/k)*(1-(1/sqrt(M)))*0.5*erfc(sqrt((3*k*a_0*a_0*((alpha)/R))./
(v_z.*sqrt(2)*(M-1))));
```